This is to certify that the
thesis entitled

Stream Transient Storage Modeling
Based On
Fractional-In-Space Dispersion

presented by

Rammesh Padmanabhan Navaneethakrishnan

has been accepted towards fulfillment
of the requirements for the

Master of Science degree in Civil and Environmental Engineering

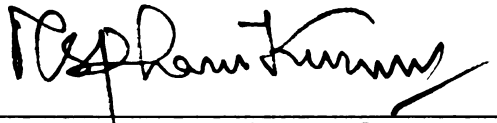

Major Professor's Signature

12/14/2007

Date

| DATE DUE | DATE DUE | DATE DUE |
|---|---|---|
| | | |
| | | |
| | | |
| | | |
| | | |
| | | |
| | | |
| | | |
| | | |
| | | |

# STREAM TRANSIENT STORAGE MODELING BASED ON FRACTIONAL-IN-SPACE DISPERSION

By

Rammesh Padmanabhan Navaneethakrishnan

A THESIS

Submitted to
Michigan State University
in partial fulfillment of the requirements
for the degree of

MASTER OF SCIENCE

Department of Civil and Environmental Engineering

2007

# ABSTRACT


## STREAM TRANSIENT STORAGE MODELING BASED ON FRACTIONAL-IN-SPACE DISPERSION

By

Rammesh Padmanabhan Navaneethakrishnan

Solute transport in natural streams is often described using the transient storage (TS) model in which two separate equations are used to describe the partitioning of the solute between the main channel and the storage zones. Several stream tracer studies have found heavy-tailed rising and falling limbs in the time-concentration breakthrough curves (BTCs) because of the long-range spatial correlation of the dispersion process as well as the exchange processes between the storage zones and the main channel respectively. Application of the TS model to field sites with multiple stream reaches is accomplished by estimating one set of parameters for each stream reach in order to describe the scale-dependent dispersion process. Dispersion and the storage zone processes are known to give rise to competing parameters in the TS model sometimes leading to singular convergence during parameter estimation. Therefore, the inability to describe dispersion accurately introduces uncertainty in the storage zone processes and parameters. In this work, we propose an alternative TS model based on the concept of anomalous diffusion described mathematically using fractional-in-space derivatives. The new Fractional-in-space Transient Storage (FSTS) model has the ability to describe the observed early (non-Fickian) dispersion in some stream reaches and is able to describe the scale-dependence of the dispersion process. The model is used to describe tracer transport in two Michigan streams using one dispersion coefficient but different fractional derivative exponents in different reaches. The new FSTS model was found to better constrain the TS model parameters by providing a superior description of dispersion.

Dedicated to my parents

and my brothers

Suresh and Srikantesh

# ACKNOWLEDGMENTS

I would like to thank my research advisor and now a friend, Mantha Phanikumar, for his constant guidance, encouragement and support and for the numerous discussions we've had during the course of this research work. He had dedicated more time, effort and energy to this work than I could have asked for. I thank him for always being willing to meet me whenever I barged into his office and also answering to my never ending emails and phone calls, even during weekends. Thank you for always being there.

I would like to thank my committee member, Shu-Guang Li, whose unconventional teaching style with emphasis on practical application of theory, encouraged me to learn and explore more about this field over a period of two years at MSU. His constructive feedback and comments have been significantly useful in shaping this work to completion. I would also like to thank my other committee members Roger Wallace and Irene Xagoraraki for their useful comments and suggestions, which helped to bring out clarity and focus to this work towards the end.

Financial support from the following two funding agencies is gratefully acknowledged: (a) NSF Biocomplexity in the Environment: Coupled Biogeochemical Cycles (b) NOAA Center of Excellence for Great Lakes and Human Health

I would also like to thank a number of other people in my everyday circle of colleagues who had enriched my professional life at MSU in various ways. First, my research group colleague and friend Chaopeng Shen for his inputs and companionship in RCE. Heather Stevens, for bugging her many a times with my never ending stories she used to listen to, when I used to get bored with programming. Finally, my roommate and friend, Sagar Rayepalli, for the same food he cooked and satisfied my unsatiable appetite during the course of this work!

In the end, I would like to thank my parents for supporting my decision to go for graduate studies and not getting mad at me for not visiting them even once after I came to US. And obviously my two big bros, Suresh and Srikantesh for being a constant inspiration throughout my life.

# TABLE OF CONTENTS

**LIST OF TABLES** . . . . . viii

**LIST OF FIGURES** . . . . . ix

**1 Introduction** . . . . . 1
- 1.1 Fractional Calculus and the Fractional Derivative . . . . . 6
- 1.2 Numerical Methods . . . . . 8
- 1.3 Outline of thesis . . . . . 11

**2 Advection Schemes** . . . . . 13
- 2.1 The Weighted Essentially Non-Oscillatory (WENO) Scheme . . . . . 15
  - 2.1.1 One-Dimensional Reconstruction . . . . . 16
- 2.2 A Fourth-Order Compact Scheme with Spectral-Like Resolution . . . . . 20
- 2.3 A Test Case: Advection of a Gaussian Pulse . . . . . 22
- 2.4 FFT Analysis of Advection Schemes . . . . . 24
- 2.5 Conclusion . . . . . 26

**3 Fractional Diffusion: Preliminaries and Numerical Approximations** . 28
- 3.1 Introduction . . . . . 28
- 3.2 Fractional-in-space Diffusion . . . . . 29
- 3.3 Fractional-in-time Derivative: Sub-Diffusion . . . . . 30
- 3.4 Fractional Derivative: Multiple Definitions . . . . . 31
  - 3.4.1 The Riemann-Liouville Derivative . . . . . 33
  - 3.4.2 The Caputo Derivative . . . . . 34
- 3.5 Numerical Approximations: The GL and Caputo Derivatives . . . . . 35
  - 3.5.1 The Caputo Derivative . . . . . 36
- 3.6 Higher Order Approximations . . . . . 37
  - 3.6.1 Higher Order Caputo Fractional Derivative Using Integer Derivatives 39
  - 3.6.2 A Test Example . . . . . 40
- 3.7 An Exact Solution: The Method of Manufactured Solutions . . . . . 41

**4 Fractional Advection Dispersion Equation** . . . . . 48
- 4.1 Semi-Analytical Solution for the fADE . . . . . 48
  - 4.1.1 Numerical methods . . . . . 49
- 4.2 Operator Splitting Methods . . . . . 51
- 4.3 Boundary Conditions . . . . . 52
- 4.4 Solution of the fADE for Continuous Release . . . . . 54
- 4.5 Instantaneous slug release . . . . . 55
  - 4.5.1 High Peclet Number: Advection-Dominated Systems . . . . . 56
  - 4.5.2 Low Peclet Number: Dispersion-Dominated Systems . . . . . 58
  - 4.5.3 Effect of fractional derivative exponent($\alpha$) . . . . . 60

**5 Stream Transient Storage Modeling** . . . . . **62**
5.1 Transient Storage Model . . . . . 64
5.2 The Fractional-in-Space Transient Storage (FSTS) Model . . . . . 65
5.2.1 Comparison of the FSTS model with the Analytical Solution for $\alpha = 2$ . . . . . 68
5.3 Application of the FSTS Model to Describe the Field Data . . . . . 69
5.3.1 The Red Cedar River, Michigan . . . . . 70
5.3.2 The Grand River, Michigan . . . . . 73

**6 Conclusions** . . . . . **80**

**APPENDICES** . . . . . **82**

**A Caputo Derivative Operator** . . . . . **82**

**B Grünwald-Letnikov Derivative Operator** . . . . . **85**

**C Grünwald-Letnikov and Caputo Weights** . . . . . **87**

**Bibliography** . . . . . **96**

# LIST OF TABLES

2.1 Coefficients of a three-stage-third-order Runge-Kutta scheme, from Lowery and Reynolds (1986) . . . . . 22

2.2 Order of accuracy for the WENO-Roe and the compact schemes . . . . . 22

3.1 Table showing the order of numerical approximation for Grünwald-Letnikov and h-Caputo derivative operators . . . . . 41

3.2 Table showing the weights for the Grünwald-Letnikov derivative for different $\alpha$ values . . . . . 46

3.3 Table showing the weights for the Caputo derivative for different $\alpha$ values . 47

5.1 Storage zone parameters for the Red Cedar River using FSTS model . . . . 78

5.2 Storage Zone Parameters for the Grand River for the three reaches with a constant $D$ using the FSTS model . . . . . 79

# LIST OF FIGURES


1.1 Illustration of transient storage mechanisms (a) when solutes enter small pockets of slow-moving water and (b) when solutes leave the main channel and enter the porous media that makes up the bed and banks of the channel. Arrows denote the solute movement between the main channel and the transient storage zone. [Runkel, 1998; Schmid, 2004] . . . . . 4

1.2 Comparison of integer and fractional derivative of $f(x) = x^2$ . . . . . 8

1.3 Fractional derivative for $f(x) = x^3$ . . . . . 12

2.1 Comparison of fifth order WENO-Roe scheme with analytical solution for $\Delta x = 0.1$, $CFL = 0.1$ at $t = 1$ . . . . . 19

2.2 Comparison of the compact, WENO and first-order upwind scheme for $\Delta x = 1$, $u = 1$, $CFL = 0.1$ at $t = 5$ . . . . . 23

2.3 Plot showing that comparison of RMSE error (log-scale) for compact, WENO and first-order scheme for different CFL and $\Delta x$ values . . . . . 24

2.4 Plot showing that comparison of the compact and the WENO scheme for $\Delta x = 1$, $u = 1$, and $CFL = 0.1$ with the analytical solution at $t = 250$. WENO scheme disperses while compact scheme oscillates . . . . . 25

2.5 Plot showing that comparison of compact and WENO scheme for $\Delta x = 1$, $u = 1$, and $CFL = 0.1$ with the analytical solution at $t = 250$. Clearly the amplitude of the WENO scheme is lower compared to compact scheme for a crude grid size . . . . . 27

3.1 The random jump in space and time in a CTRW model . . . . . 29

3.2 The left and right RL derivatives at a point $x$ . . . . . 33

3.3 Control volume approximation to the Caputo fractional derivative . . . . . 37

3.4 Higher-order approximations: The generating function $\omega$ as a function of $z$ 39

3.5 Comparison of RMSE error (log scale) for the fractional derivative with the analytical solution between GL and H-Caputo derivative (higher order Caputo) . . . . . 41

3.6 Plot showing the variation of RMSE (log scale) with fractional derivative exponents ($\alpha$) for two grid sizes $\Delta x = 0.1$ and $\Delta x = 0.01$ with $D = 1$ at time, $t = 1$ . . . . . 44

3.7 Plot showing the variation of RMSE (log scale) with dispersion coefficients, $D$, for grid sizes of $\Delta x = 0.1$ and $\Delta x = 0.01$ with $\alpha = 1.8$ and at time, $t = 1$ 45

4.1 Breakthrough curves shown at $x = 10m$ from the point of release. $u$=1ms$^{-1}$ and $D = 1$ . . . . . 50

4.2 Concentration profiles for the continuous release of a tracer in a stream simulated using the fADE. The fADE was numerically solved using the WENO-GL and WENO-Caputo schemes and compared with the semi-analytical solution of [Benson et al., 2000]. The parameters in the solution are $C_0$=1ppb at $t$= 5s, 10s and 15s with $u$ = 1ms$^{-1}$, D = 0.1m$^{1.8}/s$, $\alpha = 1.8$, $CFL = 0.1$ and $\Delta x$=0.1250m . . . . . 54

4.3 Plot showing the comparisons for all the four schemes for a $Pe = 6.6$ ($\Delta x$=0.25m, D = 0.05m$^{1.8}/s$, $u$ = 1ms$^{-1}$, $CFL$ =0.1, $t$=15s and $\alpha = 1.8$). Numerical oscillations were observed in case of compact based approaches while numerical dispersion was observed in the case of WENO based advection schemes . . . . . 57

4.4 Plot showing the comparison for a $Pe = 1.7$ for all the four schemes ($\Delta x$=0.25m, D = 0.05m$^{1.8}/s$,$u$ = 1ms$^{-1}$ , $CFL$ =0.1, $t$=15s, $\alpha$=1.8). All the schemes show reasonably good fit, although the WENO based advection scheme introduced small numerical dispersion . . . . . 58

4.5 Breakthrough curves for a low $Pe = 0.057$ ($\Delta x = 0.5$, $CFL = 0.1$, $\alpha = 1.8$, $\beta = 1$, $D$ = 10m$^{1.8}$/s, $u$ = 1ms$^{-1}$) at a distance of 5m from the spill location. . . . . 59

4.6 Breakthrough curve (without OS) for a low $Pe = 0.057$ ($\Delta x = 0.5m$, $CFL = 0.1$, $\alpha = 1.8$, $\beta = 1$, $D$ = 0.05m$^{1.8}$/s,$u$ = 1m/s) at a distance of 5m from the spill location. . . . . 60

4.7 Breakthrough curves comparison between GL and Caputo with Benson et al. [2000] for different values of $\alpha$ with $Pe = 0.1$ . . . . . 61

5.1 Numerical model showing the snapshot of concentration vs distance in the main stream at $t$ = 600s spatially for $A$ = 40 m$^2$, $A_s$ = 4 m$^2$, $D$ = 1m$^{1.8}$/s, $u$ = 1ms$^{-1}$, $\epsilon$ = 0.0 s$^{-1}$, $M$ = 1000g. The point of injection is at $x$ = 10 m 66

5.2 Breakthrough curve for the stream and storage zone concentration at a distance of $x$ = 50m from the point of injection in (a) linear scale and (b) log log scale. In log scale, it can be observed that for the falling limb the major contribution of the concentration comes from the storage zone whereas, for the rising limb it is the main channel. ($A$ = 40 m$^2$, $A_s$ = 4 m$^2$, $D$ = 1m$^{1.8}$/s, $\beta = 1$, $u$ = 0.5ms$^{-1}$, $\epsilon$ = 0.001 s$^{-1}$, $M$ = 1000 g, $\alpha = 2$) 67

5.3 FSTS vs TS model breakthrough curve in the main channel for $A = 40$ $m^2$, $A_s = 4$ $m^2$, $D = 1 m^{1.8}/s$, $\epsilon = 0.0001$ $ms^{-1}$, $M = 1000$ g, $\alpha = 2.0$, $\Delta x = 2.9950$ m and $x = 1000$ m . . . . . 68

5.4 Comparison of compact-Caputo based fADE with the analytical solution given by De Smedt et al. [2005] for $Q = 16$ $m^3 s^{-1}$, $A = 40$ $m^2$, $A_s = 4$ $m^2$, $D = 1$ $m^{\alpha} s^{-1}$, $M = 1000$ g, $\alpha = 2.0$, $\Delta x = 0.33$ m and $x = 1230$ m . 70

5.5 Comparison of compact-Caputo based fADE with the analytical solution given by De Smedt et al. [2005] for $Q = 20$ $m^3 s^{-1}$, $A = 40$ $m^2$, $A_s = 4$ $m^2$, $\epsilon = 0.0001$ $ms^{-1}$, $M = 100$ g, $\alpha = 2.0$, $\Delta x = 0.33$ m and $x = 10$ m . . 71

5.6 Comparison of compact-Caputo based fADE with the analytical solution given by De Smedt et al. [2005] for $A = 40$ $m^2$, $A_s = 4$ $m^2$, $D = 1$ $m^{\alpha} s^{-1}$, $\epsilon = 0.0001$ $ms^{-1}$, $M = 100$ g, $\alpha = 2.0$, $\Delta x = 0.33$ m and $x = 10$ m . . . . 72

5.7 Probability plot showing the normalized concentration (or probability) as a function of the Z-scores of travel time for the Reach C of the Red Cedar River. Deviation from the straight line indicates a deviation from Fickian diffusion . . . . . 73

5.8 Red Cedar River Watershed showing the Red Cedar River and the sampling locations (adapted from Phanikumar et al. [2007]) . . . . . 74

5.9 Fluorescein breakthrough curves for the three reaches A, B and C for the Red Cedar River with a constant dispersion coefficient $D = 4.14$ using the FSTS model . . . . . 75

5.10 Grand River Watershed and study region showing the sampling sites (adapted from Shen et al. [2007]) . . . . . 76

5.11 Rhodamine WT breakthrough curves for the three reaches B, C and D of the Grand River with a constant dispersion coefficient $D = 3.32$ using the FSTS model (data taken from Shen et al. [2007, in review]) . . . . . 77

# CHAPTER 1

# Introduction

More than half of the world's population lives in urban areas [Cohen, 2003] and stream ecosystems are undergoing significant changes due to rapid urbanization in many parts of the world. Changes in impervious cover and the concomitant changes in stream hydrology, geomorphology, water quality and physical habitat are a direct result of urbanization. Anthropogenic activities are the major cause of large increases in stream nutrient concentrations measured worldwide, often resulting in declining water quality (often referred to as the "urban stream syndrome" [Meyer et al., 2005]). These changes have important implications for human health and the ecological integrity of ecosystems. Understanding how streams respond to natural and anthropogenic stressors is therefore critical to managing these resources effectively. Hydrological metrics are generally used as indicators of urban impacts on stream ecosystems [Roy et al., 2005; Booth, 2005]. These include, for example, a flashier hydrograph (i.e., increased frequency of high flows as defined by the stream flashiness index), higher nutrient concentrations but less efficient nutrient uptake rates and less taxonomic diversity or species richness when compared to unaltered streams. The dynamics of solute transport in steams plays a critical role because many solutes such as Nitrogen or Phosphorus are present in short supply and therefore regulate primary or secondary productivity. Solute transport modeling is important since it allows us to explore the relationship between physical characteristics of the stream (such as geomorphology, nature of the substrate, flow etc.) and hydraulic variables such as dispersion, transient storage, and lateral inflow. A combination of tracer studies and solute transport modeling provides a framework to quantify important processes, separate physical and

biological controls and allows comparisons to be made across different scales [Dangelo et al., 1993]. Transient storage (hereinafter TS) refers to multiple processes that contribute to solute retention in a stream resulting in a delay in the downstream movement of solute mass. A distinction is usually made in the literature between in-channel storage due to surface features such as vegetation, woody debris and eddies and pools (e.g., due to extensive meandering) within the stream (called surface storage) and the retention of solutes due to interaction with near-bed sediments (called hyporheic exchange). Unless otherwise specified TS usually refers to the combined effect of both types of storage. In stream solute transport models, the dispersion coefficient $D$, the size of transient storage zones $A_S$ and the exchange rate $\alpha$ between the main channel and the storage zones are important hydraulic variables that depend on stream physical characteristics. The variables $D$ and $\alpha$ depend on properties such as discharge, velocity distribution and the channel cross-sectional area, therefore they correlate with stream order. $A_S$ strongly depends on the presence or absence of in-stream complexity (e.g., the presence or absence of leaves, cobbles/boulders). The lateral inflow $q_L$ which reflects the contributions from the sides as well as from groundwater depends on the geomorphology, streambank porosity and the location of the watertable [Dangelo et al., 1993].

Measuring stream health is one of the approaches to monitor and direct the sustainable use of streams and stream restoration efforts [Harbott et al., 2005]. Regulatory guidelines require that certain criteria be satisfied for water bodies to be considered healthy. In addition to the usual water quality parameters (such as suspended solids concentration, pH, temperature and dissolved oxygen), recent efforts have included stream organisms as indicators of stream health (e.g., fish and plant assemblages). Microbial communities respond rapidly to environmental change. Two important services are provided by microbial communities - they are a food source for higher trophic levels in the food web and they regenerate nutrients through mineralization of organic detritus [Harbott et al., 2005; Allan, 1995]. Coliforms and nitrifying bacterial counts are typically higher in urban streams (due to sewage discharges) compared to native/unaltered streams. In contrast, urban streams are known to have decreased microbial metabolism due to increased sedi-

ment metal concentrations associated with urbanization [Wei and Morrison, 1992]. One very important element of stream restoration, which had long been neglected and is still an area of active research is the hyporheic exchange zone. It is term derived from Greek roots -hypo, meaning under or beneath, and rheos, meaning a stream (rheo means to flow). Hyporheic exchange zone provides habitat for aquatic macro-invertebrates and provides conditions for heterotrophic primary production [Mulholland, 1997]. It is responsible for changes in surface water quality through physical and biogeochemical processes. There are number of variations to the definitions of hyporheic zone (Figure 1) depending upon the field they are used in as shown by the definitions given below:

1. The hyporheic zone is the zone below and adjacent to a streambed in which water from open channel exchanges with interstitial water in the bed sediments;

2. It is the zone around a stream in which the fauna of the hyporheic zone (the hyporheous) are distributed and live;

3. It is the zone in which groundwater and surface water mix.

A large number of studies have been reported in the last decade to understand the exchange between the hyporheic zone and main stream including physical mixing with groundwater [Constantz, 1998], chemical reactions [Bencala and Walters, 1983; Duff et al., 1998], microbially mediated chemical transformations [Duff and Triska, 1990] and transport of nutrients thorough groundwater-surface water interactions [Wondzell and Swanson, 1996; Valett et al., 1996; Jonsson et al., 2003]. Stream solute transport modeling is an important activity in all of the efforts reported above as it provides a means to test hypotheses about processes based on observed data. The focus of this research is on the numerical solution of the TS equations which govern solute transport in streams, therefore we will study the hyporheic zone from a hydrologist's angle, which often regards it as an extension of the stream channel, where water can spend longer duration than in the open channel [Jones and Holmes, 1996]. Conceptual models of the hyporheic zone and the processes that occur within it have been studied in many fields, but we will limit

our study to the well-known TS model as presented, for example, by Bencala and Walters [1983].

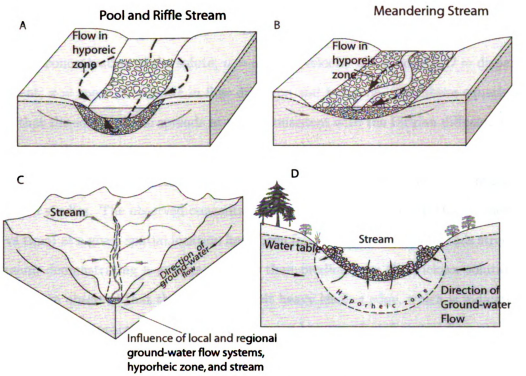


**Figure 1.1.** Illustration of transient storage mechanisms (a) when solutes enter small pockets of slow-moving water and (b) when solutes leave the main channel and enter the porous media that makes up the bed and banks of the channel. Arrows denote the solute movement between the main channel and the transient storage zone. [Runkel, 1998; Schmid, 2004]

In order to understand the physical processes occurring in the TS systems, tracer studies are typically done in the streams. The tracer studies involves releasing a slug of tracer across the cross-section of the stream or river, and measuring concentrations at various downstream locations. Breakthrough curves (time vs concentration plot) at various downstream locations helps in the understanding of transport of solute in the streams and their interaction with the storage zones. Typically, conceptual models are used to describe the transient storage processes using mathematical equations. Various parameters including dispersion coefficient, velocity and storage zone parameters are estimated by minimizing the error between the model estimates and the observed values. The estimated parameters from these models are useful in understanding the physical, chemical and biological function of streams. One of the most common mathematical models used in literature

to describe the longitudinal solute transport in surface and sub-surface systems is the classical advection-diffusion equation (ADE) defined as [Chiba et al., 2006]

$$\frac{\partial C}{\partial t} + u\frac{\partial C}{\partial x} = D\frac{\partial^2 C}{\partial x^2} \tag{1.1}$$

where $C$= concentration of the solute; $u$ = average velocity of the solute; $D$ = dispersion coefficient; $x$ = space coordinate in flow direction and $t$ = time. The above equation assumes that the solute plume spreads at a rate consistent with the Fickian diffusion theory i.e., a particle's motion has little or no long-range spatial correlation. But this is not always true in transport of solutes in rivers and streams as has been observed in many field dispersion studies. The observed concentration breakthrough curves (BTCs) (concentration vs time) at a given spatial location have been found to have a flat long tails stretching upstream, demonstrating a greater variance than predicted by the Fickian solution. It has also been observed that that BTCs exhibit heavy leading edge, which is indicative of faster-than-fickian processes, which usually occurs because of preferential flow paths in a stream. These behaviors are referred as anomalous diffusion in the literature because it does not follow the classical bell shaped breakthrough curve usually associated with Fickian diffusion. One of the possible reasons for the heavy falling edges in the BTC is that the solute particle may be sorbed to solids or get diffused into regions where the advective flux in negligible (e.g. dead zones) resulting in heavy-tailed falling limb BTCs. Therefore, in order to seek an explanation for the physics underlying the observed non-Fickian dispersion a wide range of models have been proposed in the past. Some studies have focussed on the use of TS models based on the solute exchange processes between the main channel (e.g. stream, river) and the storage zone (eg. dead zone, hyporheic zone) [Bencala and Walters, 1983; Davis et al., 2000; Fischer, 1979; Lees et al., 1999], while some models have used scale-dependent dispersion (i.e., increase in dispersion coefficient indefinitely with downstream distance) models to describe the faster-than-Fickian processes, also called super-diffusion [Berkowitz and Scher, 1995; Worman, 1998]. One of the main reasons for using scale dependent parameters were in order to describe the long-range spatial and/or temporal correlation of particle movement observed in various field studies. However, the vast majority of these models, assume, either explicitly or implicitly, an underlying Fick-

ian transport at some scales [Sposito and Jury, 1986], which assumes that the particle's motion has little or no spatial correlation. One of the approaches used in the application of the TS models based on Fickian dispersion involves the use of a set of constant parameters for each breakthrough curve within a selected stream reach. The difficulty with this approach is that since each breakthrough curve is treated separately by fitting the model to the observed data, the estimated dispersion coefficients contain errors associated with the non-Fickian behavior of the solute plume. This situation is further complicated due to the fact that other parameters in the TS model produce an effect that is essentially similar to the dispersion coefficient (e.g., changing the peak in the breakthrough curve). The result is a set of parameters that do not describe the observed data. Examples of situations in which the TS model produced physically unrealistic parameters are described in Fernald et al. [2001] and Phanikumar et al. [2007]. One of the objectives of this work is to propose an alternative method of describing dispersion using the concept of fractional-in-space diffusion in-order to describe the non-Gaussian rising-limb of the BTCs observed in field studies as well as better constraining the stream solute transport models. When the second order diffusion term is replaced with a fractional order term, the classical ADE becomes the fractional ADE (fADE). We use the term "fADE"with the understanding that only the dispersion term is described using a fractional-in-space derivative. In a similar way, when the Fickian diffusion term is replaced with a fractional diffusion term in the well-known TS model [Bencala and Walters, 1983], we get the fractional-in-space TS model which we refer to as the FSTS model in this work. More discussion about the fADE, FSTS and their mathematical properties as well as their numerical solution will follow in Chapters 3, 4 and 5. Fractional diffusion relies on the concept of fractional derivative operators which we discuss in the next section briefly.

## 1.1 Fractional Calculus and the Fractional Derivative

Fractional calculus has a long history, having been mentioned in a letter from Leibniz to L'Hospital in 1695 [Weilbeer, 2006]. In his letter Leibniz writes:

"You can see here sir, that one can express a term like $d^{\frac{1}{2}}\overline{xy}$ or $d^{1:2}\overline{xy}$ by an infinite series, even though it seems to be far from the geometry, which usually only considers the differences of positive integer exponents or the negatives with respect to sums, but not yet those, whose exponents are fractional. It is true that it is still to show that it is this series for $d^{1:2}x$ ; but not only this can be explained in a way. Because the ordinates $x$ are expresses in a geometric series, such that by choosing a constant $d\beta$ it follows that $dx = x d\beta$: $a$ ,or (if one chose $a$ as unit) $dx = x d\beta$ , meaning $ddx$ would be $x.\overline{d\beta}^2$, and $d^3x$ would be $= x.\overline{d\beta}^3$ etc. and $d^e x = x\overline{d\beta}^e$ . And thus the differential exponent has been changed by the exponents and by replacing $d\beta$ with $dx : x$, yielding $d^e x = \overline{dx : x}^e.x..$ Thus it follows that $d^{\frac{1}{2}}x$ will be equal to $x\sqrt[2]{dx : x}$. It seems like one day very useful consequences will be drawn from this paradox, since there are little paradoxes without usefulness."

Other leading mathematicians like Fourier, Bernoulli, Euler and Laplace were among the many who had dabbled with fractional calculus and the mathematical consequences of it [Nishimoto, 1991]. The fractional integral and derivative operators are an extension of definitions from integral values to real values, similar to fractional exponents from integral exponents. There exist numerous definitions of fractional derivatives including the definitions of Riemann-Liouville, Grünwald-Letkinov, Weyl, Caputo, Marchaud, Riesz, and Miller Ross [Kumar and Agrawal, 2006]. The most popular definitions in the world of fractional calculus are the Riemann-Liouville, Grünwald-Letnikov (GL) and the Caputo definitions. A number of textbooks have also been published over the past few decades in the field of fractional calculus which treats the subject in-depth [Miller and Ross, 1993; Oldham and Spanier, 1974; Podlubny, 1999].

One of the main differences between the integer-order derivatives and fractional-order derivatives is that while integer-order derivatives are local, fractional-order derivatives have a non-local behavior. Due to this fundamental difference, the fractional derivative at a point depends upon the characteristics of the entire function and not just the values in the vicinity of a point; hence a differintegral operator (function consisting of both

differential as well as integral operators) is used to define them [Ochoa-Tapia et al., 2007]. As the function is defined using an differintegral operator a lower limit and an upper limit is required to define the fractional derivative. The plot shows the comparison between fractional derivative and integer order derivative of a function $f(x) = x^2$ and $f(x) = x^3$. We present the formal definitions, various properties and numerical approximations to the fractional derivatives in Chapter 3

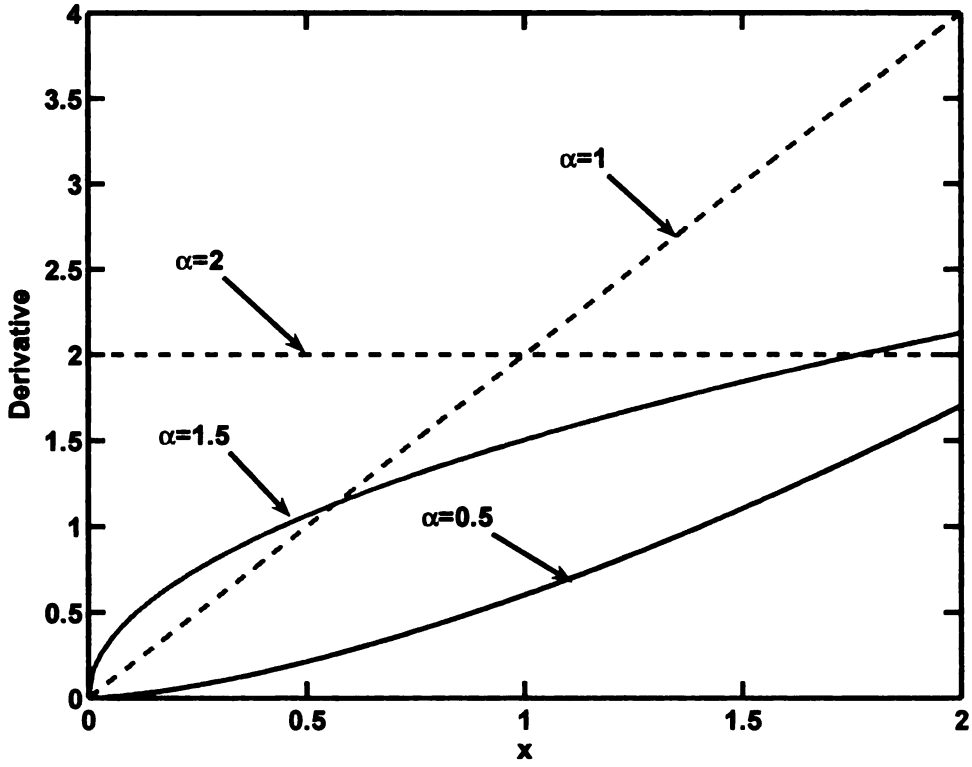


**Figure 1.2.** Comparison of integer and fractional derivative of $f(x) = x^2$

## 1.2 Numerical Methods

Closed-form solutions of the governing equations exist only for limited cases (i.e., boundary and initial conditions). For the TS model, such solutions are even rare and the few solutions that exist need to be evaluated numerically by evaluating infinite series and complex integrals. The computational time and effort required to evaluate complex analytical solutions is comparable to the time it takes to numerically solve the governing equations,

therefore numerical solution of the governing partial differential equations (PDEs) is the preferred approach in recent years, especially with the advent of high-speed processors and compilers that exploit the architecture of these processors. The main advantages of using numerical methods are that they are not limited to constant parameters or simple initial and boundary conditions common to analytical solutions. Additionally, they are computationally effective and easier to program and more effective when running parameter estimation models.

One can use any of the three approaches to solve the ADE numerically - Eulerian, Lagrangian, or mixed Eulerian-Lagrangian [Neuman, 1984] approaches. Similarly the fADE can be solved using the above three approaches but most of the work reported in the literature used an Eulerian approach [Schumer et al., 2001; Meerschaert and Tadjeran, 2004; Deng et al., 2004] or a mixed Eulerian-Lagrangian method. In the Eulerian approach, the advection and fractional diffusion terms are solved simultaneously by numerically approximating them individually. Since, we find many situations in surface as well as sub-surface flow are advection dominated; a finer finite difference mesh is required to minimize the errors and capture the advection front accurately. Since, hydrologic simulations are run for large time intervals, any reduction in grid size will translate into a significantly lesser computational time. By using a higher order scheme for solving the advection term better accuracy can be achieved using a larger grid size. In the literature, there are many higher order numerical schemes (e.g. compact, WENO, spectral methods) to solve the hyperbolic system of partial differential equation (e.g. advection ) as well as parabolic system of partial differential equation (e.g. diffusion) but these schemes have not been used for solving the fADE. Operator splitting methods in which the advection and dispersion terms are solved using separate numerical schemes (best suited for their class) are an attractive alternative but such methods have not been solved in the context of the fADE or the FSTS models. One of the objectives of this work is to fill this gap. We solve the advection and the fractional diffusion equations independently using Eulerian techniques and combine them using operator-splitting methods. We restrict our study to the usage of two higher order accurate advection schemes: a weighted essentially non-oscillatory (WENO)

scheme [Liu et al., 1994] and a fourth-order accurate compact scheme [Demuren et al., 2001] for solving the advection terms. The fractional diffusion term is solved using the Grünwald-Letnikov [Oldham and Spanier, 1974] and Caputo [Caputo and Mainardi, 1971] definitions. Although fractional calculus has a history that is as old as the calculus itself, numerical solution of fractional differential equations is a relatively new area of research. Some of the traditional approaches to handling boundary conditions and approximating derivatives are not directly applicable while dealing with fractional PDEs. For example, depending on the definition of the fractional derivative being used, the (fractional) derivative of a constant may not be equal to zero. This result has immediate consequences from the point of specifying boundary conditions to transport problems based on conservation laws. This means that certain definitions of the fractional derivative, although mathematically well defined, can not be used in describing solute transport in streams. Therefore a systematic evaluation of different definitions of the fractional derivative is important to understand the relative merits of various approximations. The main objectives of this study are as follows:

1. To use fractional-in-space dispersion in the TS model (i.e., the FSTS model) to describe the non-Gaussian rising-limb of the BTCs, in order to better constrain the stream solute transport model;

2. To evaluate operator-splitting approaches applied to the fADE and compare the performance of two higher order accurate advection schemes (WENO and compact);

3. To compare the numerical approximation of a fractional order dispersion term using the Caputo and the Grünwald -Letnikov definitions to model fractional diffusion;

4. To demonstrate that the new FSTS model can be used to describe field data by estimating the TS model parameters in two Michigan streams.

The next section gives the brief outline of the thesis.

## 1.3 Outline of thesis

In this thesis, we systematically analyze all the model equations (or sub-components) of the FSTS model: the hyperbolic advection equation, the parabolic fractional dispersion equation, the fADE and the fractional transient storage (FSTS) model . This approach allows us to examine the numerical approximations and the errors involved by comparing numerical solutions with analytical solutions for the respective sub-models.

In Chapter 2, a brief overview of the finite difference techniques to solve one-dimensional hyperbolic equations is discussed. A comparison of the WENO and fourth-order compact scheme is reported using a test case whose solution resembles the movement of a slug of tracer in a river. Our main objective here is to discuss the two advection schemes and identify the better method for solving the advection part of the fADE equation.

In Chapter 3, we discuss the two well known definitions of approximating the fractional derivative numerically: GL and Caputo. A higher order numerical approximation to the Caputo derivative will be discussed. Additionally, different forms of fractional diffusion equations will be discussed. A comparison of the GL and Caputo for the space-fractional diffusion equation will made with the analytical solution using method-of-manufactured solutions (MMS) approach.

In Chapter 4, we propose the new fADE model based on the operator-splitting (OS) approach to solve the fADE. The higher order numerical scheme for hyperbolic PDE (WENO and compact) discussed in Chapter 2 will be used for solving the advection term while the fractional derivative operators (Caputo and GL ) discussed in Chapter 3 will be used to solve fractional dispersion using OS method. A comparison of the the new numerical model will be made for describing the movement of a slug of tracer in a river.

In Chapter 5, we use the new numerical fADE model proposed in Chapter 4 for solving the solute transport using the fractional transient storage model (FSTS) and compare it with the analytical solution by De Smedt et al. [2005] for second-order diffusion case. We test our FSTS model by estimating various field parameters for the Red Cedar River and the Grand River.

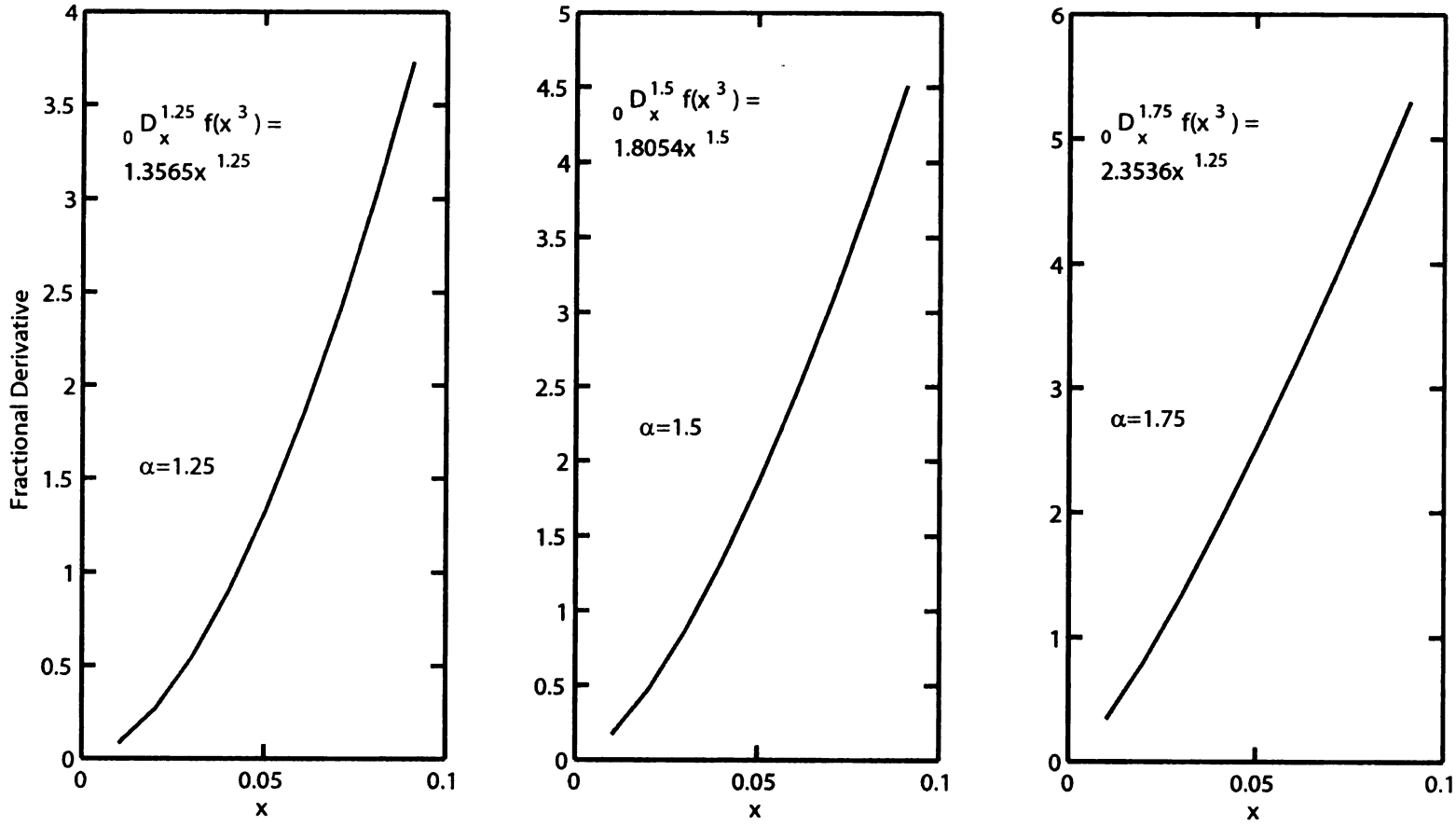


**Figure 1.3.** Fractional derivative for $f(x) = x^3$

# CHAPTER 2

# Advection Schemes

Advection and diffusion processes fall into hyperbolic and parabolic systems of partial differential equations respectively. The combination of these classes of equations is among the most widespread in all of science, engineering, finance and other fields where mathematical modeling is involved. Very often one of the processes is dominant, as is the case in surface and sub-surface contaminant transport where advection is dominant. Advection-dominated transport processes are characterized by sharp fronts which are often difficult to capture without using a higher order numerical method or fine grid resolution. Since numerical methods that work best for diffusion (parabolic class of PDEs) are not always well-suited for describing advection (hyperbolic class of PDEs), we take advantage of operator-splitting approaches to solve the fractional advection dispersion (fADE) equation by using different numerical schemes to describe the two processes. In what follows, we limit ourselves to one spatial dimension due to our interest in stream solute transport in the longitudinal direction. Extensions to multiple dimensions are generally straightforward and can be based on the concept of dimensional splitting [Khan and Liu, 1998; van der Houwen and Sommeijer, 1997].

The unsteady one-dimensional advection equation written in conservative form is given by:

$$\frac{\partial c}{\partial t} + u\frac{\partial c}{\partial x} = 0, \quad 0 < x < \infty,\ t > 0 \tag{2.1}$$

where $c$ denotes the concentration, $u$ the mean velocity, $x$ the distance and $t$ denotes time. The analytical solution to this problem is simply the advection of the profile given

by the initial condition without any attenuation in the peak. For a finite-difference numerical scheme to be useful for solving the above equation, it must satisfy certain requirements such as accuracy, stability, consistency, convergence and efficiency [Roache, 1998]. Lower-order schemes introduce significant smearing while describing sharp fronts due to excessive numerical diffusion. Numerical errors generally build up with time and contaminate the solution, particularly in situations where transport simulations must be run for large time durations. Since, numerical (or false) diffusion results from an error in the finite-difference approximation of its continuum counterpart (i.e., discarding the higher-order terms in a Taylor series expansion), grid refinement can be used to obtain accurate solutions using lower-order schemes. However, this is not an attractive option for describing field data since parameter estimation (which requires thousands of model runs if global search algorithms are used) is often an important component and lower-order schemes are unattractive as the computational effort involved can be prohibitive. Spectral, compact and essentially non-oscillatory (ENO) schemes are attractive classes of high resolution numerical methods that are known to have higher resolving power (points per wavelength or PPW) compared to lower-order schemes. Upwind and high-resolution schemes belong to an active area of research and a comprehensive review of all these methods is beyond the scope of this work. Hussaini et al. [1997] provides the background and a review of some of the earlier developments in this field. In this chapter we consider and evaluate two types of numerical methods in their ability to describe the hyperbolic advection process - a fifth-order accurate Weighted Essentially Non-Oscillatory (WENO) scheme [Shu, 1997] and a fourth-order accurate compact scheme [Demuren et al., 2001]. Although spectral methods are attractive in situations where the imposition of periodic boundary conditions does not pose a problem (e.g., in atmospheric science), they are generally less flexible in specifying boundary conditions for stream solute transport modeling; therefore these methods are not considered in this work. An important class of numerical methods for solving the advection equation includes the Lagrangian and semi-Lagrangian schemes [Wallis, 2007]. These methods are particularly attractive as they do not exhibit false numerical diffusion and their time-step is not limited by the Courant condition. The

Courant condition can be restrictive when spatial variations in velocity are encountered (e.g., groundwater). Solute transport equations for streams are often applied on a reach basis using a constant average velocity for each reach. Therefore, the Courant condition may not be very restrictive depending on the scheme used. Lagrangian advection schemes are therefore not considered in this work.

## 2.1 The Weighted Essentially Non-Oscillatory (WENO) Scheme

The weighted essentially non-oscillatory (WENO) finite difference schemes have become one of the most popular methods in solving equations based on hyperbolic conservation laws. These methods are often used in computational fluid dynamics (CFD) to simulate incompressible and subsonic compressible flows. The primary motivation for using these schemes has to do with their ability to reduce or eliminate spurious oscillations near discontinuities (Gibbs phenomenon). Traditional finite difference schemes (e.g., upwind and central schemes) are based on fixed stencil interpolation which works for globally smooth problems. For example, in a simple finite difference scheme information for cell $i$ is based on information at neighboring cells (e.g., ....$i-2$, $i-1$, $i$, $i+1$...). It is well established in literature that the oscillations encountered in using the fixed stencil approximations suffer from numerical instabilities in nonlinear problems containing discontinuities. The oscillations do not decay even when the finite difference mesh is refined. In order to remove these oscillations the essentially non-oscillatory scheme (ENO) was first proposed by Harten et al. [1987].

In the ENO scheme instead of using a fixed stencil for interpolating the concentration at cell $i$, a functional criterion based on the size of the Newton divided differences between the candidate stencils on the left ( e.g., $i-1$, $i-2$, ...) and right (e.g., $i+1$, $i+2$, ....) is used to determine the local stencil for interpolation. This technique is more robust compared to other functional criteria such as highest degree divided differences among all candidate stencils and picking the one with the least absolute values. Even though this approach is robust for a wide range of grid sizes, $\Delta x$, the scheme is usually of lower order accuracy, because all candidate stencils are not used in the final interpolations. In order to address

the problem of achieving higher order acuracy without any oscillations Liu et al. [1994] proposed a new scheme which uses all the candidate stencils by assigning specific weights to each of them. This class of schemes are called weighted essentially non-oscillating schemes (WENO) in which a convex combination of all candidate stencils is used instead of just one as in the original ENO. The WENO schemes thus achieve uniformly higher-order accuracy throughout the domain which is preserved for piecewise-smooth functions as well.

The WENO schemes have been extensively used, in particular to simulate shock turbulence interactions [Pirozzoli, 2002], relativistic hydrodynamics [Dolezal and Wong, 1995], gas dynamic problems [Serna and Marquina, 2004] as well as in image processing [Burgel et al., 2002; Fedkiw et al., 2003]. Most of the problems solved using WENO are of the type in which solutions contain both shocks and rich smooth-region structures [Cadiou and Tenaud, 2004; Sebastian and Shu, 2003; Tai et al., 2002]. In environmental engineering and the earth sciences, shocks can occur while describing the transport of conservative and reactive solutes in streams and ground water, sediment transport [Tsai et al., 2004], dam break situations, chemotaxis and bioremediation [Gallo and Manzini, 1998].

### 2.1.1 One-Dimensional Reconstruction

Consider the model equation for unsteady, one-dimensional advection in conservative form:

$$\frac{\partial c}{\partial t} + \frac{\partial (uc)}{\partial x} = 0 \tag{2.2}$$

In the above equation $uc$ represents the advective flux. Replacing the flux ($uc$ ) with the function $f(c)$ we get

$$\frac{\partial c}{\partial t} + \frac{\partial f(c)}{\partial x} = 0 \tag{2.3}$$

which is the one-dimensional conservation law [Costa and Don, 2007]. We discretize the space into uniform intervals of size $\Delta x$ and denote $x_i = i\Delta x$. Variables evaluated at the spatial location $x_i$ will be identified by the subscript $i$. The conservative finite difference

form of equation 2.2 can be written as:

$$\frac{\partial c}{\partial t} = -\frac{1}{\Delta x}\left(\hat{f}_{i+\frac{1}{2}} - \hat{f}_{i-\frac{1}{2}}\right) \tag{2.4}$$

where the numerical flux $\hat{f}_{i+\frac{1}{2}}$ is the average value of the flux over cell $i$. This is determined using WENO reconstruction. For a $(2k-1)^{\text{th}}$ order WENO scheme, we first compute $k$ numerical fluxes given by:

$$\hat{f}^r_{i+\frac{1}{2}} = \sum_{j=0}^{k-1} \hat{f}_{i-r+j} \quad r = 0, ..., k-1 \tag{2.5}$$

Since we are considering a fifth order scheme, $k = 3$ and the concentration in cell $i$ is given by:

$$\hat{f}_{i+\frac{1}{2}} = \hat{f}(c_{i-2}, \cdots, c_{i+2}) \tag{2.6}$$

where $\hat{f}()$ is determined using the WENO algorithm, which takes into account any shocks observed in neighboring cells using nonlinear weights. For the fifth order WENO scheme the numerical flux is estimated by using a convex combination of all the three numerical fluxes ($k = 3$) as shown below

$$\begin{aligned}\hat{f}_{i+\frac{1}{2}} = w_0^+\left(\tfrac{2}{6}f^+_{i-2} - \tfrac{7}{6}f^+_{i-1} + \tfrac{11}{6}f^+_i\right) + w_1^+\left(-\tfrac{1}{6}f^+_{i-1} + \tfrac{5}{6}f^+_i + \tfrac{2}{6}f^+_{i+1}\right) \\ + w_2^+\left(\tfrac{2}{6}f^+_i + \tfrac{5}{6}f^+_{i+1} - \tfrac{1}{6}f^+_{i+2}\right)\end{aligned} \tag{2.7}$$

where the nonlinear weights $w_k^+$ ($k$ = 0,1,2) are defined in the following way

$$w_0^+ = \frac{\alpha_0^+}{\alpha_0^+ + \alpha_1^+ + \alpha_2^+} \quad w_1^+ = \frac{\alpha_1^+}{\alpha_0^+ + \alpha_1^+ + \alpha_2^+} \quad w_2^+ = \frac{\alpha_2^+}{\alpha_0^+ + \alpha_1^+ + \alpha_2^+} \tag{2.8}$$

where

$$\alpha_0^+ = \tfrac{1}{10}\left(\frac{1}{\epsilon + IS_0^+}\right)^2 \alpha_1^+ = \tfrac{6}{10}\left(\frac{1}{\epsilon + IS_1^+}\right)^2 \alpha_2^+ = \tfrac{3}{10}\left(\frac{1}{\epsilon + IS_2^+}\right)^2 \tag{2.9}$$

Here the $IS_k$ ($k = 0, 1, 2$) are the so called "smoothness indicators" which measures the smoothness of the function $f(x)$ in the stencil and $\epsilon$ is a small constant used to avoid the denominator to become zero and is typically taken as $10^{-6}$. The smoothness indicators ($IS_k$) are given by:

$$\begin{aligned} IS_0^+ &= \tfrac{13}{12}\left(f_{i-2} - 2f_{i-1} + f_i\right)^2 + \tfrac{1}{4}\left(f_{i-2} - 4f_{i-1} + 3f_i\right)^2 \\ IS_1^+ &= \tfrac{13}{12}\left(f_{i-1} - 2f_i + f_{i+1}\right)^2 + \tfrac{1}{4}\left(f_{i-1} - f_{i+1}\right)^2 \\ IS_2^+ &= \tfrac{13}{12}\left(f_i - 2f_{i+1} + f_{i+2}\right)^2 + \tfrac{1}{4}\left(3f_i - 4f_{i+1} + f_{i+2}\right)^2 \end{aligned} \tag{2.10}$$

Similarly, $\hat{f}_{i-\frac{1}{2}}$ can be found by replacing $i$ with $i-1$. Substituting $\hat{f}_{i+\frac{1}{2}}$ and $\hat{f}_{i-\frac{1}{2}}$ in equation 2.3, we get an approximation to the derivative $(\partial c/\partial t)$. For stability, it is important that upwinding is used in constructing the flux. Therefore, in order to determine the direction of flow, the easiest and most inexpensive way is by determining the Roe speed [Shu, 1997] which is given by:

$$a_{i+\frac{1}{2}} = \frac{f_{i+1} - f_i}{c_{i+1} - c_i} \tag{2.11}$$

If $a_{i+\frac{1}{2}} \geq 0$ , the flow direction is from left to the right and we would use $f^-_{i+\frac{1}{2}}$ while for $a_{i+\frac{1}{2}} < 0$, the flow direction is from right to left and we would be using $f^-_{i+1/2}$. In the above discussion we estimated $f^+_{i+1/2}$. In a similar manner one can estimate $f^-_{i+1/2}$, which is similar to the above method with different weight coefficients [Shu, 1997].

So far, we have discussed only spatial discretization. In order to achieve higher order accuracy in time, a third order Total Variational Diminishing (TVD) Runge-Kutta method [Shu, 1997] was used. TVD-based time discretization is used since non-TVD based Runge-Kutta time discretizations can generate oscillations even for WENO-based spatial discretization [Gottlieb et al., 2006]. The following TVD Runge-Kutta algorithm was found to produce excellent results [Shu, 1997].

$$\begin{aligned} c^1 &= c^n + u\Delta t\left(-\frac{\partial f(c)^{(n)}}{\partial x}\right) \\ c^2 &= \tfrac{3}{4}c^n + \tfrac{1}{4}c^1 + u\Delta t\left(-\frac{\partial f(c)^{(1)}}{\partial x}\right) \\ c^{n+1} &= \tfrac{1}{3}c^n + \tfrac{2}{3}c^2 + \tfrac{2}{3}u\Delta t\left(-\frac{\partial f(c)^{(2)}}{\partial x}\right) \end{aligned} \tag{2.12}$$

The above algorithm is stable for a $CFL < 1/4$ [Gottlieb and Shu, 1997]. The scheme was found to be uniformly fifth order accurate including at smooth extrema [Jiang and Shu, 1996]. We considered a test case to examine the order of the above scheme with periodic boundary conditions by considering the following example in which a sine wave is advected in the positive x-direction with a constant speed.

$$\frac{\partial c}{\partial t} + u\frac{\partial c}{\partial x} = 0, \qquad -1 < x < 1 \tag{2.13}$$

$$u = 1, c(x,0) = \sin(\pi x) \tag{2.14}$$

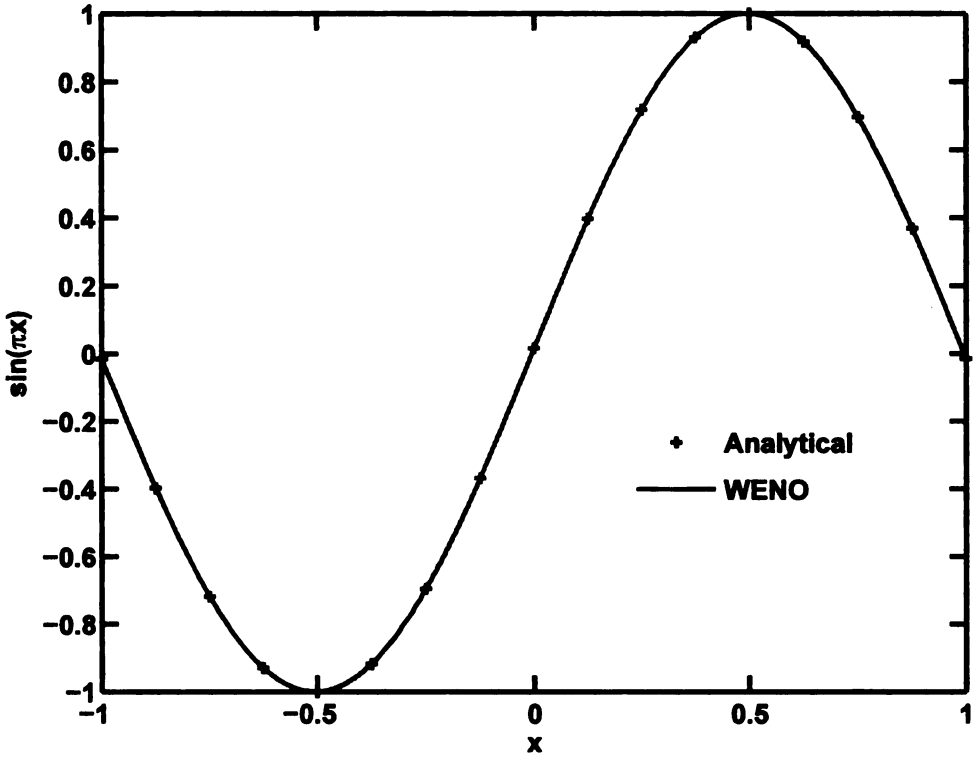


**Figure 2.1.** Comparison of fifth order WENO-Roe scheme with analytical solution for $\Delta x = 0.1$, $CFL = 0.1$ at $t = 1$

We found the order of the scheme using $L_\infty$ and $L_1$ error norms given by:

$$L_1 = \frac{2}{N} \sum \left( \left| C_{analy} - C_{num} \right| \right) \tag{2.15}$$

$$L_\infty = \max \left( \left| C_{analy} - C_{num} \right| \right) \tag{2.16}$$

where $N$ is the number of grid points and $C_{analy}$ and $C_{num}$ are the analytical and numerical solutions, respectively. The fifth order accuracy was achieved at about 40 grid points (Table 2.1) which is in agreement with the results of [Shu, 1997]. We therefore conclude that in order to achieve fifth-order accuracy for a WENO scheme, a minimum grid resolution is required. Based on our test case this requirement can be expressed as: $\Delta x \leq 0.0250$ for $u = 1$.

## 2.2 A Fourth-Order Compact Scheme with Spectral-Like Resolution

To produce $n^{\text{th}}$-order accuracy, most numerical schemes require a stencil of $(n+1)$ grid points. compact schemes, on the other hand, require fewer than $(n+1)$ points to achieve the same level of accuracy (hence the name compact). A well-known example involves the central difference approximation of the second derivative of a function. To achieve second-order accuracy (in space or time), the scheme uses information from three grid cells $i$, $i+1$ and $i-1$. Compact schemes are attractive as they can achieve higher-order accuracy using just two points. At least two other reasons make the compact schemes attractive - the two-point stencil is ideally suited for making computations on highly irregular or stretched grids (e.g., to resolve the structure of a turbulent boundary layer) and the schemes have exponential error convergence similar to the classical spectral methods. By contrast, the error convergence rate for the WENO schemes discussed above is linear, which limits their ability to achieve higher-order accuracy in large computational domains.

Compact schemes achieve higher-order accuracy by treating the derivative terms in the governing equation as unknown functions to be solved (in addition to the function itself). This means that for the advection equation, the concentration $c$ and its first derivative $c'$ will be solved at the end of every time step. A fourth-order compact scheme was introduced by Gupta, Manohar and Stephenson in the early 80's for solving the advection-diffusion equation (ADE). It has also been used to solve the Navier-Strokes equation [Li; Phanikumar, 1994] and Euler equations [Abarbanel and Kumar, 1988]. Lele [1992] found that implicit compact schemes have better fine-scale resolution, and yield better global accuracy than standard higher-order finite difference schemes. Here we briefly describe the algorithm used to solve equation 2.1 using a fourth-order implicit compact scheme. Additional details and examples applications to other areas (e.g., aero-acoustics) are available in [Demuren et al., 2001]. This scheme was also used to model solute transport in soil columns [Phanikumar and Hyndman, 2003]. The first derivative term appearing in equation 2.1 was obtained by solving the following tri-diagonal matrix system [Lele, 1992]:

$$\alpha_I c'_{i-1} + c'_i + \alpha_I c'_{i+1} = \frac{a_I}{2\Delta x}(c_{i+1} - c_{i-1}) \tag{2.17}$$

where $c_i' = \frac{\partial c}{\partial x_i}$, $\alpha_I = \frac{1}{3}$, and $a_I = \frac{14}{9}$.

The LHS of equation 2.17 contains the unknown derivatives at grid points $i$ and $i \pm 1$, while the $RHS$ contains the known function values (e.g. concentration) $c_i$ at the grid points $i \pm 1$ . In matrix form the system of equation 2.17 can be written as

$$\mathbf{A_x} c' = \mathbf{B_x} \tag{2.18}$$

where $\mathbf{A_x}$ is a tridiagonal $N_x \times N_x$ matrix ($N_x$ is the number of grid points), and $\mathbf{B_x}$ is a vector. The resulting tridiagonal system of equations was solved using Thomas algorithm [Press, 2002]. For nonperiodic boundaries, one sided finite difference approximations are required to close the system of equations at the boundary points: $i = 1$ and $i = N$. A third-order approximation was used at $i$ and $i = N$ given by [Demuren et al., 2001]

$$c_1' + 2c_2' = \frac{1}{\Delta x}\left(\frac{-5}{2}c_1 + 2c_2 + \frac{1}{2}c_3\right) \tag{2.19}$$

A similar approximation was used at $i = N$. Storage of variables could potentially become an issue while using the compact schemes. Therefore, we used a three-stage-third order Runge-Kutta scheme proposed by [Lowery and Reynolds, 1986] with low-storage requirements for temporal differencing. By low-storage we mean only two storage locations (one for time derivative and one for the variable itself) are required for time advancement, which is achieved by continuously overwriting the storage location for the time derivatives and unknown variables at each substage for $M = 1, 2$ and 3 as

$$\hat{H}_i^{(M)} = a^M \hat{H}_i^{M-1} \tag{2.20}$$

$$c_i^{(M+1)} = c_i^M + b^{M+1} u \Delta t \hat{H}_i^{(M)} \tag{2.21}$$

$$\hat{H}_i^{(M)} = \hat{H}_i^{(M)} - u\frac{\partial c}{\partial x_i}^{(M)} \tag{2.22}$$

where coefficients $a^M$ and $b^M$ are given in Table 2.1 and

$$\hat{H}_i^{(M-1)} = -u\frac{\partial c}{\partial x_i}^{(M-1)} \tag{2.23}$$

**Table 2.1.** Coefficients of a three-stage-third-order Runge-Kutta scheme, from Lowery and Reynolds (1986)

| M | $a^M$ | $b^M$ |
|---|---|---|
| 1 | 0 | 0.500 |
| 2 | -0.68301270 | 0.91068360 |
| 3 | -1.33333333 | 0.36602540 |

**Table 2.2.** Order of accuracy for the WENO-Roe and the compact schemes

| Method | $N$ | $L_\infty$ | $L_\infty order$ | $L_1$ | $L_1 order$ |
|---|---|---|---|---|---|
| | 5 | 0.311 | | 0.394 | |
| **WENO-Roe-Fifth-order** | 10 | 0.030 | 3.64 | 0.039 | 3.40 |
| | 20 | 1.438e-5 | 4.44 | 1.474e-5 | 4.36 |
| | 40 | 4.32e-5 | 5.07 | 4.62e-5 | 5.06 |
| | | | | | |
| | 5 | 0.285 | | 0.190 | |
| **Fourth-order compact** | 10 | 0.019 | 3.84 | 0.012 | 3.97 |
| | 20 | 1.30e-4 | 3.92 | 7.25e-4 | 4.06 |
| | 40 | 8.13e-5 | 4.00 | 4.44e-5 | 4.03 |

## 2.3 A Test Case: Advection of a Gaussian Pulse

To evaluate the performance of the two advection schemes and to assess the nature and magnitude of errors introduced by the schemes, we used a test case for which the solution is similar to the instantaneous release of a slug of tracer in an infinite domain. The slug will maintain the same initial profile (in our case Gaussian) for all times since dispersion is zero. The initial condition (which is also equal to the exact solution for all times) is given by:

$$c(x,0) = 0.5 \exp\left[-\left(\frac{x}{3}\right)^2 \ln(2)\right], \quad -20 \leq x \leq 450; \quad u = 1 \tag{2.24}$$

This solution will test the time-advancement of the initial profile using these schemes with the equation 2.1. Table 2.2 below summarizes the comparison of the results obtained using the WENO and the compact schemes. All the comparison were done at time $t = 5$. We used two criteria to determine which scheme will be preferred for solving the fADE equation. Since our interest was in running the models for large times (while describing field data), schemes that give stable results for the largest times step size $\Delta t$ with the least numerical dispersion will be preferred. Additionally, the domain sizes for simulations used in surface water modeling are typically large, therefore, schemes that give reasonably accurate solutions with a larger step size will be preferred because of the

lower computational time. The stability of the numerical schemes is determined using CFL (Courant-Friedrichs-Lewy) number defined by:

$$CFL = \frac{u\Delta t}{\Delta x} \tag{2.25}$$

For a scheme to be stable the general criterion is that $CFL \leq 1$. For an explicit scheme, if $CFL \geq 1$, the scheme will become unstable and will not converge.

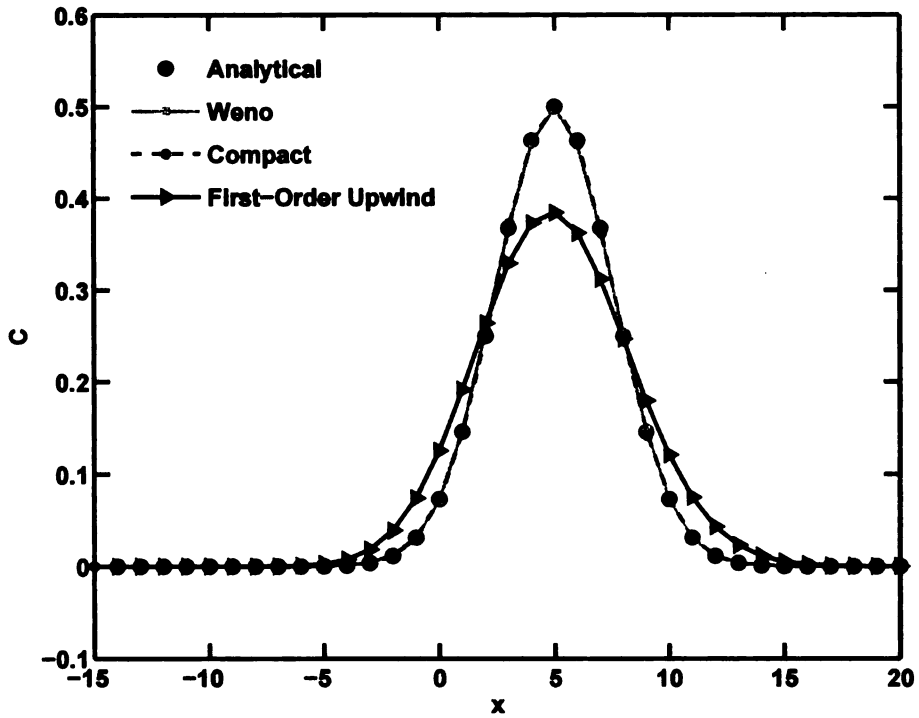


**Figure 2.2.** Comparison of the compact, WENO and first-order upwind scheme for $\Delta x = 1$, $u = 1$, $CFL = 0.1$ at $t = 5$

We initially used a crude grid size and found that for $CFL = 0.1$, both WENO and compact schemes perform reasonably well in describing the peak with the WENO scheme giving a lower Root Mean Squared Error (RMSE) (Figure 2.3). The first order upwind scheme introduced significant numerical dispersion and was not able to describe the peak accurately (Figure 2.3). Comparisons for a larger time using the same crude grid showed that while the compact scheme tends to produce oscillations, the WENO scheme introduces numerical dispersion. It is therefore, clear that a more refined grid size should be used for accurately describing the peak. In a second simulation using fine grids, we found

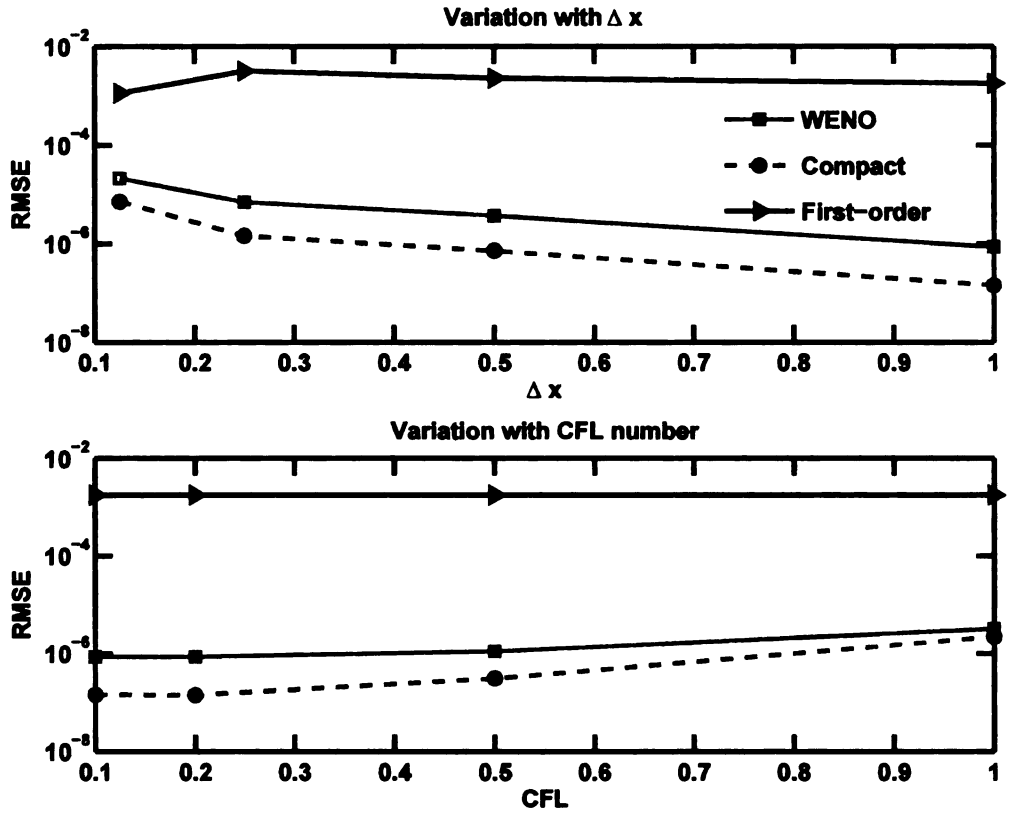


**Figure 2.3.** Plot showing that comparison of RMSE error (log-scale) for compact, WENO and first-order scheme for different CFL and $\Delta x$ values

that both compact and WENO schemes were able to describe the peak without any oscillations. As the grid size ($\Delta x$) decreased the compact scheme was found to give a lower RMSE error (see Figure 2.3) while as CFL number decreased both of them approached similar orders of RMSE error.

## 2.4 FFT Analysis of Advection Schemes

Numerical solutions of differential equations generally contain both dissipative (i.e., errors in the peak or amplitude) and dispersive (i.e., phase errors) errors even if the model equation is non-dispersive as is the case for the pure advection test case considered here. Numerical solutions can be compared and analyzed based on a number of metrics such as the truncation errors and rates of convergence of the schemes, as well as dispersive and dissipative behavior. It is often a challenge to select criteria that fairly evaluate different

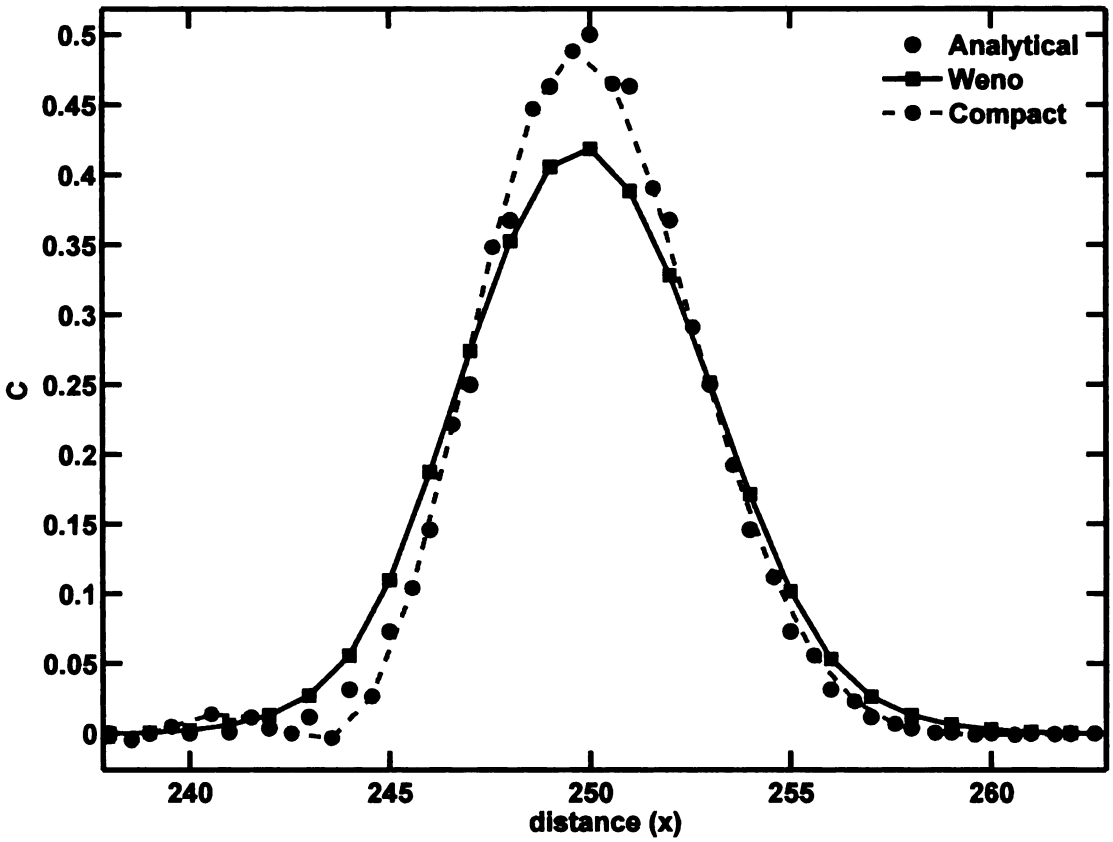


**Figure 2.4.** Plot showing that comparison of the compact and the WENO scheme for $\Delta x = 1$, $u = 1$, and $CFL = 0.1$ with the analytical solution at $t = 250$. WENO scheme disperses while compact scheme oscillates

classes of numerical methods. A general methodology which can be used to compare numerical solutions obtained from different schemes is a mathematical framework based on Fourier analysis since the method provides a great deal of information about the errors involved. Fourier analysis is most commonly used to find the frequency components buried in a noisy signal in the time domain (e.g., time series of discharge data at a gaging station). To analyze the resolution properties of the schemes, the concentration profiles as a function of distance at a given time can be transformed from the physical space to the wave number space and analyzed using FFT analysis. Results of the FFT analysis are shown in Figure 2.5. We noticed that the WENO scheme introduced significant numerical dissipation in addition to producing considerable phase errors at high wave numbers.

## 2.5 Conclusion

Based on the above results, we conclude that the compact scheme provides a superior description of advection and is therefore the preferred choice for solving the fADE since WENO scheme for large time simulations seems to disperse higher compared to the compact scheme. It is important to capture the peak accurately since it allows us to understand various effects of fractional dispersion. If numerical dispersion is introduced with an advection scheme, it will be difficult to understand whether the dispersion observed is due to numerical dispersion or due to fractional dispersion. Our results indicated that the compact scheme produced superior solutions without any oscillations as long as low CFL numbers were used to maintain stability.

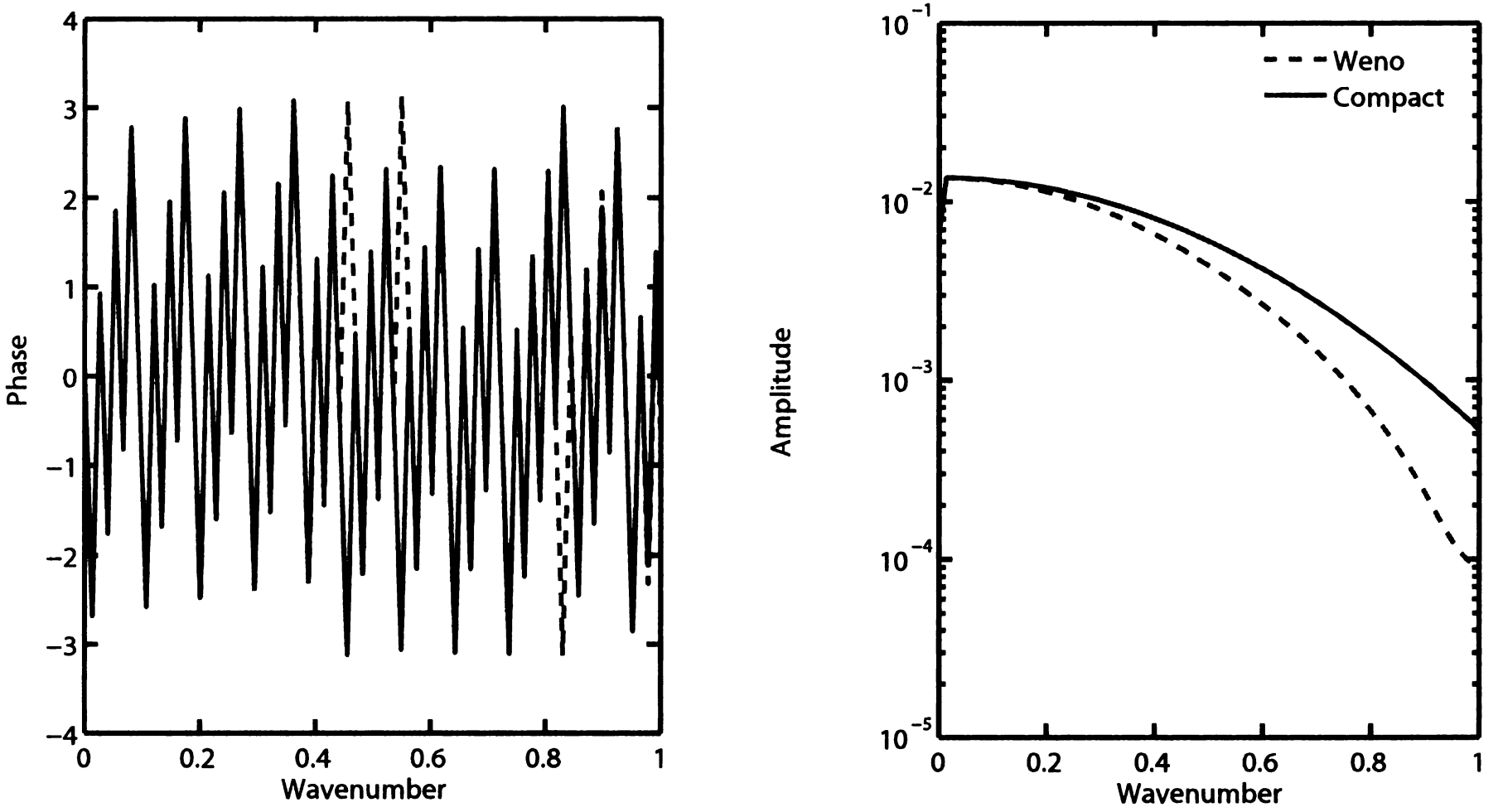


**Figure 2.5.** Plot showing that comparison of compact and WENO scheme for $\Delta x = 1$, $u = 1$, and $CFL = 0.1$ with the analytical solution at $t = 250$. Clearly the amplitude of the WENO scheme is lower compared to compact scheme for a crude grid size

# CHAPTER 3

# Fractional Diffusion: Preliminaries and Numerical Approximations

## 3.1 Introduction

Transport of solute particles in surface and subsurface water can be viewed as a purely probabilistic problem. The classical Fickian diffusion model is based on the assumption of Brownian motion. Brownian motion assumes that the particle's motion has no long-range spatial correlation i.e., long walks in the same direction are rare. But what happens to particles with long-range spatial correlation? One can answer the above question using fractional calculus and a class of probability density functions (PDFs) described using continuous time random walks (CTRW). Using CTRW, the diffusion process can be viewed as a result of random walk in space and time. In other words, a particle can undergo jumps of random size at random times. The random walk in time and space can be represented by the joint probability density function $P(x,t)$, which describes each particle "transition" over a distance, $x-x'$, in time $t-t'$, using the master equation given by [Montroll and Weiss, 1965].

$$P(x,t) = \underbrace{\delta(x)\int_{t}^{\infty}\psi(t')dt'}_{\substack{\text{Contribution from particles that} \\ \text{have not moved during } (0,\mathrm{t})}} + \int_{0}^{\mathrm{t}}\psi(t-t')\left[\int_{-\infty}^{\infty}\lambda(x-x')P(x'-t')dx'\right]dt' \qquad (3.1)$$

$$\text{Contribution from particles located at x and jumping to x}' \text{ during } (0,\mathrm{t})$$

This equation may be used to describe various kinds of diffusion equations, depending

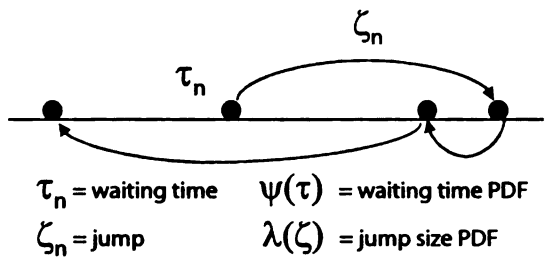


**Figure 3.1.** The random jump in space and time in a CTRW model

upon how the waiting time ($\tau_n$) and jump distributions ($\lambda(\zeta)$) are chosen. Fickian diffusion is the limiting case of CTRW. The assumptions being that the waiting times between the jumps ($\tau_n$) are exponentially distributed and the jump distances ( $\zeta_n$) are normally (Gaussian) distributed. But in case of anomalous diffusion, which is a more general case, the jump distributions are non-Gaussian with divergent moments to account for anomalously large particle movements also known as "Lévy flights". Similarly, the waiting times can have an arbitrary distribution instead of an exponential distribution for a second-order diffusion. An increasing number of processes are being described by anomalous diffusion where the random waiting times and jumps do not follow the Gaussian distribution. In these cases, the overall transport is better described by steps that are not independent (long range) and can have arbitrarily large waiting times.

## 3.2 Fractional-in-space Diffusion

Fractional-in-space diffusion is used to describe faster-than-Fickian growth rates, skewness and heavy leading limbs of BTCs in streams and heterogenous aquifers. The diffusive flux for fractional-in-space diffusion can either be based on a fractional Fickian flux [Zhang et al., 2007] or on a regular integer order flux (the well-known Ficks law) [Schumer et al., 2001].

In the first case, the diffusive flux is fractional order and non-local, and is given by [Yong et al., 2006].

$$\frac{\partial C}{\partial t} = \frac{\partial}{\partial x}\left[D(x)\frac{\partial^{\alpha-1}C}{\partial x^{\alpha-1}}\right] \tag{3.2}$$

While for the the second case, the integer order divergence in the above formulation was

replaced by a fractional analogue resulting in fractional-in-space diffusion given by:

$$\frac{\partial C}{\partial t} = \frac{\partial^{\alpha-1}}{\partial x^{\alpha-1}}\left[D(x)\frac{\partial C}{\partial x}\right] \tag{3.3}$$

Both equations 3.2 and 3.3 are equivalent for the case, when $D(x)$ is constant and independent of the spatial variable $x$ [Yong et al., 2006], reducing it to

$$\frac{\partial C}{\partial t} = D\frac{\partial^{\alpha} C}{\partial x^{\alpha}} \tag{3.4}$$

## 3.3 Fractional-in-time Derivative: Sub-Diffusion

Fractional-in-time derivatives are used to describe long waiting times between the random jumps, usually accompanied with travel times of particles longer than the expected classical Fickian diffusion, called sub-diffusion. For example, Haggerty et al. [2000] used fractal, or power law to describe a distribution of rates instead of using a single rate model. This can be thought to be as scaling in time, where the coefficients on the time operators need to be adjusted with time. A fractional-in-time derivative can be used to describe rate coefficients which are scale invariant in time. One classic example of a sub-diffusive process involves solute transport in a stream in which the exchange process is between the main channel and the storage zones. The storage zones trap the contaminant particles, hence the longer time, characterized by heavy falling limb in BTCs. In a stream transient storage (TS) models, this exchange process is usually described as a first-order mass transfer process, which can be viewed as a special case of the processes described by a fractional-in-time derivative. The governing equation for the sub-diffusion is given by Gorenflo et al. [2002].

$$\frac{\partial^{\beta} C}{\partial t^{\beta}} = D\frac{\partial^2 C}{\partial x^2} \quad \text{where} \quad 0 < \beta \leq 1 \tag{3.5}$$

Other variations of the fractional-in-time diffusion are as follows

$$\frac{\partial^{\alpha} C}{\partial t^{\alpha}} = \frac{\partial}{\partial x}\left(D\frac{\partial C}{\partial x}\right) \tag{3.6}$$

One form of the diffusion equation that is fractional in both space and time can be represented as

$$\frac{\partial^{\alpha'} C}{\partial t^{\alpha'}} = \frac{\partial^{\alpha-1}}{\partial x^{\alpha-1}}\left(D\frac{\partial C}{\partial x}\right) \tag{3.7}$$

where $\alpha$ and $\alpha'$ are fractional exponents in space and time, respectively.

Fractional diffusion relies on the concept of fractional derivative operators which we discuss in the next section. We limit our discussion to the definitions and theory relevant to this study. We introduce formal definitions of fractional derivatives and discuss the numerical methods to approximate them. Additionally, a comparison between the two well known definitions of fractional derivatives (Caputo and Grünwald-Letnikov) will be presented.

## 3.4 Fractional Derivative: Multiple Definitions

Although the integer derivatives of a function are mathematically well-defined with well-known physical and geometrical interpretations, the fractional derivatives are much less explored and understood. For example, it is well-known that there are no geometrical interpretations of a fractional derivative as of today [Podlubny, 1999]. While there are a number of areas in which physical interpretations of the fractional derivative are meaningful and useful, one has to come to terms with the fact that there are multiple definitions of the same fractional derivative. While some definitions are well-suited for certain types of applications, other definitions are not. Therefore, as mentioned in chapter 1, we consider (and evaluate) three main approaches to defining the fractional derivative: the Riemann-Liouville definition, the Grünwald-Letnikov (GL) definition and the Caputo definition. Here we introduce their formal definitions and in the next section we introduce numerical methods to approximate these derivatives. In order to understand the fractional derivative it is important to understand the concept of a fractional integral, both of which are closely related. This section summarizes some of the properties of the fractional order integral and differential operators relevant to our work. Additional details can be found in Podlubny [1999] and Oldham and Spanier [1974]. The traditional expression of repeated integration of a function for an integer order is given by:

$$ {}_aD_x^{-n} f(x) = \int_a^x dx_1 \int_a^{x_1} dx_2 \int_a^{x_2} dx_3 \ldots \int_a^{x_{n-1}} dx_n f(x_n) \tag{3.8} $$

The order of integration can be interchanged and equation 3.8 can be written as

$$ {}_aD_x^{-n} f(x) = \frac{1}{(n-1)!} \int_a^x (x-y)^{n-1} f(y) dy \tag{3.9} $$

To extend the above equation to non-integers, the integer is replaced with a real number and the factorial in the denominator is replaced with the more general gamma function $\Gamma()$, which is an extension of the factorial function to complex and real number arguments. The gamma function is defined as

$$ \Gamma(x) = \int_0^\infty e^{-t} t^{x-1} dt \tag{3.10} $$

and satisfies the following property

$$ \Gamma(n) = (n-1)! \tag{3.11} $$

Replacing the factorial with the more general gamma function, we get the Riemann-Liouville (RL) fractional integral defined as [Oldham and Spanier, 1974]

$$ {}_aD_x^{-\nu} f(x) = \frac{1}{\Gamma(\nu)!} \int_a^x (x-y)^{\nu-1} f(y) dy \tag{3.12} $$

Fractional derivative operators of order $\alpha$ act as an inverse of the fractional integral of order $\alpha$, i.e.,

$$ {}_aD_x^{\alpha} {}_aD_x^{-\alpha} f(x) = f(x) \tag{3.13} $$

$$ {}_aD_x^{\alpha} f(x) = \frac{d^N}{dx^N} \left[ {}_aD_x^{-\nu} f(x) \right] \quad \text{where} \quad \nu = N - \alpha \tag{3.14} $$

$$ {}_aD_x^{\alpha} f(x) = \frac{d^N}{dx^N} \left[ {}_aD_x^{-(N-\alpha)} f(x) \right] = \frac{d^{\alpha}}{dx^{\alpha}} f(x) \tag{3.15} $$

In a similar way, the RL derivative can be defined as [Samko et al., 1993]

$$ {}_0D_x^{\alpha} f(x) = \left\{ \begin{array}{ll} \frac{1}{\Gamma(n-\alpha)} \left(\frac{d}{dx}\right)^n \int_0^x \frac{f(u)}{(x-u)^{\alpha-n+1}} du & n-1 \leq \alpha < n \\ \\ \frac{d^n}{dx^n} f(x) & \alpha = n \end{array} \right\} \tag{3.16} $$

### 3.4.1 The Riemann-Liouville Derivative

Fractional derivative of a function $f$ at a point $x$ can be defined based entirely on information either on the left-hand side or the right-hand side of a spatial location in question (Figure 3.2). If the independent variable is time instead of space, then the left fractional derivative can be interpreted as an operation on the past states of the function ($f$) while the right derivative can be interpreted as an operation performed on the futures states of $f$ [Podlubny, 1999]. The left RL derivative at $x$ is defined as

$$ {}_aD_x^{\alpha} f(x) = \frac{1}{\Gamma(n-\alpha)} \frac{\partial^n}{\partial x^n} \int_a^x \frac{f(u)}{(x-u)^{\alpha-n+1}} du \tag{3.17} $$

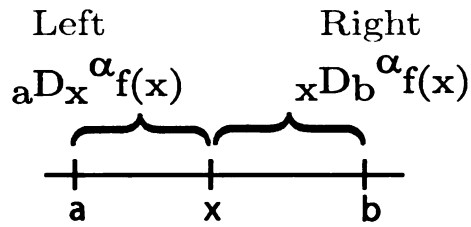


**Figure 3.2.** The left and right RL derivatives at a point $x$

while the right RL derivative at $x$ is defined as

$$ {}_xD_b^{\alpha} f(x) = \frac{(-1)^n}{\Gamma(n-\alpha)} \frac{\partial^n}{\partial x^n} \int_x^b \frac{f(u)}{(u-x)^{\alpha-n+1}} du \tag{3.18} $$

where $n-1 \leq \alpha \leq n$ and $\Gamma()$ is the gamma function. Although the RL derivative is a well-defined mathematical function, one can easily encounter problems when applying it to physical problems. In particular, the fact that the RL derivative of a constant is not zero can cause problems while specifying boundary conditions (e.g., continuous slug release of a tracer of a known constant concentration in a stream). For example, consider the fractional derivative of a constant $C$,

$$ {}_aD_x^{\alpha} C = \frac{C}{\Gamma(1-\alpha)(x-a)^{\alpha}} \tag{3.19} $$

where $1 \leq \alpha \leq 2$. As observed, the RL derivative is singular at the lower limit. This presents a problem when using the RL expression for estimating the derivative at the initial boundary since

$$ \lim_{x \to a} {}_aD_x^{\alpha} f(x) = \infty \tag{3.20} $$

$$f^k(a) = 0 \tag{3.21}$$

where $k = 0, 1, 2...n-1$ and $1 \leq \alpha \leq 2$ . Similarly, the Laplace transform of the RL derivative depends on the fractional derivative at zero, which introduces initial value problems (refer Podlubny [1999] for details). These drawbacks of the RL derivative operator can be resolved by using the Caputo definition of the fractional derivative.

### 3.4.2 The Caputo Derivative

As the RL derivative, Caputo derivative is also a *differintegral* expression but the operation of integral and derivative is interchanged in case of Caputo derivative. The Caputo derivative can be defined as Podlubny [1999]

$${}_a^C D_x^\alpha f(x) = \frac{1}{\Gamma(n-\alpha)} \left[ \int_a^x \frac{f^{(n)}(u)}{(x-u)^{\alpha-n+1}} du \right] \tag{3.22}$$

where $n-1 \leq \alpha \leq n$ and the superscript $C$ is used to distinguish the Caputo derivative from the regular RL derivative. One of the main differences between Caputo and RL definitions is that the initial value of the Caputo derivative is in terms of integer-order derivative in Caputo unlike in RL. For example, consider the case of $1 \leq \alpha \leq 2$ commonly encountered in describing the transport of solutes, for which the Caputo derivative is defined as

$${}_a^C D_x^\alpha f(x) = \frac{1}{\Gamma(2-\alpha)} \left[ \int_a^x \frac{f''(u)}{(x-u)^{\alpha-2+1}} du \right] \tag{3.23}$$

The Riemann-Liouville fractional derivative requires initial conditions expressed in terms of initial values of fractional derivatives of the unknown function [Podlubny, 1999; Samko et al., 1993] while the Caputo derivative, in comparison, requires that the initial condition are expressed in terms of initial values of integer order derivatives. Therefore, Caputo derivative can be used in physical problem where one can interpret the integer-order initial values whereas in case of RL derivative the fractional initial value is difficult to interpret and not known easily. This can be avoided by treating only the cases of zero initial conditions. However, for zero initial conditions the Riemann-Liouville and Caputo fractional derivatives coincide [Podlubny, 1999].

From the above definitions of non-integer fractional derivatives, it is apparent that these derivative are non-local operators and these derivatives find important applications in various fields. A fractional derivative at a certain point in space or time contains information about the function at earlier points in space or time, respectively. Thus, fractional derivatives possess a memory effect, which they share with several materials like viscoelastic materials and polymers and this property is also important to applications in hydrology such as anomalous diffusion.

## 3.5 Numerical Approximations: The GL and Caputo Derivatives

In this section we discuss the finite difference approximations to a fractional derivative using the Grünwald-Letnikov and Caputo derivative operators. The GL based fractional derivative operator is a fractional formulation using backward difference for any arbitrary function $f(x)$, although the convergence of the infinite sum cannot be ensured for all functions. There exists a link between the Riemann-Liouville and GL approaches to fractional derivative operators and the exact equivalence between the two approaches has been shown in Podlubny [1999]. The GL approximation to the fractional derivative is given by

$$ {}_aD_x^\alpha f(x) = \lim_{N\to\infty} \frac{1}{\Delta x^\alpha \Gamma(-\alpha)} \sum_{j=0}^{N} \frac{\Gamma(j-\alpha)}{\Gamma(j+1)} f(x-jh) \tag{3.24} $$

where $N = (x-a)/\Delta x$ and is a positive integer . The above equation can be simplified to the following sum of series given by:

$$ {}_aD_x^\alpha f(x) = \sum_{j=0}^{N} w_j f(x-jh) \tag{3.25} $$

where the weights $w_j$ are defined as

$$ w_j = \left(1 - \frac{\alpha+1}{j}\right) w_{j-1} \tag{3.26} $$

The right sided GL fractional derivative can similarly be defined as

$$ {}_xD_b^\alpha f(x) = \lim_{N\to\infty} \frac{1}{\Delta x^\alpha \Gamma(-\alpha)} \sum_{j=0}^{N} \frac{\Gamma(j-\alpha)}{\Gamma(j+1)} f(x+jh) $$

### 3.5.1 The Caputo Derivative

The Caputo derivative can be approximated for the fractional diffusion equation using finite volume method. The scheme described below was adapted from Zhang et al. [2006] who used this method for solving the fractional advection dispersion equation (fADE). We use essentially the same approach but we only consider the fractional diffusion equation. The transport domain $[0, L]$ is divided into $N$ equal elements of size $\Delta x$. Using the mass-balance equation based on the diffusive flux during time period $\Delta t$ the fractional diffusion equation can be written as

$$\frac{C_i^{t+\Delta t} - C_i^t}{\Delta t} = Q_{i-1/2}^{t+\Delta t/2} - Q_{i+1/2}^{t+\Delta t/2} \tag{3.27}$$

where the subscripts $i \pm 1$ and $i \pm 1/2$ represent locations $x_{i\pm1}$ and $x_{i\pm1/2}$, respectively as show in Figure 3.3. The two fractional diffusive fluxes are estimated using the Caputo derivative given by:

$$Q_{i-1/2} = \frac{-D}{\Gamma(2-\alpha)} \left( \int_0^{x_{i-1/2}} \frac{1}{(x_{i-1/2} - y)^{\alpha-1}} \frac{\partial C}{\partial y} dy \right) \tag{3.28}$$

$$Q_{i+1/2} = \frac{-D}{\Gamma(2-\alpha)} \left( \int_0^{x_{i+1/2}} \frac{1}{(x_{i+1/2} - y)^{\alpha-1}} \frac{\partial C}{\partial y} dy \right) \tag{3.29}$$

which can be simplified and written in finite difference form as follows. Further details are provided in Appendix A.

$$Q_{i-1/2} = \frac{D}{\Gamma(2-\alpha)\Delta x^\alpha} \left[ \sum_{j=1}^{i-1} w_j (C_{i-j}^t - C_{i-j-1}^t) \right] \tag{3.30}$$

$$Q_{i+1/2} = \frac{D}{\Gamma(2-\alpha)\Delta x^\alpha} \left[ \sum_{j=1}^{i} w_j (C_{i+1-j}^t - C_{i-j}^t) \right] \tag{3.31}$$

The above value of diffusive flux can be substituted back in equation 3.27 to get the final form of the discretized fractional diffusion equation as

$$\frac{C_i^{t+\Delta t} - C_i^t}{\Delta t} = \frac{D}{\Gamma(2-\alpha)\Delta x^\alpha} \left\{ \begin{array}{l} \left( C_{i-1}^{t+\Delta t} - 2C_i^{t+\Delta t} + C_{i+1}^{t+\Delta t} \right) \\ + \sum_{j=1}^{i} w_j (C_{i+1-j}^t - C_{i-j}^t) \\ + \sum_{j=1}^{i-1} w_j (C_{i-j}^t - C_{i-j-1}^t) \end{array} \right\} \tag{3.32}$$

where

$$w_j = (j+1)^{2-\alpha} - (j)^{2-\alpha} \tag{3.33}$$

The above equation is solved using a semi-implicit approach described by Lynch et al. [2003], where the Gaussian terms ($i-1$, $i$ and, $i+1$) are solved implicitly while the "tail" terms ($i-2, i-3....1, 0$) are solved explicitly. The above equation reduces to the classical Fickian diffusion for $\alpha = 2$.

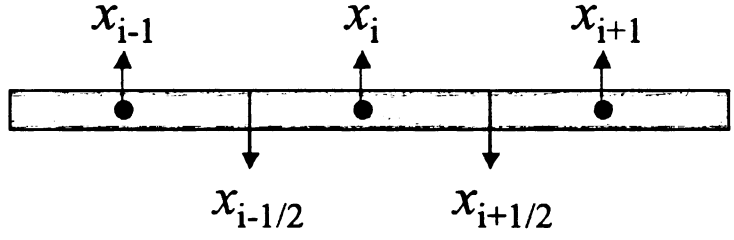


**Figure 3.3.** Control volume approximation to the Caputo fractional derivative

## 3.6 Higher Order Approximations

Most numerical solutions of differential equations involving fractional derivatives are first order accurate (either in time or space or both depending on which of the derivatives is being approximated). This is true for both the GL as well as the Caputo definitions. Higher-order accurate approximations are attractive when solutions need to be obtained with minimum computational effort, especially when parameters are being estimated. In order to implement higher order finite difference approximations we need to approximate the weights in GL or Caputo to a higher order. Podlubny [1999] showed that the weights $w_k^{(\alpha)}$ can be obtained as the coefficients of the power series expansion of a generating function $\omega$. The generating function $\omega_1(z)$ generates the coefficients for the first order derivative to first order approximation while its $\alpha$-th power, given by the function $\omega_1^{\alpha}$ generates the coefficients for the first order approximation of the $\alpha$-th fractional derivative. Here $z$ denotes a complex number. Once the generating function is selected, the weights can be obtained by evaluating the Fourier integral of the generating function. For example, the weights for the first order formulas presented in the previous sections can be obtained using the generating function for the $\alpha$-th derivative (to first order approximating) using

the function $\omega_1(z) = (1-z)^\alpha$:

$$(1-z)^\alpha = \sum_{k=0}^{\infty} (-1)^k \frac{\Gamma(\alpha+1)}{\Gamma(\alpha-k+1)} z^k = \sum_{k=0}^{\infty} w_k^{(\alpha)} z^k \tag{3.34}$$

Substituting $z = e^{-i\varphi}$ we have

$$(1-e^{-i\varphi})^\alpha = \sum_{k=0}^{\infty} w_k^{(\alpha)} e^{-ik\varphi} \tag{3.35}$$

and the coefficients $w_k^{(\alpha)}$ can be obtained from the relation:

$$w_k^{(\alpha)} = \frac{1}{2\pi i} \int_0^{2\pi} f_\alpha(\varphi) e^{ik\varphi} d\varphi, \qquad f_\alpha(\varphi) = (1-e^{-i\varphi})^\alpha \tag{3.36}$$

The coefficients $w_k^{(\alpha)}$ can be computed using the fast Fourier transform. In order to compute higher order approximations to the fractional derivative instead of using$(1-z)^\alpha$ as a generating function, one needs to use higher order generating functions. Lubich [1986] obtained higher order approximations of order 2, 3, 4, 5 and 6 for the GL fractional derivative using the following generating functions. These are plotted as a function of the complex number $z$ in Figure 3.6

$$\omega_2^{(\alpha)}(z) = \left(\frac{3}{2} - 2z + \frac{1}{2}z^2\right)^\alpha \tag{3.37}$$

$$\omega_3^{(\alpha)}(z) = \left(\frac{11}{6} - 3z + \frac{3}{2}z^2 - \frac{1}{3}z^2\right)^\alpha \tag{3.38}$$

$$\omega_4^{(\alpha)}(z) = \left(\frac{25}{12} - 4z + 3z^2 - \frac{4}{3}z^3 + \frac{1}{4}z^4\right)^\alpha \tag{3.39}$$

$$\omega_5^{(\alpha)}(z) = \left(\frac{137}{60} - 5z + 5z^2 - \frac{10}{3}z^3 + \frac{5}{4}z^4 - \frac{1}{5}z^5\right)^\alpha \tag{3.40}$$

$$\omega_6^{(\alpha)}(z) = \left(\frac{147}{60} - 6z + \frac{15}{2}z^2 - \frac{20}{3}z^3 + \frac{15}{4}z^4 - \frac{6}{5}z^5 + \frac{1}{6}z^6\right)^\alpha \tag{3.41}$$

While the approach described above is mathematically elegant and requires that the weights be computed only once, we describe another approach to obtain a higher order approximations to the fractional derivative. The method is based on directly integrating a higher order accurate integer derivative (based on the Caputo definition). This approach is attractive for simulating advection dispersion problems since the advection term (first derivative) is already computed to higher order accuracy using a compact scheme

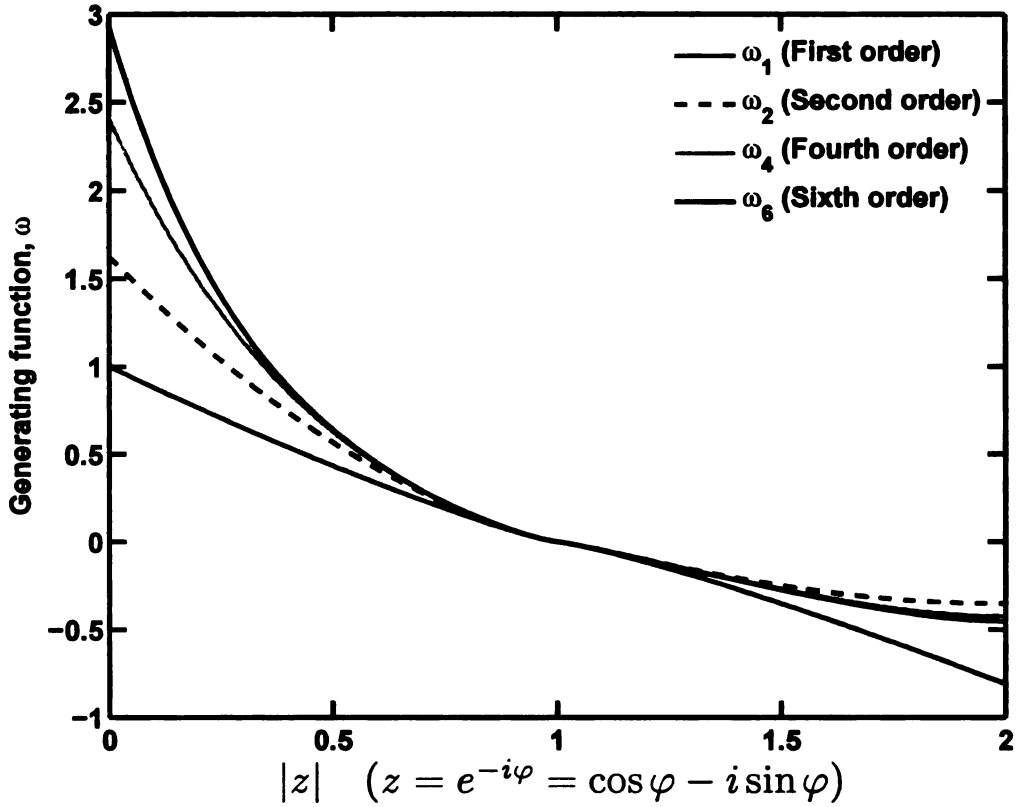


**Figure 3.4.** Higher-order approximations: The generating function $\omega$ as a function of $z$

### 3.6.1 Higher Order Caputo Fractional Derivative Using Integer Derivatives

In order to approximate the Caputo derivative to a higher order, two steps are involved. In the first step an integer order derivative inside the integral is computed to a higher order. In the second step, the integral is computed to a higher order approximation. Several methods exists to approximate the definite integral using finite difference approaches including Simpson's rule, Trapezoidal rule, Gaussian quadrature etc. Here, we use the modified form of trapezoidal rule described by Odibat [2006] to approximate the integral in the Caputo derivative. The advantage of using this method is that the numerical approximation is second order accurate and is computationally easy to implement, since it uses a weighted sum of the function and its integer order derivatives at specified points. Since the points at which the integer order derivatives are estimated are fixed, we can easily approximate the derivative using any higher order numerical approximation. The overall order of the fractional derivative is governed by the lowest order between the

definite integral approximation and integer order derivative.

The algorithm to approximate the Caputo fractional derivative of arbitrary order $\alpha > 0$ for a given function using the trapezoidal numerical approximation is as follows. Consider a function $f(x)$ between interval $[0, a]$ divided into $k$ subintervals $\left[x_j, x_{j+1}\right]$ of equal width $h = \frac{a}{k}$ by using the nodes $x_j = jh$ for $j = 0, 1, 2, 3, ...., k$. The Caputo fractional derivative is given by [Odibat, 2006]

$$
{}_0^C D_x^\alpha f(x) = \frac{h^{n-\alpha}}{\Gamma(n+2-\alpha)} \left\{ \begin{array}{l} \left[(k-1)^{n-\alpha+1} - (k-n+\alpha-1)k^{n-\alpha}\right] f^n(0) \\ +f^n(a) \\ +\sum_{j=1}^{k-1} \left[ \begin{array}{l} (k-j+1)^{n-\alpha+1} \\ -2(k-j)^{n-\alpha+1} \\ +(k-j-1)^{n-\alpha+1} \end{array} \right] f^n(x_j) \end{array} \right\} \tag{3.42}
$$

where $n-1 < \alpha < n$. The integer order derivatives ($f^n$) in the above expression can be approximated using any regular finite difference numerical approximation. We used the fourth order compact scheme discussed in Chapter 2 to approximate the first derivative ( for $0 < \alpha \leq 1$) and second derivative (for $1 < \alpha \leq 2$).

### 3.6.2 A Test Example

We tested the new numerical method by taking the $\alpha$-th fractional derivative ($\alpha = 0.5$) for the test function $f(x) = \sin(x)$. Using the new numerical method discussed above, we estimated the first derivative of the function $f(x) = \sin(x)$ using the fourth-order compact scheme at all the finite difference mesh points between $0 \leq x \leq 1$. The analytical solution to the fractional derivative of $f(x) = \sin(x)$ is given by [Odibat, 2006]

$$
{}_0^C D_x^\alpha \sin x = x^{1-\alpha} \sum_{i=0}^{\infty} \frac{(-1)^i x^{2i}}{\Gamma(2i+2-\alpha)} \quad \text{for} \quad 0 < \alpha < 1 \tag{3.43}
$$

$$
{}_0^C D_x^\alpha \sin x = x^{2-\alpha} \sum_{i=0}^{\infty} \frac{(-1)^{i+1} x^{2i+1}}{\Gamma(2i+4-\alpha)} \quad \text{for} \quad 1 < \alpha < 2 \tag{3.44}
$$

The order of the scheme was estimated systematically using various grid sizes ($\Delta x$) by computing the errors ($\epsilon$) relative to the analytical solution. The order of the scheme was estimated by fitting a power-law equation of the form $y = a\Delta x^b$ in a $\Delta x$ vs $\epsilon$ plot shown in Figure 3.5. The values for $a$ and $b$ comparison for the GL and H-Caputo (higher order

Caputo) derivative is illustrated in Table 3.1. We find from the table that the new higher order scheme based on the Caputo definition gives a second order accurate approximation to the fractional derivative.

**Table 3.1.** Table showing the order of numerical approximation for Grünwald-Letnikov and h-Caputo derivative operators

| | $f(x) = ax^b$ | | 95% Confidence Interval | |
|---|---|---|---|---|
| Model | $a$ | $b$ | $a$ | $b$ |
| GL | 0.135 | 0.998 | 0.131 - 0.139 | 0.987 - 1.009 |
| Caputo | 0.06 | 2.021 | 0.045 - 0.074 | 1.915 - 2.127 |

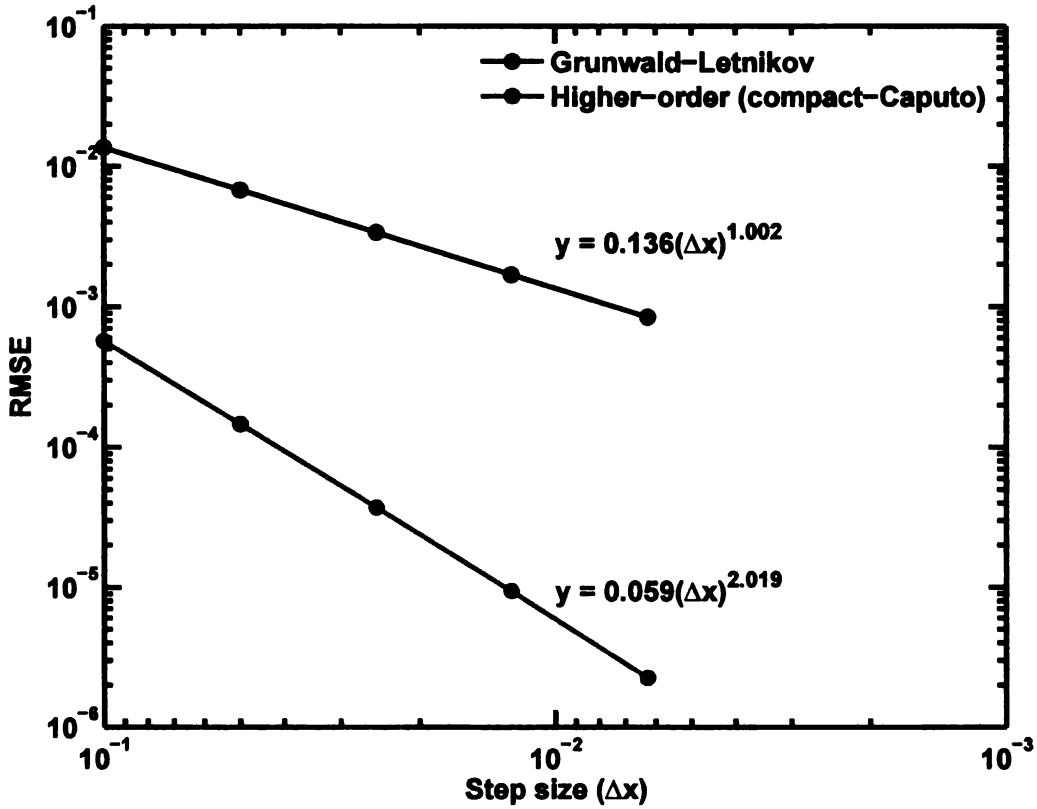


**Figure 3.5.** Comparison of RMSE error (log scale) for the fractional derivative with the analytical solution between GL and H-Caputo derivative (higher order Caputo)

## 3.7 An Exact Solution: The Method of Manufactured Solutions

The method of manufactured solutions [Roache, 1998] is a technique which can be used for verifying the numerical algorithm in situations where analytical solutions do not exist.

There are various instances where either the PDE does not have any closed-form solution or the closed-form solution is limited to specific initial and boundary conditions. For example, if a new finite difference numerical scheme is developed for a PDE, which has no analytical solution, then it is difficult to access the accuracy of the new scheme. The MMS is a useful approach in such cases. The idea of the MMS is that one can proceed by assuming a solution and substituting it back in the PDE for which we require the analytical solution. Since the assumed solution is not the exact solution for the PDE, we find the remainder by substituting the assumed solution in the PDE and subtracting that reminder from the the original PDE. The assumed (or "manufactured") solution will then satisfy the modified PDE (original PDE minus the remainder). The details of the above approach will be demonstrated with an example for comparing the Caputo and GL based fractional-in-space diffusion equation. We used the MMS approach because the analytical solutions to the fractional-in-space diffusion equation given below are limited to specific initial and boundary conditions.

$$\frac{\partial C}{\partial t} = D\frac{\partial^{\alpha} C}{\partial x^{\alpha}} \tag{3.45}$$

For comparing the numerical solution with the analytical solution, we chose a function whose fractional derivative was easy to estimate and could be used to estimate the analytical solution easily of equation 3.45 using the MMS approach. A zero initial conditions was chosen for solving equation 3.45, in order to make a fair comparison between the Caputo and GL derivatives, since both derivatives become equal for zero initial condition. We chose the function $f(x,t) = e^{-t}x^3$ where $t$ represent time and $x$ the spatial location. The fractional derivative of the function $f(x,t)$ with respect to $x$ is given by:

$$\frac{\partial^{\alpha} f}{\partial x^{\alpha}} = e^{-t}\left(\frac{\Gamma(4)}{\Gamma(4-\alpha)}x^{3-\alpha}\right) \tag{3.46}$$

Substituting the above value in equation 3.45 we get

$$\frac{\partial f}{\partial t} = De^{-t}\left(\frac{\Gamma(4)}{\Gamma(4-\alpha)}x^{3-\alpha}\right) \tag{3.47}$$

Clearly, $f(x,t)$ is not the solution for the above equation since the $LHS$ $(-te^{-t}x^3)$ is not equal to $RHS$ $(De^{-t}\left(\frac{\Gamma(4)}{\Gamma(4-\alpha)}x^{3-\alpha}\right))$. We modify the existing equation so that $f(x,t)$ is the solution to the fractional diffusion equation. Therefore, we estimate the remainder

$R$, and substitute back to the $RHS$ side of equation 3.45 so that $f(x,t)$ will satisfy the fractional diffusion equation.

$$R = e^{-t}\left(-x^3 - \frac{D\Gamma(4)}{\Gamma(4-\alpha)}x^{3-\alpha}\right) \tag{3.48}$$

Adding $R$ to $RHS$ of equation 3.45 we get

$$\frac{\partial f}{\partial t} = D\frac{\partial^\alpha f}{\partial x^\alpha} + e^{-t}\left(-x^3 - \frac{D\Gamma(4)}{\Gamma(4-\alpha)}x^{3-\alpha}\right) \tag{3.49}$$

whose closed-form solution is now $f(x,t) = e^{-t}x^3$. We use a finite domain size ($0 \leq x \leq 1$) and vary $\alpha$ ($1 \leq \alpha \leq 2$) to compare the GL and Caputo based approaches for solving the fractional-in-space diffusion equation. The initial and boundary condition used were:

**Initial Condition:**

$$f(x,0) = x^3 \quad 0 \leq x \leq 1 \tag{3.50}$$

**Boundary Conditions:**

$$\left.\begin{array}{l} f(0,t) = 0 \\ f(1,t) = e^{-t} \end{array}\right\} \quad \text{for all other time} \quad t \tag{3.51}$$

In order to find which of the schemes gave better results, we ran simulations for different grid sizes ($\Delta x$), dispersion coefficients ($D$), and fractional exponents ($\alpha$). The plot (Figure 3.6 and 3.7) below shows the comparison of RMSE error between the GL and Caputo fractional derivative operators for different grid sizes of $\Delta x = 0.1$ and $\Delta x = 0.01$. We observe that for a larger step size the Caputo derivative produced greater error compared to the GL derivative, and vice-versa. In order to understand the difference in behavior due to the grid size, we compared the weights of both Caputo and GL derivatives. We tried to use this approach, since fractional derivatives contains information of earlier spatial locations and assigns weights to each of them.

The weights of the GL are based on the modified GL definition given by Deng et al. [2004] where the fractional derivative of the function $C(x)$ is given by:

$$\frac{\partial^\alpha C}{\partial x^\alpha} \approx \frac{1}{\Delta x^\alpha}\sum_{j=0}^{N+1} w_j^\alpha C_{N+1-j}^t \tag{3.52}$$

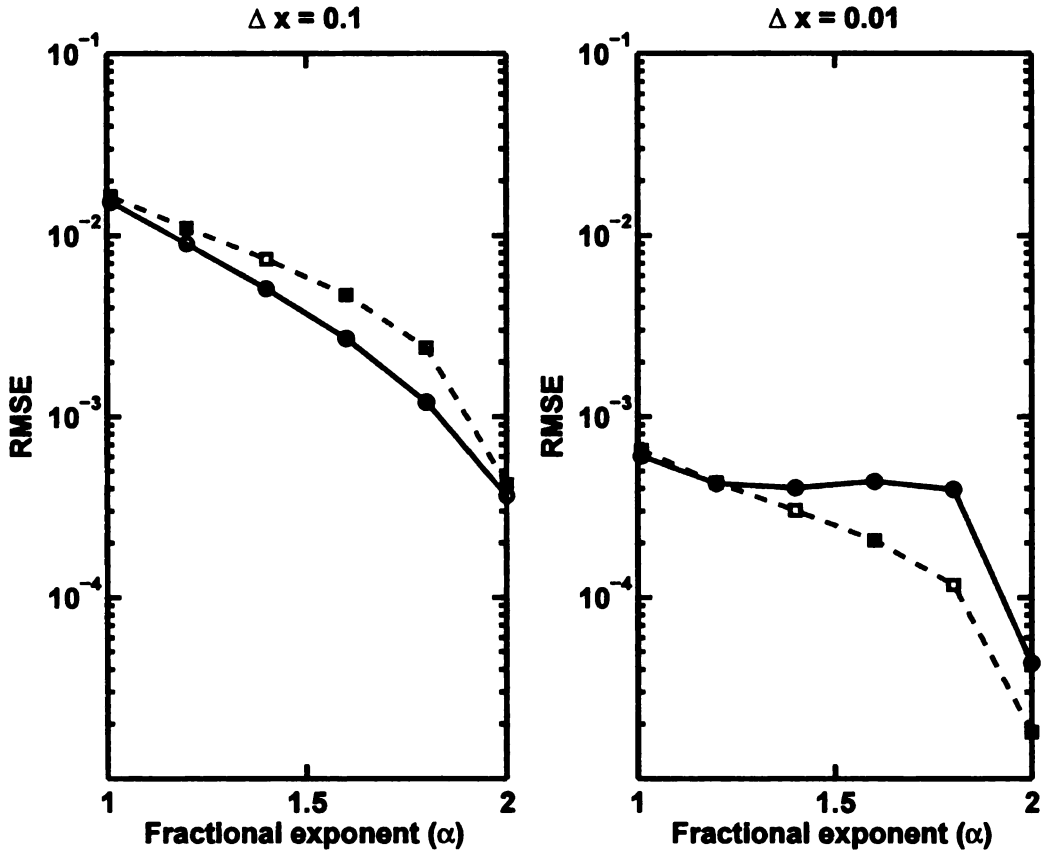


**Figure 3.6.** Plot showing the variation of RMSE (log scale) with fractional derivative exponents ($\alpha$) for two grid sizes $\Delta x = 0.1$ and $\Delta x = 0.01$ with $D = 1$ at time, $t = 1$

The concentration at location $i$ can be thought to be as a function of concentrations at other locations given by:

$$C_i = f\left[\sum_{j=0}^{N} w_j C_{i+1-j}\right] \tag{3.53}$$

where

$$w_j = \left(1 - \frac{\alpha - 1}{i}\right) w_{j-1}, \quad \mathrm{w}_0 = 1, \quad j = 1, 2, 3... \tag{3.54}$$

For a GL derivative the value of the function at a spatial location $i$ is dependent on the function value at spatial locations $i+1, i, i-1, i-2, .....0$. The coefficients decrease rapidly when $j \geq 3$ for all values of $\alpha$. Similarly, for the Caputo derivative defined using the finite volume approach given by equation 3.27, one can collect the terms and using algebraic manipulation (See Appendix C for details) arrive at the following:

$$C_i = f\left[w_0^c C_{i+1} + (-2w_0^c + w_1^c)C_i + \sum_{j=0}^{N} (w_j^c - 2w_{j+1}^c + w_{j+2}^c)C_{i-j-1}\right] \tag{3.55}$$

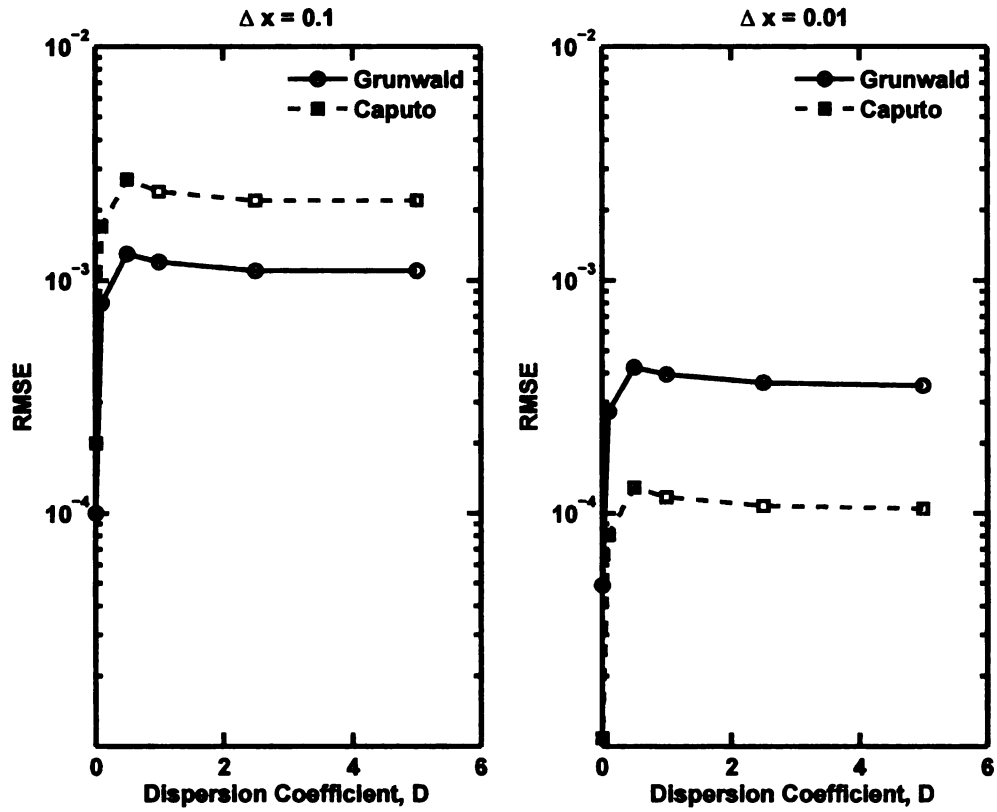


**Figure 3.7.** Plot showing the variation of RMSE (log scale) with dispersion coefficients, $D$, for grid sizes of $\Delta x = 0.1$ and $\Delta x = 0.01$ with $\alpha = 1.8$ and at time, $t = 1$

where

$$w_j^c = \frac{(j+1)^{2-\alpha} - (j)^{2-\alpha}}{\Gamma(3-\alpha)} \tag{3.56}$$

Tables 3.2 and 3.3 show the relative influence of the weights at all spatial locations for finite difference mesh points between the Caputo and GL derivatives. We found that the Caputo derivative has a higher relative weights at the $i$ point compared to the GL derivative, which may be one of the factors contributing to a more accurate Caputo derivative approximation compared to GL. There may be other reasons for the differences, which has not been explored in this study. Overall, we found that for the fractional-in-space diffusion equation, Caputo based fractional derivative performed better for reasonably fine step sizes.

**Table 3.2.** Table showing the weights for the Grünwald-Letnikov derivative for different $\alpha$ values

| Grünwald Weights - Fractional derivative exponent($\alpha$) | | | | | | | | | | |
|---|---|---|---|---|---|---|---|---|---|---|
| **Location** | **1.1** | **1.2** | **1.3** | **1.4** | **1.5** | **1.6** | **1.7** | **1.8** | **1.9** | **2.0** |
| i+1 | 1.0000 | 1.0000 | 1.0000 | 1.0000 | 1.0000 | 1.0000 | 1.0000 | 1.0000 | 1.0000 | 1.0000 |
| i | -1.1000 | -1.2000 | -1.3000 | -1.400 | -1.5000 | -1.6000 | -1.7000 | -1.8000 | -1.9000 | -2.0000 |
| i-1 | 0.0550 | 0.1200 | 0.1950 | 0.2800 | 0.3750 | 0.4800 | 0.5950 | 0.7200 | 0.8550 | -1.0000 |
| i-2 | 0.0165 | 0.0320 | 0.0455 | 0.0560 | 0.06250 | 0.0640 | 0.05950 | 0.0480 | 0.0285 | 0.0000 |
| i-3 | 0.0078 | 0.0144 | 0.0193 | 0.0224 | 0.0234 | 0.0224 | 0.0595 | 0.0144 | 0.0078 | 0.0000 |
| i-4 | 0.0045 | 0.0081 | 0.0104 | 0.0116 | 0.0117 | 0.0108 | 0.0193 | 0.0063 | 0.0033 | 0.0000 |
| i-5 | 0.0030 | 0.0051 | 0.0064 | 0.0070 | 0.0068 | 0.0061 | 0.0089 | 0.0034 | 0.0017 | 0.0000 |
| i-6 | 0.0021 | 0.0035 | 0.0043 | 0.0046 | 0.0044 | 0.0038 | 0.0049 | 0.0020 | 0.0010 | 0.0000 |
| i-7 | 0.0015 | 0.0025 | 0.0031 | 0.0032 | 0.0030 | 0.0026 | 0.0030 | 0.0013 | 0.0006 | 0.0000 |
| i-8 | 0.0012 | 0.0019 | 0.0023 | 0.0024 | 0.0022 | 0.0018 | 0.0020 | 0.0009 | 0.0004 | 0.0000 |
| i-9 | 0.0009 | 0.0015 | 0.0018 | 0.0018 | 0.0016 | 0.0014 | 0.0010 | 0.0007 | 0.0003 | 0.0000 |
| i-10 | 0.0007 | 0.0012 | 0.0014 | 0.0014 | 0.0013 | 0.0010 | 0.0008 | 0.0005 | 0.0002 | 0.0000 |

**Table 3.3.** Table showing the weights for the Caputo derivative for different $\alpha$ values

| Caputo Weights - Fractional derivative exponent ($\alpha$) | | | | | | | | | | |
|---|---|---|---|---|---|---|---|---|---|---|
| **Location** | **1.1** | **1.2** | **1.3** | **1.4** | **1.5** | **1.6** | **1.7** | **1.8** | **1.9** | **2.0** |
| i+1 | 1.0000 | 1.0000 | 1.0000 | 1.0000 | 1.0000 | 1.0000 | 1.0000 | 1.0000 | 1.0000 | 1.0000 |
| i | -1.1339 | -1.2589 | -1.3755 | -1.4843 | -1.5858 | -1.6805 | -1.7689 | -1.8513 | -1.9282 | -2.0000 |
| i-1 | 0.0168 | 0.0301 | 0.0395 | 0.0450 | 0.0465 | 0.0441 | 0.0380 | 0.0284 | 0.0156 | 0.0000 |
| i-2 | 0.0077 | 0.0132 | 0.0166 | 0.0182 | 0.0180 | 0.0164 | 0.0135 | 0.0097 | 0.0051 | 0.0000 |
| i-3 | 0.0044 | 0.0073 | 0.0090 | 0.0096 | 0.0092 | 0.0082 | 0.0066 | 0.0046 | 0.0023 | 0.0000 |
| i-4 | 0.0028 | 0.0047 | 0.0056 | 0.0058 | 0.0055 | 0.0047 | 0.0037 | 0.0025 | 0.0013 | 0.0000 |
| i-5 | 0.0020 | 0.0032 | 0.0038 | 0.0039 | 0.0036 | 0.0030 | 0.0023 | 0.0016 | 0.0008 | 0.0000 |
| i-6 | 0.0015 | 0.0023 | 0.0027 | 0.0027 | 0.0025 | 0.0021 | 0.0016 | 0.0010 | 0.0005 | 0.0000 |
| i-7 | 0.0011 | 0.0018 | 0.0020 | 0.0020 | 0.0018 | 0.0015 | 0.0011 | 0.0007 | 0.0004 | 0.0000 |
| i-8 | 0.0009 | 0.0014 | 0.0016 | 0.0015 | 0.0014 | 0.0011 | 0.0008 | 0.0005 | 0.0003 | 0.0000 |
| i-9 | 0.0007 | 0.0011 | 0.0012 | 0.0012 | 0.0011 | 0.0009 | 0.0006 | 0.0004 | 0.0002 | 0.0000 |
| i-10 | 0.0006 | 0.0009 | 0.0010 | 0.0010 | 0.0008 | 0.0007 | 0.0005 | 0.0003 | 0.0001 | 0.0000 |

# CHAPTER 4
# Fractional Advection Dispersion Equation

In this chapter we present the numerical methods for solving the one-dimensional fractional-in-space advection dispersion equation (hereinafter fADE) based on operator splitting. The fADE is given by:

$$\frac{\partial C}{\partial t} + u\frac{\partial C}{\partial x} = D\left(\beta\frac{\partial^{\alpha}C}{\partial x^{\alpha}} + (1-\beta)\frac{\partial^{\alpha}C}{\partial(-x)^{\alpha}}\right) \tag{4.1}$$

where $C$ is the concentration, $t$ is the time, $x$ is the spatial coordinate, $u$ is the mean velocity, $\alpha$ is the order of fractional derivative, $D$ is the dispersion coefficient and $\beta$ ($0 \leq \beta \leq 1$) is the skewness parameters that controls the bias of the dispersion. We will discuss the operating-splitting (OS) technique to solve equation 4.1.

## 4.1 Semi-Analytical Solution for the fADE

Closed-form solutions to the fADE do not exist in the literature but semi-analytical solutions to boundary value problems can be found using the Laplace or the Fourier transform in a manner similar to what was described in Ogata and Banks [1961]. Benson et al. [2000] gave a semi-analytical solution for the fADE equation for boundary conditions similar to an instantaneous release of a slug of tracer in a stream (the instantaneous release can be mathematically represented using the Dirac-delta function). The solution for the fADE for an infinite domain given by [Benson et al., 2000] is

$$\hat{C}(k,t) = \exp\left[\frac{1}{2}(1-\beta)(-ik)^{\alpha}t + \frac{1}{2}(1-\beta)(-ik)^{\alpha}Dt - ikut\right] \tag{4.2}$$

where $i = \sqrt{-1}$ and $-1 \leq \beta \leq 1$ indicates the relative weight of the forward versus backward transition probability and $1 < \alpha \leq 2$ is the scaling exponent in the one-dimensional space, $u$ is the velocity, $D$ is the dispersion coefficient with units $L^{\alpha}T^{-1}$.

With the notational simplification $B = |\cos(\pi\alpha/2)D|$, and with the identities $i = e^{i\pi/2}$ and $e^{i\theta} = \cos\theta + \sin\theta$, equation 4.2 can be rewritten as

$$\begin{aligned}\hat{C}(k,t) = \exp\{&-Bt\,|k|^{\alpha}\,[1 + i\beta(sign\ (k)] \\ &.\tan(\pi\alpha/2)) - ikvt\}\end{aligned} \tag{4.3}$$

The above Fourier-transformed solution does not have a closed form inverse solution, but can be put into a canonical form of the characteristic function of the $\alpha-$stable density (see Benson et al. [2000]for details) to get the final solution of fADE as

$$\hat{C}(k,t) = \exp\left(Bt\,|k|^{\alpha} - ikut\right) \tag{4.4}$$

where $\sigma = (Bt)^{1/\alpha}$ indicates the stable density that is shifted by the mean $(ut)$ and is invariant upon scaling by $t^{1/\alpha}$.

This analytical solution suffers from the limitations similar to most analytical solutions, i.e., they are applicable only when the parameters are constant, and when relatively simple initial and boundary conditions are used. In real world problems this can pose serious limitations on the practical applicability of these solutions; for example, for a spatially or temporally varying velocity and dispersion coefficients analytical solutions do not exist. Additionally, the analytical solution exists only for an infinite domain with zero flux boundary conditions at both the ends. Figure 4.1 shows the BTCs for an instantaneous release of slug of mass $m = 1$ kg for different values of $\alpha$, using the analytical solution code written by Benson [1998]. Note that for $\alpha = 2$, the classical ADE is recovered. One can observe from Figure 4.1 heavy-rising limbs for $\alpha < 2$, indicating faster-than-Fickian process.

### 4.1.1 Numerical methods

The classical ADE is a mixed system of hyperbolic (advection) and parabolic (dispersion) partial differential equations (PDEs). The hyperbolic equation is generally difficult to solve accurately because of the lower order accuracy of spatial differencing. Since generally both advection and dispersion terms are solved simultaneously, lower order accurate methods introduce significant error in the advection term in the form of numerical dispersion compared to dispersion term. In the classical ADE, higher order accurate numerical

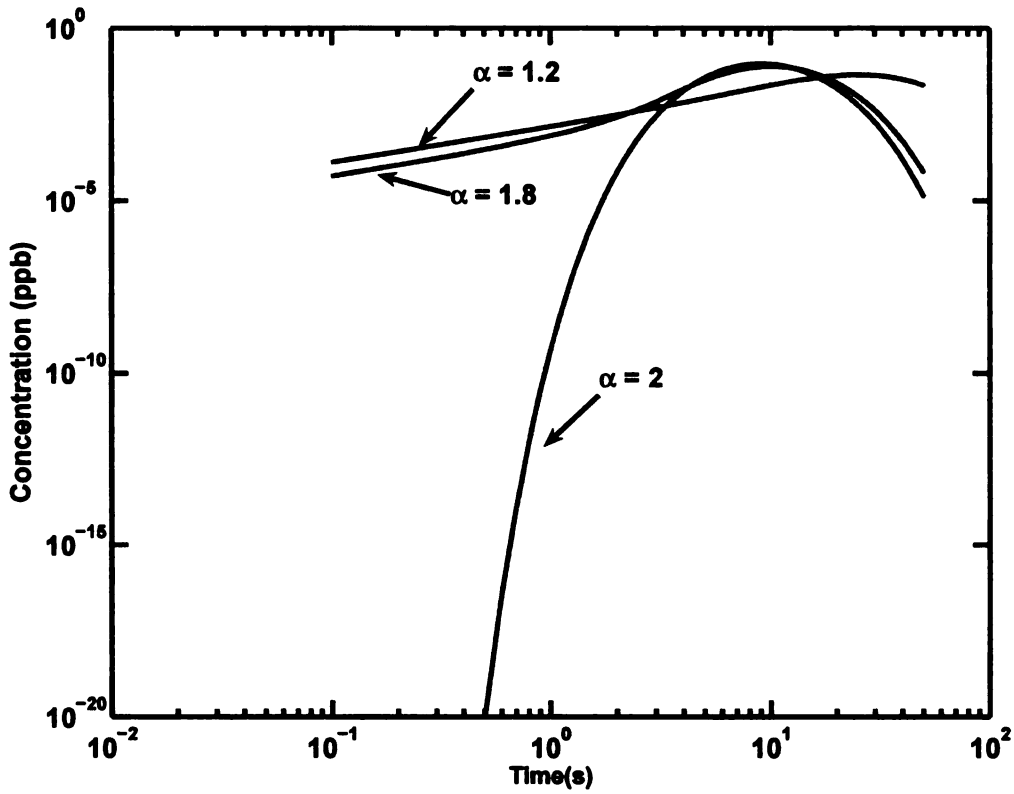


**Figure 4.1.** Breakthrough curves shown at $x = 10m$ from the point of release. $u$=1ms$^{-1}$ and $D = 1$

schemes exists for both the advection as well as the second-order dispersion term, however as discussed in Chapter 3 there exists only first-order accurate numerical methods for the fractional dispersion term. Therefore, for the fADE equation the numerical approximation is limited by the order of accuracy of fractional dispersion term, which results in a relatively crude resolution overall. There are three solutions to resolve the problem of not using a high-resolution finite-difference mesh: (i) Use a higher-order accurate numerical approximation for both the advection and the fractional dispersion terms; (ii) Solve the advection and fractional dispersion terms independently using the operator-splitting technique; and finally (iii) Use the semi-Lagrangian approach for the advection term and existing numerical approximation for the fractional dispersion term. We chose the second approach of using the OS technique to separate the advection and the fractional dispersion terms and solving them using the numerical methods discussed in Chapters 2 and 3. The advection terms were approximated using the WENO and the fourth-order com-

pact schemes, while the fractional dispersion terms were approximated using Caputo and Grünwald-Letnikov (GL) derivative operators.

## 4.2 Operator Splitting Methods

Operator splitting (OS) methods were originally developed for reasons of speed, accuracy, and stability. These methods present a divide-and-conquer strategy where the unwieldy systems of PDEs are broken down into simpler subproblems and treated individually using specialized numerical algorithms best suited for their class. Depending upon the PDE problem to be addressed, one can use different types of OS methods. In differential splitting the PDEs was split time before space and can be represented as

$$\frac{\partial f}{\partial t} + \pounds f = 0, \quad \pounds = \sum_{s=1}^{S} \pounds_s \tag{4.5}$$

where $\pounds_s$ represents the physical processes of interest (e.g. advection, diffusion, reaction etc.). In case of algebraic splitting, the order of splitting is reversed with space splitting done before time. It is commonly used for segregated solution of the semi-discretized equations. The OS method is applied to $L = L_s$ resulting from the space discretization before applying the time splitting.

$$\frac{\partial f}{\partial t} + Lf = 0, \quad L = \sum_{s=1}^{S} L_s \tag{4.6}$$

where $L_s$ represents the discrete operators (sparse matrices of arbitrary origin). Since this study is limited to one-dimensional space, there is no need for dimensional splitting, but we will be taking advantage of the differential splitting to solve the fADE. OS methods can introduce errors in the final solution and depending upon the type of OS technique used the order of errors changes. Generally the order of the OS is bounded by the lowest order of the numerical algorithm which in our case is fractional diffusion since both GL and Caputo derivative operators are first-order accurate while compact and WENO are of fourth and fifth-order accurate respectively.

OS algorithms can be solved using different orders of accuracy. For example, the first-order accurate OS method includes methods by Marchuk and Yanenko [1964] while

the second-order accurate methods include Strang splitting [Khan and Liu, 1995]. In this study, we use the second-order accurate Strang splitting algorithm to solve the fADE, since our aim is to minimize the time-splitting error introduced by OS and at the same time have an OS method which has higher order accuracy compared to the first-order fractional dispersion. The Strang OS method can be applied to the fADE by rewriting equation 4.1 as

$$\frac{\partial C}{\partial t} + \pounds C = 0 \quad \text{and} \quad \pounds = \pounds_1 + \pounds_2 \tag{4.7}$$

where

$$\pounds_1 = \frac{\partial}{\partial x}, \quad \pounds_2 = \frac{\partial^\alpha}{\partial x^\alpha} \tag{4.8}$$

We split the time step $\Delta t$ into half-time steps and solved the equations using the Strang-splitting algorithm. In the first half-time step $\Delta t/2$, the advection term is solved using the higher order numerical methods (WENO or compact), while the fractional dispersion is solved using semi-implicit approach for the complete time of $\Delta t$. Since, advection and dispersion processes take place simultaneously for the complete time step $\Delta t$, we advect for the remaining time step $\Delta t/2$.

$$\frac{\partial C}{\partial t} + u\frac{\partial C}{\partial x} = 0 \quad \text{in} \quad (t^n, t^{n+1/2}) \tag{4.9}$$

$$\frac{\partial C}{\partial t} + \left(-D\frac{\partial^\alpha C}{\partial x^\alpha}\right) = 0 \quad \text{in} \quad (t^n, t^{n+1}) \tag{4.10}$$

$$\frac{\partial C}{\partial t} + u\frac{\partial C}{\partial x} = 0 \quad \text{in} \quad (t^{n+1/2}, t^n) \tag{4.11}$$

Strang splitting is second-order accurate and unconditionally stable if the discrete counterparts of $\pounds_1$ and $\pounds_2$ are positive-definite matrices. Positive-definiteness is not a problem in our case since our governing equations were based on conservation laws.

## 4.3 Boundary Conditions

We used the Strang OS approach described above to simulate tracer transport in a stream for two cases: (a) a continuous release and (b) an instantaneous release ("spill") of a slug of tracer. Both cases were simulated by considering an infinite domain. Two types of boundary conditions were considered: (i) a prescribed concentration boundary and (ii)

a prescribed flux boundary. These boundary conditions are well known in contaminant hydrology, however, we need to modify these well-known boundary conditions for the case of fractional dispersion, therefore they are discussed below in more detail.

**Prescribed-Concentration:** The LHS boundary was simulated using constant concentration is given by:

$$C(0,t) = C_0 \quad t \geq 0 \tag{4.12}$$

while the RHS boundary (at an infinite distance) was simulated using zero prescribed flux for all times and is given for the classical ADE by

$$\left.\frac{\partial C}{\partial x}\right|_{x\to\infty} = 0 \tag{4.13}$$

**Prescribed Flux boundary:** The LHS and RHS boundaries were simulated using the prescribed flux boundary conditions for an infinite domain $x \in (-\infty, \infty)$ with instantaneous release of slug of tracer at $x = 0$. For the classical ADE with an infinite domain, the prescribed flux at the two boundaries is equal to the dispersive flux at the inlet and outlet boundaries and can be written as

$$\begin{aligned} -D\left.\frac{\partial C}{\partial x}\right|_{x\to-\infty} &= 0 \\ -D\left.\frac{\partial C}{\partial x}\right|_{x\to\infty} &= 0 \end{aligned} \tag{4.14}$$

The above is not the correct boundary condition in case of fractional dispersion, since the dispersive flux at the two outlets is a fractional dispersive flux unlike the integer-order flux in the ADE. The fractional-order flux at the two boundaries is given by:

$$\begin{aligned} -D\left(\beta\frac{\partial^{\alpha-1}C}{\partial x^{\alpha-1}} + (1-\beta)\frac{\partial^{\alpha-1}C}{\partial(-x)^{\alpha-1}}\right)_{x\to-\infty} &= 0 \\ -D\left(\beta\frac{\partial^{\alpha-1}C}{\partial x^{\alpha-1}} + (1-\beta)\frac{\partial^{\alpha-1}C}{\partial(-x)^{\alpha-1}}\right)_{x\to\infty} &= 0 \end{aligned} \tag{4.15}$$

The two dispersive fluxes at the two boundaries are approximated using the control volume approach described by Zhang et al. [2006] and are given by (details in the Appendix A)

$$\begin{aligned} Q_{-N+1/2} &= -\frac{D}{\Gamma(2-\alpha)\Delta x^{\alpha}}\left[\begin{array}{l}\beta w_0(C_{-N+1} - C_{-N}) \\ +\sum_{j=0}^{N-1}(1-\beta)(C_{-N+1+j} - C_{-N})\end{array}\right] \\ Q_{N-1/2} &= -\frac{D}{\Gamma(2-\alpha)\Delta x^{\alpha}}\left[\begin{array}{l}\sum_{j=0}^{N-1}\beta w_j(C_{N-j} - C_{N-j-1}) \\ +(1-\beta)(C_{N-1} - C_N)\end{array}\right] \end{aligned} \tag{4.16}$$

We equated both the above fluxes to zero, since we were using infinite boundary conditions.

## 4.4 Solution of the fADE for Continuous Release

For simulating the fADE using a prescribed-concentration boundary for the case of continuous release of a tracer, we chose a domain of size $L = 20$m with zero concentration everywhere in the domain initially. At $t = 0$ a conservative tracer with a constant concentration of $C_0$ was imposed at the LHS boundary at $x = 0$ and the boundary condition remains constant throughout the period of simulation. The RHS boundary at $x = L$ was simulated by using zero-flux prescribed flux given by . We used $\beta = 1$ , a case also studied by Benson et al. [2004] and Liu et al. [2004]. The fADE was solved using strang OS approach, with the advection term solved using WENO numerical approximation and fractional dispersion term was solved using GL and Caputo derivative approximations (see Figure 4.4).

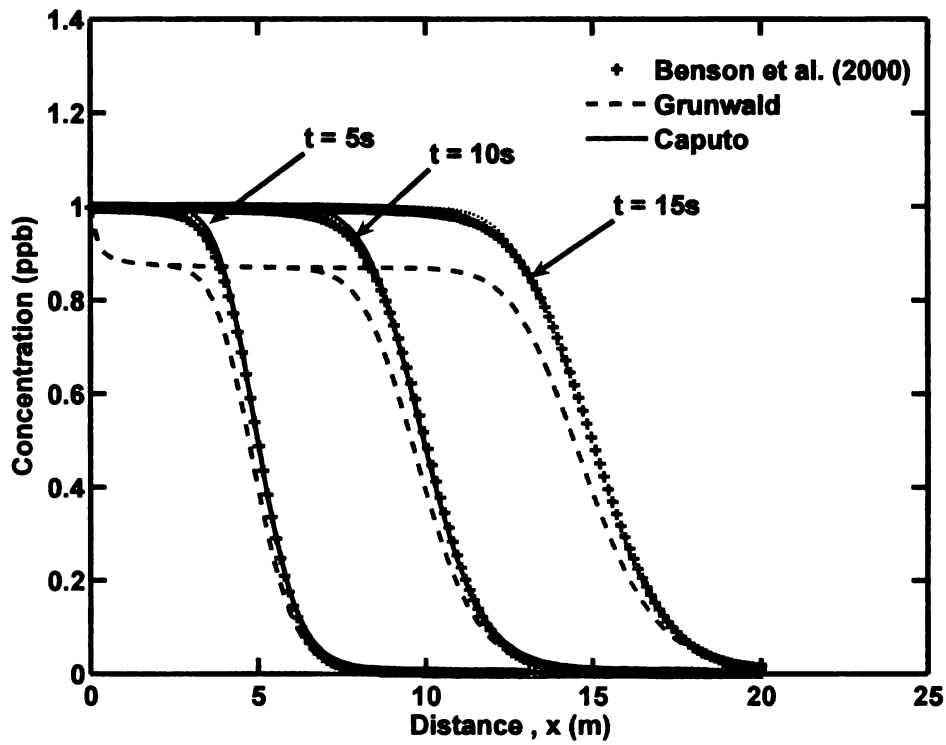


**Figure 4.2.** Concentration profiles for the continuous release of a tracer in a stream simulated using the fADE. The fADE was numerically solved using the WENO-GL and WENO-Caputo schemes and compared with the semi-analytical solution of [Benson et al., 2000]. The parameters in the solution are $C_0$=1ppb at $t$= 5s, 10s and 15s with $u = 1\text{ms}^{-1}$, $\text{D} = 0.1\text{m}^{1.8}/s$, $\alpha = 1.8$, $CFL = 0.1$ and $\Delta x$=0.1250m

We find that the comparison based on the GL approach does not match with the semi-

analytical solution by Benson et al. [2000]. This has also been observed by Zhang et al. [2006], where the fractional dispersion was solved using the Riemann-Liouville definition which has been been shown to have exact equivalence to the GL approach used here by Podlubny [1999]. The inability of the GL-based numerical solution to correctly describe solute transport as given by the analytical solution was attributed to the fact that the fractional derivative of a constant (in our case the prescribed concentration $C_0$) does not vanish (that is not equal to zero) in the case of the GL approach. This was not an issue while using the Caputo derivative based numerical scheme which agreed well with the analytical solution. We therefore conclude that the Caputo derivative is the preferred approach for simulating continuous release in a stream.

## 4.5 Instantaneous slug release

We simulated the instantaneous release using a prescribed-total-flux-boundary at $x = 0$ and a free drainage outlet at $x = L$, commonly encountered in hydrology by using the following boundary condition, described earlier in Chapter 3

$$uC - D\left(\beta\frac{\partial^{\alpha-1}C}{\partial x^{\alpha-1}} + (1-\beta)\frac{\partial^{\alpha-1}C}{\partial(-x)^{\alpha-1}}\right)_{x=-L} = 0 \tag{4.17}$$

$$-D\left(\beta\frac{\partial^{\alpha-1}C}{\partial x^{\alpha-1}} + (1-\beta)\frac{\partial^{\alpha-1}C}{\partial(-x)^{\alpha-1}}\right)_{x=L} = 0 \tag{4.18}$$

where an initial slug of conservative mass of tracer equal to $m = M_0$ was released at $t = 0$ at the spatial location $x = 0$. The domain of simulation is $x = [-L, L]$. We simulated this boundary using an "infinite" domain with the tracer slug released at $x = 0$. We wanted to understand which combination of numerical schemes works best in describing the instantaneous slug release, which will be used later to describe field data. Therefore, we tested both WENO and compact schemes for solving the advection process while the GL and the Caputo derivative operators were used for approximating fractional dispersion. Hence, we tested all the four possible combinations of schemes, i.e., WENO-GL, WENO-Caputo, compact-GL and compact-Caputo for simulating this case using the OS technique.

During our initial runs, we found that the RMSE error was not a true measure of whether or not the scheme was reasonable enough to capture the peak or the tail accurately. Therefore, we ran many simulations and visually checked to see within what reasonable range the schemes perform well. We wanted to know if the numerical solution can describe both the peak and the tail and if it is in reasonable agreement with the semi-analytical solution by [Benson et al., 2000]. In order to accurately capture the effects of various flow conditions occurring in the field including high advection or high dispersion, we used the cell Peclet ($Pe$) number as a metric to represent various conditions. For example, using the cell Peclet number we can capture the effects of fractional derivative exponent ($\alpha$), velocity ($u$), dispersion coefficient $D$ and the mesh size $\Delta x$ using a single parameter. The cell Peclet number for the fADE can be defined as:

$$Pe = \frac{u\Delta x^{\alpha-1}}{D} \tag{4.19}$$

Note that for $\alpha = 2$, the fADE cell $Pe$ number is equivalent to the ADE cell $Pe$ number. All the breakthrough curves were plotted at a distance of $x = 10m$ from the point of injection of the tracer. We compared all the four schemes by plotting the BTCs and comparing then with the semi-analytical solution by Benson et al. [2000]. We used forward skewed fractional dispersion ($\beta = 1$), since in an advection-dominated flow (e.g., streams) dispersion will be biased forward which was also noted by Benson [1998] and Zhang et al. [2006].

### 4.5.1 High Peclet Number: Advection-Dominated Systems

We simulated a high Peclet number condition to compare the four schemes listed above with the analytical solution. A comparison is shown in Figure 4.3.

We found the that the compact-based advection scheme gave oscillations in the tail region of the breakthrough curve using both the GL as well as the Caputo based fractional derivative operators. This supports the well-known fact (see Demuren et al. [2001]) that the compact scheme introduces oscillations at high Peclet number. The WENO based advection scheme was not able to simulate the peak or the tail correctly using any of the fractional dispersion schemes but did not suffer from oscillations because of its non-

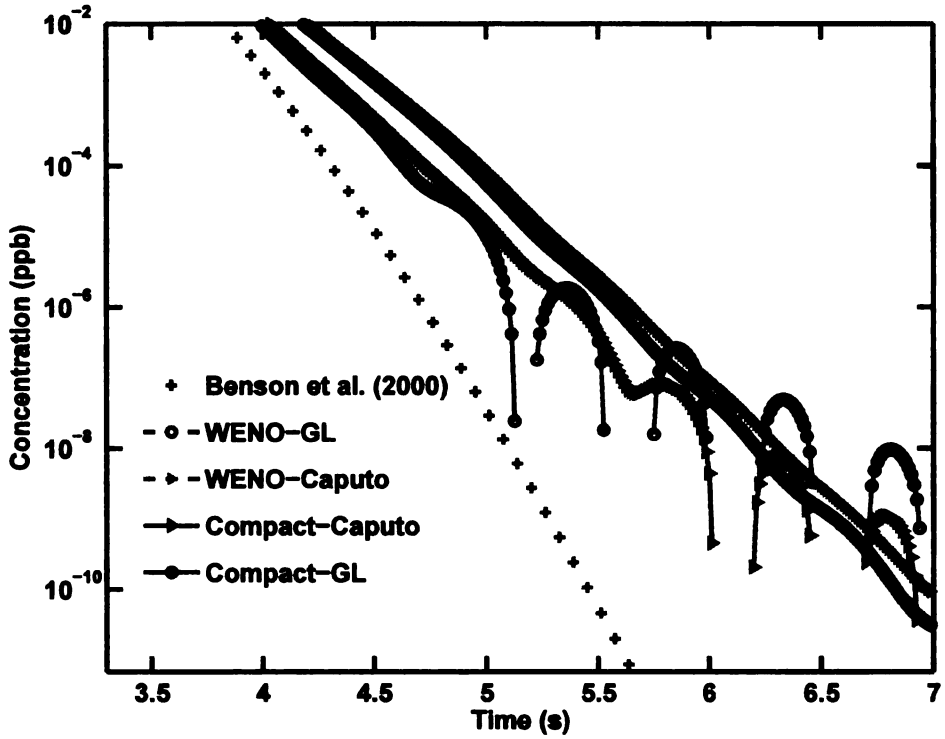


**Figure 4.3.** Plot showing the comparisons for all the four schemes for a $Pe = 6.6$ ($\Delta x$=0.25m, D = 0.05m$^{1.8}/s$, $u$ = 1ms$^{-1}$, $CFL$ =0.1, $t$=15s and $\alpha$ = 1.8). Numerical oscillations were observed in case of compact based approaches while numerical dispersion was observed in the case of WENO based advection schemes

oscillatory nature. The WENO scheme is a little dispersed as it requires a minimum grid size to achieve the fifth-order accuracy as illustrated in Chapter 2. Since a crude grid size of $\Delta x$=0.25 is used in the above simulation, dispersion error is noticed. Our runs show that for $Pe < 2$ all the four schemes were able to simulate the peaks well but the GL-based fractional dispersion did not simulate the tail well. This is in agreement with the higher RMSE errors for the GL derivative operator compared to the Caputo-based approximation which we had discussed in Chapter 3. For $Pe < 2$ both the compact and the WENO-based fADE solutions were not able to simulate the analytical solution well. We find that as the $Pe$ number increases, there exists a significant difference between outputs from the two models. We decreased the $Pe$ number and found that all the four schemes give a reasonably good fit without any significant difference. The advantage of using the compact based advection for $Pe < 2$ is that it performs the best in explaining the peak compared to the WENO for various crude grid sizes. This is important since the

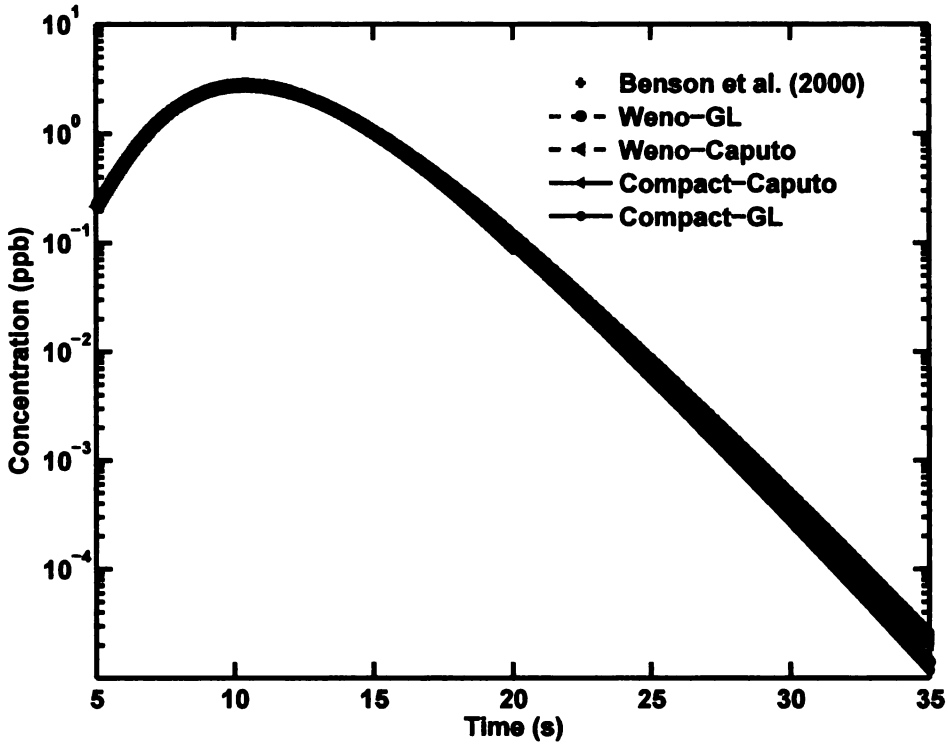


**Figure 4.4.** Plot showing the comparison for a $Pe = 1.7$ for all the four schemes ($\Delta x$=0.25m, D = $0.05\text{m}^{1.8}/s$,$u = 1\text{ms}^{-1}$ , $CFL$ =0.1, $t$=15s, $\alpha$=1.8). All the schemes show reasonably good fit, although the WENO based advection scheme introduced small numerical dispersion

tracer studies are performed in rivers over long reaches. A crude grid size will result in a faster simulation which in turn will result in a lesser computational time during parameter estimation. On the other hand, the WENO scheme performs satisfactorily even for high $Pe$ number without oscillations although significant dispersion errors are introduced for crude grid sizes. We conclude that for simulating advection-dominated systems, the grids should be refined such that the condition $Pe < 2$ is satisfied.

### 4.5.2 Low Peclet Number: Dispersion-Dominated Systems

In order to understand whether Caputo or GL based fractional dispersion scheme explains the dispersion better for a spill case, we ran simulations for another limiting case, i.e. high dispersion. For a high dispersion situation , there will be no significant difference between the advection schemes because the physical dispersion far exceeds any numerical dispersion in WENO or compact schemes. A test case for $D = 10\text{m}^{1.8}/\text{s}$, $u = 1\text{m/s}$ with $Pe = 0.0574$ was used. We found that using the GL fractional diffusion, the peak

was higher than the analytical solution, while the Caputo based fractional diffusion was able to simulate the analytical solution (both tail and peak) accurately. Both WENO and compact based advection schemes were able to explain the analytical solution well with almost no apparent difference as expected. Therefore, the moving front was highly smeared (due to physical dispersion), so the effect of any numerical smearing was negligible in comparison. It was also observed that as one approaches lower $Pe$ number,the GL based fractional dispersion was unable to explain the peak. This is consistent with the results in chapter 3 (Figures 3.6 and 3.7) where we demonstrated that the Caputo derivative provides a superior description of fractional dispersion. We found that the GL dispersion peaks and tail concentration were higher compared to the analytical solution as shown in Figure 4.5 below

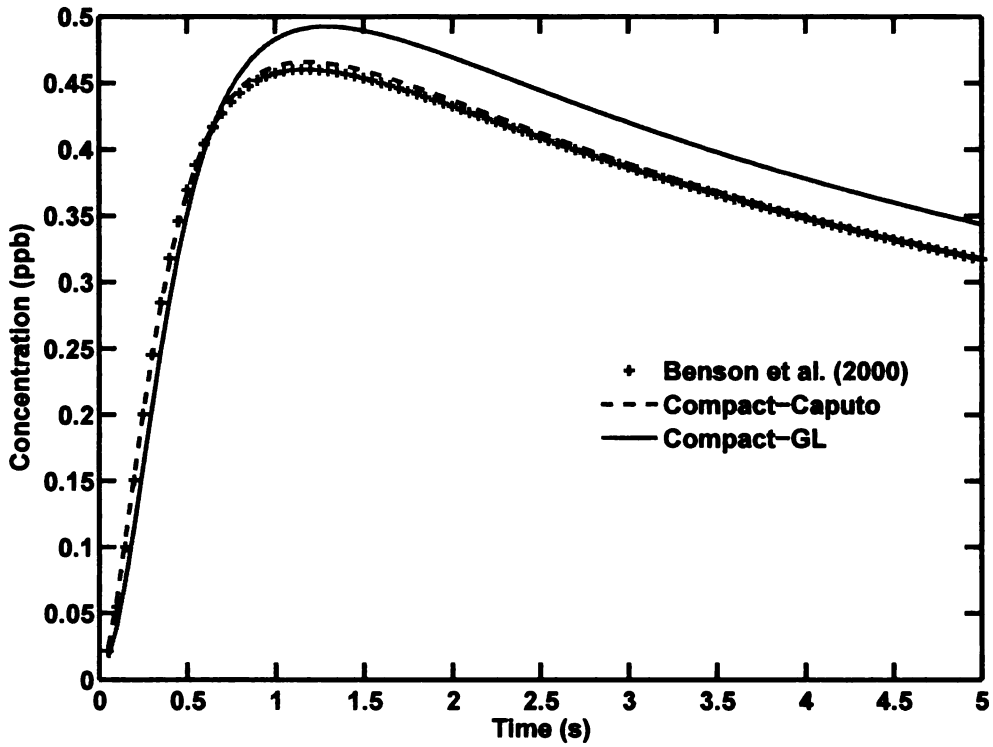


**Figure 4.5.** Breakthrough curves for a low $Pe = 0.057$ ($\Delta x = 0.5$, $CFL = 0.1$, $\alpha = 1.8$, $\beta = 1$, $D = 10\text{m}^{1.8}/\text{s}$, $u = 1\text{ms}^{-1}$) at a distance of 5m from the spill location.

In order to confirm whether significant errors are introduced due to OS, a first order upwind based advection scheme using GL and Caputo was used to solve the fADE without any OS using the same parameters (see Figure 4.6). As observed from figure 4.6 both OS

and the no-OS approaches gave similar results, which implies that the OS does not introduce any significant errors. This implies that Caputo based fractional-in-space provides a superior description compared to GL, supporting the earlier results in Chapter 3.

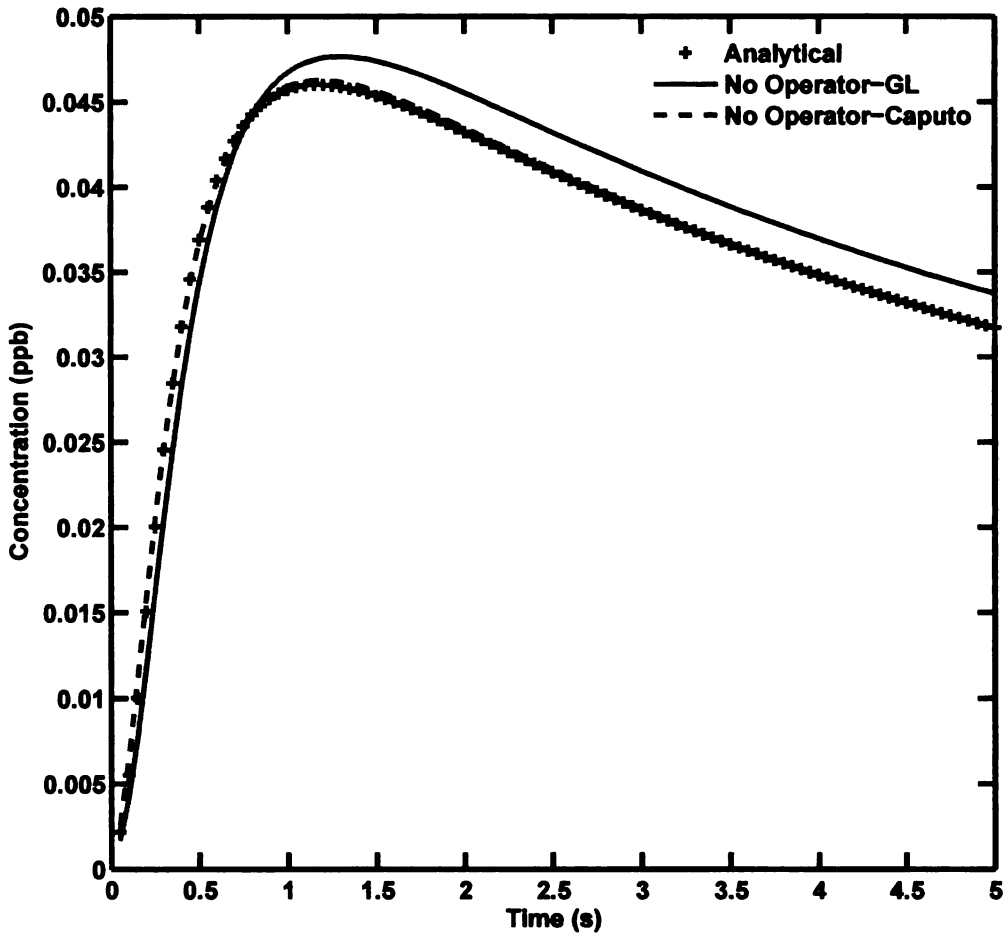


**Figure 4.6.** Breakthrough curve (without OS) for a low $Pe = 0.057$ ($\Delta x = 0.5m$, $CFL = 0.1$, $\alpha = 1.8$, $\beta = 1$, $D = 0.05\text{m}^{1.8}/\text{s}$,$u = 1\text{m/s}$) at a distance of 5m from the spill location.

### 4.5.3 Effect of fractional derivative exponent($\alpha$)

To understand the effect of the fractional derivative exponent $\alpha$ with $Pe$ number less than 1, we plotted the breakthrough curves for three different values of $\alpha$. It was found that as $\alpha$ tends towards 1, the fractional dispersion term becomes similar to the advection term. It was found that both caputo and GL based fractional dispersion schemes are not able to simulate the tail. Also, there seems to be a phase error introduced as $\alpha$ approaches 1. The observed difference between the analytical and numerical solutions as $\alpha \rightarrow 1.0$ is

attributed to a change in the nature of the partial differential equation from parabolic (for any value of $\alpha > 1.0$) to hyperbolic (for $\alpha = 1.0$). Therefore the point $\alpha = 1.0$ may be treated as a singularity as far as the validity of the numerical solution is considered.

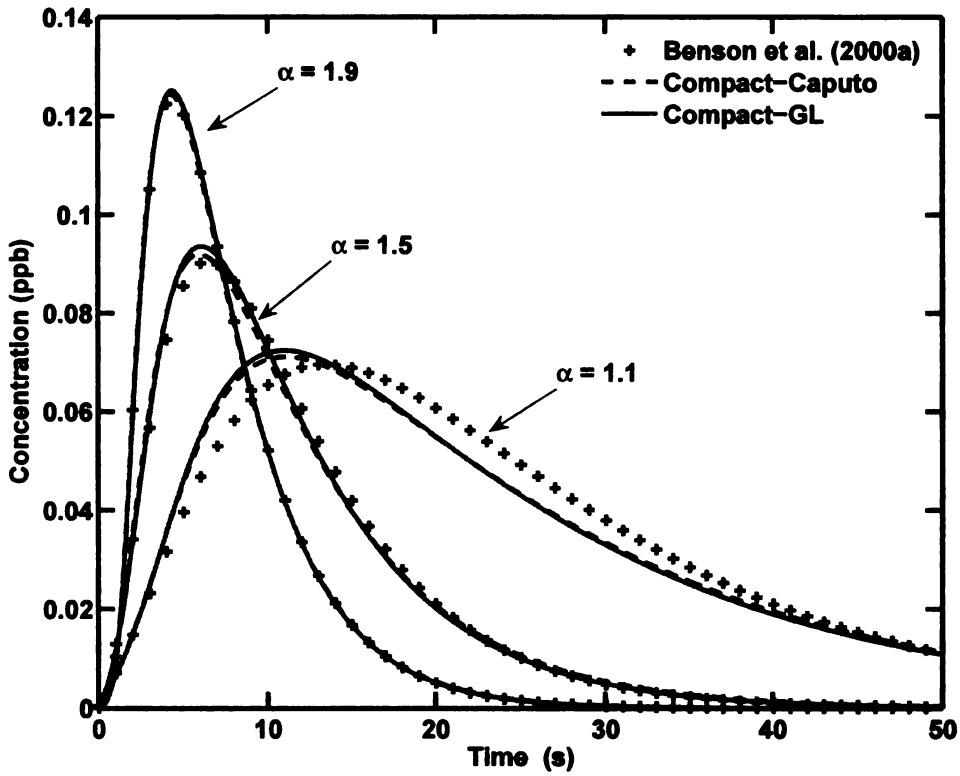


**Figure 4.7.** Breakthrough curves comparison between GL and Caputo with Benson et al. [2000] for different values of $\alpha$ with $Pe = 0.1$

In conclusion, the operator splitting approach was found to produce accurate numerical solutions to the fractional advection dispersion equation as long as the cell Peclet number was sufficiently low (typically less than 2.0). The combination of a compact scheme for advection and the Caputo-based approximation of the fractional dispersion was found to produce the best results (that is, describing the peak as well as the tail in the breakthrough curves). The WENO scheme did not introduce oscillations (not a surprising result considering the nature of this scheme), but significant dispersion errors were introduced at high Peclet numbers.

# CHAPTER 5

# Stream Transient Storage Modeling

It has been observed in various studies that the dispersion process traditionally described using Fickian diffusion fails to explain the field measurements. Data collected from nearly 100 streams and rivers shows that the unit-peak concentration tends to attenuate in proportion to the travel time with the 0.89 power, not the 0.5 power predicted by second-order dispersion [Jobson, 2001]. This is indicative of a non-Fickian diffusion process sometimes also called as anomalous diffusion. This can result in a heavy leading and falling limbs in the time-concentration breakthrough curves (BTCs) [Schumer et al., 2003]. The heavy leading limb is indicative of faster-than-Fickian growth rate, usually because of preferential flow paths. On the other hand, heavy falling limb is indicative of the delay of solute in the main channel because of the exchange processes between the main channel and storage zone. In order to understand both these processes, we examine solute transport processes in a stream.

Solute dispersion in rivers or streams primarily consists of contributions from four mechanisms: molecular diffusion, turbulent diffusion, shear-flow dispersion and scaling dispersion [Fischer, 1979]. The most important among them being the shear-flow dispersion, which typically involves mixing due to spatial variability in the flow field. This process produces progressive spreading of the dissolved and suspended substances that causes the variance of the concentration distribution with time. Taylor [1954] showed that after sufficient mixing distance, the variance grows linearly with time and then the concentration distribution follows Fick's law of diffusion. However, this is not always

true because of the substantial water influx across channel boundaries, which results in a far less uniform velocity field than what has been previously assumed while using a second-order dispersion in these systems [Bencala and Walters, 1983; Harvey and Gorelick, 2000]. Additionally, the exchange of solute in the stream with the hyporheic zone has been shown to produce a consistent delay in the solute transport relative to the main stream flow, leading to a heavy falling limb in the BTCs. On the other hand, the heavy leading or rising limb in the BTC is observed because of the long-range spatial correlation of the dispersion process. This leads to an enhanced diffusion (super-diffusion) than what the second-order diffusion solution estimates [Sahimi, 1993]. It is a result of the infinite-variance particle jump distributions that arise during transport of solute in heterogenous media [Schumer et al., 2001].

There have been many approaches in the past to describe the non-Fickian processes. For example, to model the long-range spatial correlation of the dispersion process, some of these models have used variable dispersion coefficient, by varying the dispersion coefficient linearly with downstream distance [Berkowitz and Scher, 1995; Wheatcraft and Tyler, 1988]. However, it is difficult to justify this approach, unless there is a some definite trend in the heterogeneity of the stream. There have also been many cases where these adjusted models gave physically unreasonable parameters for the observed field data [Constantz, 1998]. One of the other approaches used in the past is to use the fractional-in-space advection-dispersion equation (fADE) to model the long-range spatial correlation [Deng et al., 2004]. The drawback of using fADE is that it does not account for the transient storage of solutes in the river banks or the hyporheic zones. These exchange processes can be of an arbitrary order depending upon the type of processes occurring. For example, the hyporheic exchange process typically follows a power law residence time distribution (RTD) because of the large waiting times of solute along the subsurface flow paths and due to adsorption. On the other hand, surface storage exchange processes typically follow an exponential law RTD because of comparatively shorter waiting times. The fADE model does not account for these processes which includes adsorption and desorption, and the effects of vegetation and reactions [Deng et al., 2006]. To account for the transient storage

of the solute in these storage zones, we use the transient storage (TS) model in this study.

## 5.1 Transient Storage Model

The transient storage model describes solute transport in streams taking the physical, chemical and biological characteristics into account. Most of the previous TS models used the standard advection-dispersion equation (ADE) for solute transport with additional terms accounting for transient storage, lateral inflow and other processes (e.g., decay, sorption) depending upon the scope and complexity of the problem. Generally, the TS model is used in conjunction with the observed field studies to estimate the hydrologic parameters affecting solute transport. The standard one-dimensional TS model is described using equations 5.1 and 5.2 for the main channel and the storage zones respectively [Runkel and Broshears, 1991]

$$\frac{\partial C}{\partial t} + u\frac{\partial C}{\partial x} = \frac{1}{A}\frac{\partial}{\partial x}\left(AD\frac{\partial C}{\partial x}\right) + \frac{q_L}{A}(C_L - C) + \varepsilon(C_s - C) \tag{5.1}$$

$$\frac{\partial C_s}{\partial t} = \varepsilon\frac{A}{A_s}(C - C_s) \tag{5.2}$$

where $C$ = cross-sectional average of concentration in the main stream ($ML^{-3}$); $C_s$ = concentration in the storage zone ($ML^{-3}$); $C_L$ = lateral inflow solute concentration ($ML^{-3}$); $u$ = cross-sectional average of water velocity ($LT^{-1}$); $D$ = coefficient of longitudinal dispersion ($L^2T$); $x$ = space coordinate in the flow direction (L); $t$ = time (T); $\varepsilon$ = a first-order storage exchange coefficient ($T^{-1}$); $A$ = main channel cross-sectional area ($L^2$); $A_s$= storage zone cross-sectional area ($L^2$) and $q_L$ = lateral inflow rate ($L^3T^{-1}L^{-1}$). These equations are applicable to conservative (non-reactive) solutes such as tracers, but nonconservative (reactive) solutes may be accounted for by adding chemical reaction terms (e.g., kinetic sorption and decay) to equations 5.1 and 5.2.

This conceptual model assumes a first-order mass exchange between the main channel and the storage zones. However, field studies have reported breakthrough curves with heavier power law tails as opposed to the exponential tails modeled using a first-order exchange process [Becker and Shapiro, 2000; Haggerty et al., 2000]. This deviation has been attributed to the longer or deeper hyporheic flow paths [Worman, 2002; Marion

et al., 2003] which are generally not described properly using first-order exchange kinetics. Additionally, equations 5.1 and 5.2 assume that the subsurface is a well-mixed reservoir, while in reality hyporheic exchange is generally characterized by a strong exchange due to spatial variations of properties such as permeability in the subsurface [Marion and Zaramella, 2005]. Some researchers have used a fractional-in-time derivative to describe more complex exchange patterns between the main channel and the storage zones in aquifers [Schumer et al., 2003], however, time fractional derivatives is beyond the scope of the current work. In this study, we use the existing TS model assumptions, of describing the heavy-tailed falling limb, using the first-order exchange process between the main channel and the storage zones. Additionally, we replace the second-order dispersion using fractional-in-space dispersion to model the heavy rising limb observed due to faster-than-fickian processes. We refer to this new model as the fractional-in-space transient storage model (FSTS).

## 5.2 The Fractional-in-Space Transient Storage (FSTS) Model

The FSTS model can describe the non-Gaussian rising and falling limb in a BTC by using fractional-in-space dispersion and a first-order exchange process between the main channel and the storage zones respectively. The FSTS model is based on fADE instead of ADE and can be rewritten as

$$\frac{\partial C}{\partial t} + u\frac{\partial C}{\partial x} = D\frac{\partial^{\alpha} C}{\partial x^{\alpha}} + \frac{q_L}{A}(C_L - C) + \varepsilon(C_s - C) \tag{5.3}$$

$$\frac{\partial C_s}{\partial t} = \varepsilon\frac{A}{A_s}(C - C_s) \tag{5.4}$$

where $\alpha$ is the fractional derivative exponent and $\beta$ is the skewness parameter that controls the bias of the dispersion. We ran a number of simulations in order to understand the differences between the FSTS and TS models. All the simulations were run subject to $\beta = 1$, for a concentration profile skewed forward, a case also studied by [Benson et al., 2004] to represent preferential transport along pathways such as fractures and macropores. We simulated the injection of a tracer in a stream, subject to the following initial and

boundary conditions

$$C(0,0) = C_0 \quad \text{and} \quad C(x,0) = 0, \forall\, x(x \neq 0) \quad \text{and} \quad t = 0 \tag{5.5}$$

$$-D\left(\beta\frac{\partial C}{\partial x} + (1-\beta)\frac{\partial C}{\partial(-x)}\right)_{x\to-\infty} = 0$$

$$-D\left(\beta\frac{\partial^{\alpha-1}C}{\partial x^{\alpha-1}} + (1-\beta)\frac{\partial^{\alpha-1}C}{\partial(-x)^{\alpha-1}}\right)_{x\to\infty} = 0 \qquad \text{for} \quad 0 \leq t < \infty \tag{5.6}$$

Figure 5.1 (the figure is a spatial snapshot of concentration at a given time) shows that higher concentration is observed for $\alpha < 2$ compared to $\alpha = 2$ at larger downstream distances in the main channel at $t = 600s$. This is due to the faster-than-fickian process discussed earlier, which results in solutes moving faster than the standard second-order dispersion based TS model.

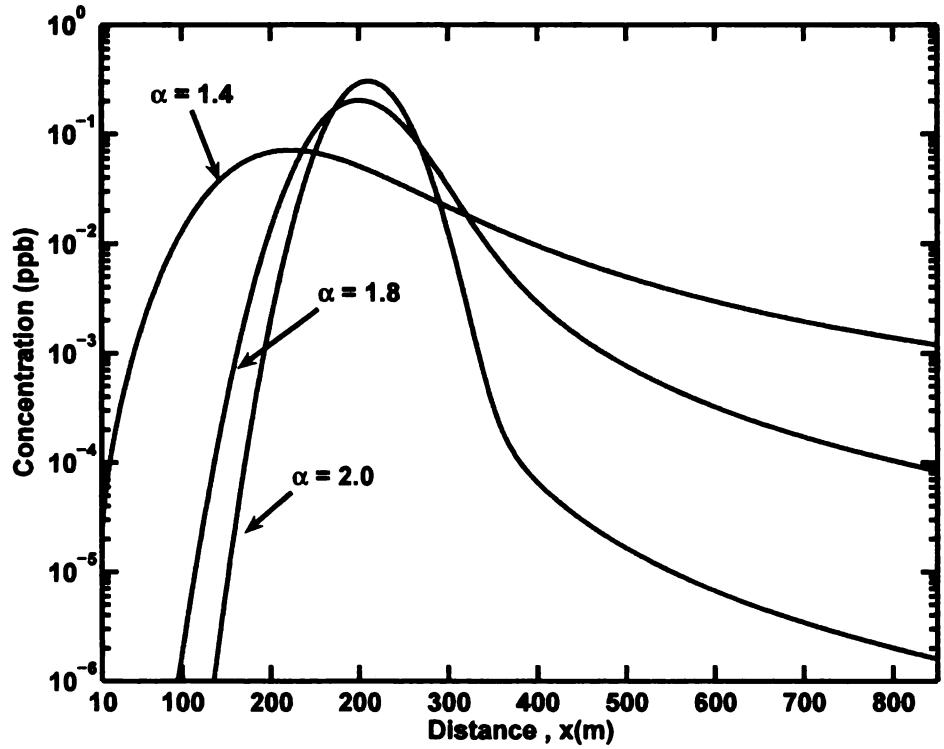


**Figure 5.1.** Numerical model showing the snapshot of concentration vs distance in the main stream at $t = 600$s spatially for $A = 40$ m$^2$, $A_s = 4$ m$^2$, $D = 1\text{m}^{1.8}/\text{s}$, $u = 1\text{ms}^{-1}$, $\epsilon = 0.0$ s$^{-1}$, $M = 1000$g. The point of injection is at $x = 10$ m

We also ran the FSTS model with $\alpha = 2.0$, to understand how the concentrations in the stream and the storage zones change with time. In Figure 5.2 we plot the distribution of concentration in the main channel and the storage zone for $\alpha = 2$ and storage exchange coefficient, $\epsilon = 0.001$. We can observe that the major contribution to the rising limb of

the BTC comes from the main channel (stream). However, the opposite is true for the falling limb of the BTC (Figure 5.2 log scale). This is because of the large waiting times of the solute in the storage zones before releasing back into the main channel.

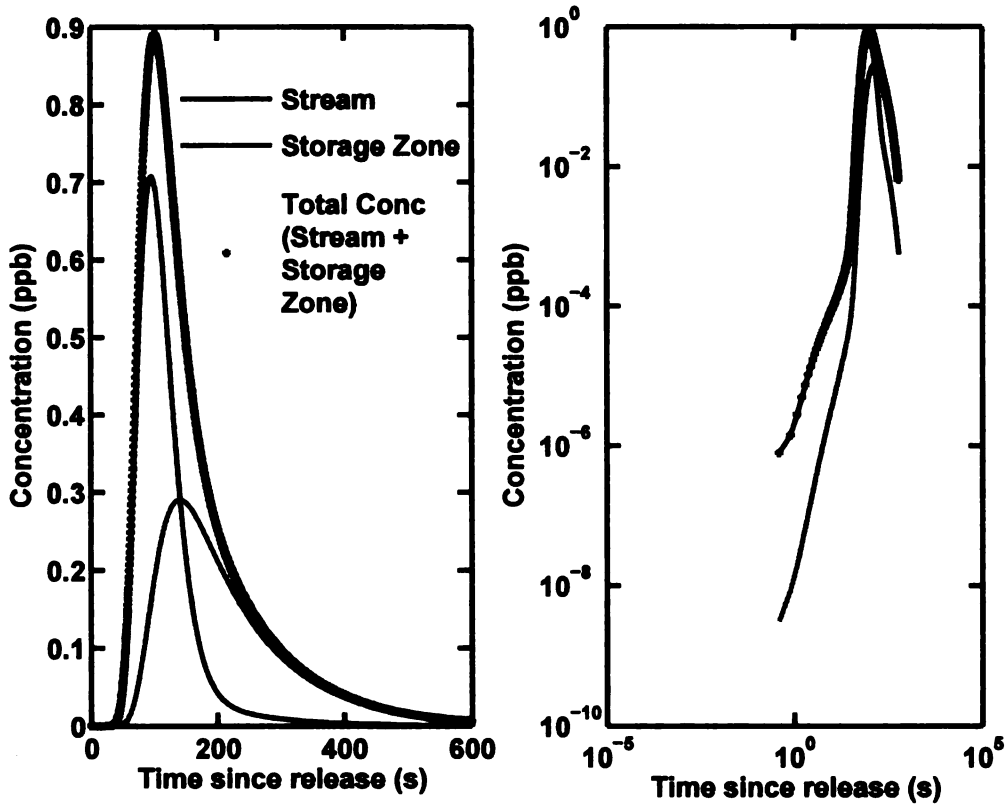


**Figure 5.2.** Breakthrough curve for the stream and storage zone concentration at a distance of $x = 50$m from the point of injection in (a) linear scale and (b) log log scale. In log scale, it can be observed that for the falling limb the major contribution of the concentration comes from the storage zone whereas, for the rising limb it is the main channel. ($A = 40$ m$^2$, $A_s = 4$ m$^2$, $D = 1\text{m}^{1.8}/\text{s}$, $\beta = 1$, $u = 0.5\text{ms}^{-1}$, $\epsilon = 0.001$ s$^{-1}$, $M = 1000$ g, $\alpha = 2$)

We also compared the FSTS model with the TS model in order to compare the behavior of the BTCs in the main channel for these models. We ran the model for the parameters mentioned in Figure 5.2 and observed that the heavy falling limb for both of these models gave almost similar concentration while significantly higher concentration for the rising limb in case of FSTS model. This reinforces our earlier discussion that both these models uses first-order exchange processes between the main channel and the storage zone, which controls the falling limb, and therefore give similar concentration magnitude. On the other hand, the rising limb is controlled by the fractional-in-space dispersion, therefore

the FSTS model gives a heavier rising limb compared to the TS model.

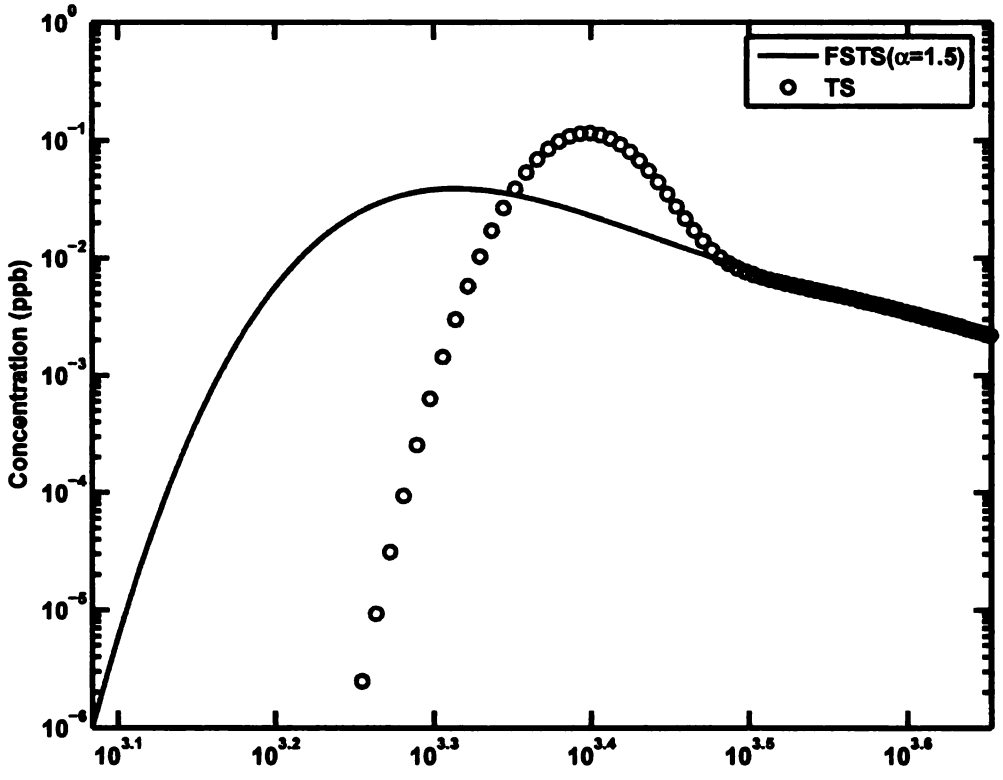


**Figure 5.3.** FSTS vs TS model breakthrough curve in the main channel for $A = 40$ m$^2$, $A_s = 4$ m$^2$, $D = 1\text{m}^{1.8}/\text{s}$, $\epsilon = 0.0001$ ms$^{-1}$, $M = 1000$ g, $\alpha = 2.0$, $\Delta x = 2.9950$ m and $x = 1000$ m

### 5.2.1 Comparison of the FSTS model with the Analytical Solution for $\alpha = 2$

We used the analytical solution by De Smedt et al. [2005] to evaluate the accuracy of our FSTS model for the special case of Fickian diffusion, i.e., $\alpha = 2$. There exists no analytical solution for the FSTS model, hence we compared our numerical model for $\alpha = 2$, which effectively reduces it to a TS model. Analytical solution for the TS model exists and is given by De Smedt et al. [2005] for an instantaneous injection of a tracer in a river with uniform flow in an "infinite" domain. The analytical solution to equations 5.1 and 5.2 is given by [De Smedt et al., 2005]

$$C(x,t) = \int_0^t \left[ \begin{array}{l} \varepsilon + \left( \frac{x^2 - \nu^2\tau^2}{4D\tau^2} - \frac{1}{2\tau} - \varepsilon \right) J\left( \varepsilon\tau, \frac{\varepsilon(t-\tau)}{\beta} \right) \\ -\varepsilon J\left( \frac{\alpha(t-\tau)}{\beta}, \varepsilon\tau \right) \end{array} \right] C_1(x,\tau)d\tau \qquad (5.7)$$

where $\beta = A_s/A$ and $C_1(x,t)$ is the classical solution to the ADE for an instantaneous

slug release and is given by:

$$C_1(x,t) = \frac{M}{A\sqrt{4\pi Dt}} \exp - \left( \frac{(x-ut)^2}{4Dt} \right) \tag{5.8}$$

The $J$ function in the above equation can be evaluated using the following relation

$$J(a,b) = 1 - e^{-b} \int_0^a e^{-\lambda} I_0 \left( 2\sqrt{b\lambda} \right) d\lambda = 1 - e^{-a-b} \sum_{n=1}^{\infty} \frac{a^n}{n!} \sum_{m=0}^{n-1} \frac{b^m}{m!} \tag{5.9}$$

where $I_0$ is the modified Bessel function of zero order. One of the drawbacks of the above analytical solution is the problem of convergence for higher values of $\varepsilon$ due to the large computational time required to evaluate the $J$ functions. Therefore, if this equation is used for parameter estimation it will increase the computational time significantly which makes the numerical model more attractive. The above analytical solution was also found to agree well with other numerical models like OTIS [Runkel, 1998]. The FSTS model was found to be in excellent agreement with this analytical solution for $\alpha = 2$, for different values of $\varepsilon$, $D$, and $u$ as shown in Figures 5.4, 5.5, and 5.6 respectively.

## 5.3 Application of the FSTS Model to Describe the Field Data

We applied the FSTS model to describe tracer transport in two Michigan streams. One of the streams had a large reach length (The Grand River, Reach Length - 42 km) while the other had a smaller reach length (The Red Cedar River, Reach Length - 5 km). In order to apply the FSTS model to the streams, we first confirmed whether the BTCs of the observed tracer concentration for these sites exhibited non-Gaussian behavior during early or the late time. This was done by plotting the concentration on a probability scale against the Z-scores of the travel time. A deviation from the straight line is indicative of the non-Gaussian behavior. One can observe from the Figure 5.3, that the rising limb for the Reach C of the Red Cedar River shows a deviation from the straight line, which indicates non-Fickian early breakthrough. This justifies the use of fractional-in-space dispersion based TS model to describe the field data for the site.

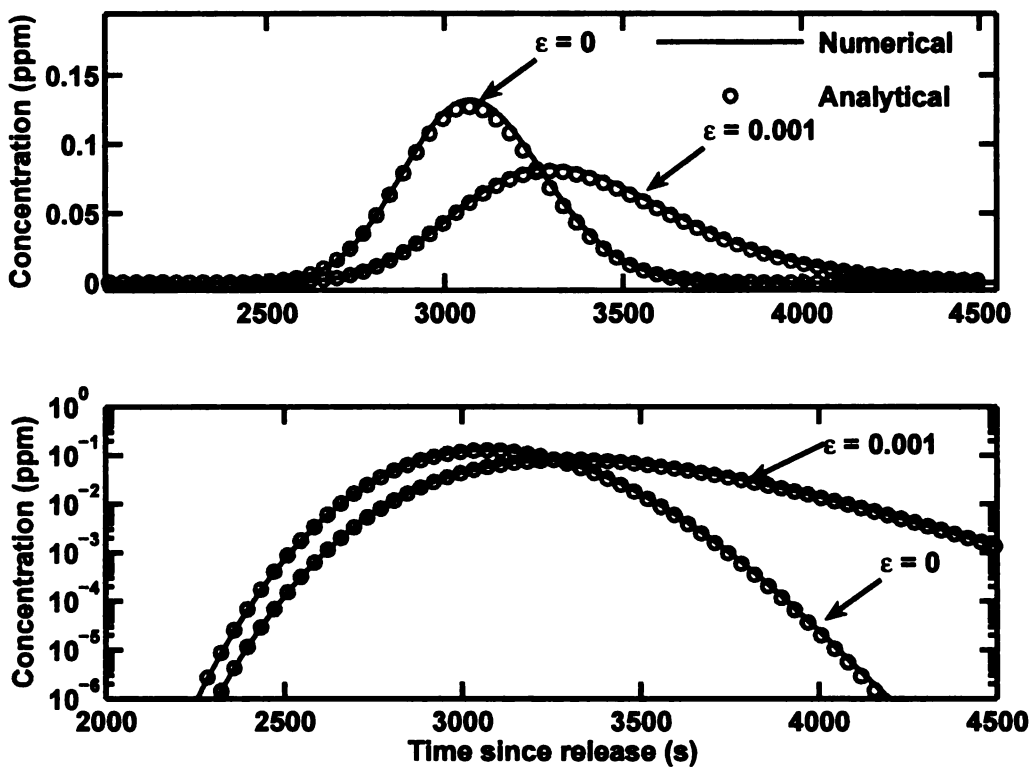


**Figure 5.4.** Comparison of compact-Caputo based fADE with the analytical solution given by De Smedt et al. [2005] for $Q = 16$ m$^3$s$^{-1}$, $A = 40$ m$^2$, $A_s = 4$ m$^2$, $D = 1$ m$^\alpha$s$^{-1}$, $M = 1000$ g, $\alpha = 2.0$, $\Delta x = 0.33$ m and $x = 1230$ m

### 5.3.1 The Red Cedar River, Michigan

The Red Cedar River (RCR) is a fourth-order stream in south central Michigan. It originates as an outflow from Cedar lake, Michigan, and flows into East Lansing and Michigan State University (MSU). The RCR meanders through the MSU campus over a stretch of 5km (our study reach) and has an average slope of 0.413 m/km. The study reach was bounded by Hagadorn Bride on the East and the Kalamazoo Street Bridge on the West (Figure 5.8). Out of the many tracer studies done on this river in 2002 we used the tracer test conducted on 19th March, 2002 [Phanikumar et al., 2007] with a discharge rate of $Q = 19.89$ m$^3$/s. Fluorescein dye was injected at the Hagadorn Bridge and samples were collected at downstream locations at the Farm Lane (1400m), Kellog (3100m) and Kalamazoo Bridge (5079m), respectively (Figure 5.8). The total mass injected was equal to 10.70 kg Phanikumar et al. [2007]. Since it was a small reach, the influence of the lateral inflow (contribution from tributaries and baseflow) was negligible [Phanikumar

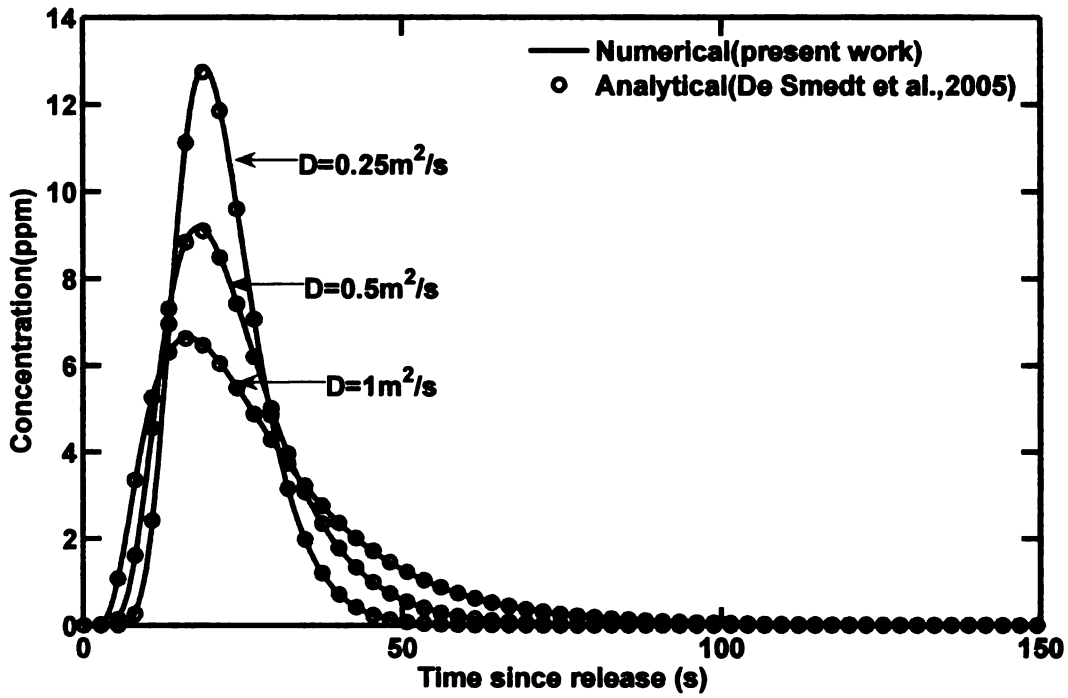


**Figure 5.5.** Comparison of compact-Caputo based fADE with the analytical solution given by De Smedt et al. [2005] for $Q = 20$ m$^3$s$^{-1}$, $A = 40$ m$^2$, $A_s = 4$ m$^2$, $\epsilon = 0.0001$ ms$^{-1}$, $M = 100$ g, $\alpha = 2.0$, $\Delta x = 0.33$ m and $x = 10$ m

et al., 2007] and therefore, we used $q_L = 0$ for all the simulations.

Phanikumar et al. [2007] applied the TS model on a reach-by-reach basis for the three reaches A, B and C as shown in Figure 5.8. They used a global optimization algorithm to estimate parameters for each of the three reaches (total of 15). They were able to estimate parameters for the reaches A and B , but for the reach C parameters were found to suffer from singular convergence [Runkel, 1998; Fernald et al., 2001], likely due to competition between processes. Our FSTS model uses a constant $D$ and variable $\alpha$ values for each of the reaches, to capture the long-range correlation of the dispersion process. Using this approach we were able to describe the scale dependency of the dispersion process and better constrain the model parameters. We estimated the $\alpha$ value on a reach-by-reach basis to account for the intra-reach variability that can not be captured using a constant $\alpha$. In the FSTS model we estimated the six parameters (i.e.,$A$, $A_S$, $q_L$, $\epsilon$, $D$ and $\alpha$) instead of five for the TS model for each of the reaches because of the introduction of an extra parameter, $\alpha$. For the three reaches A, B, and C where we tested our FSTS model,

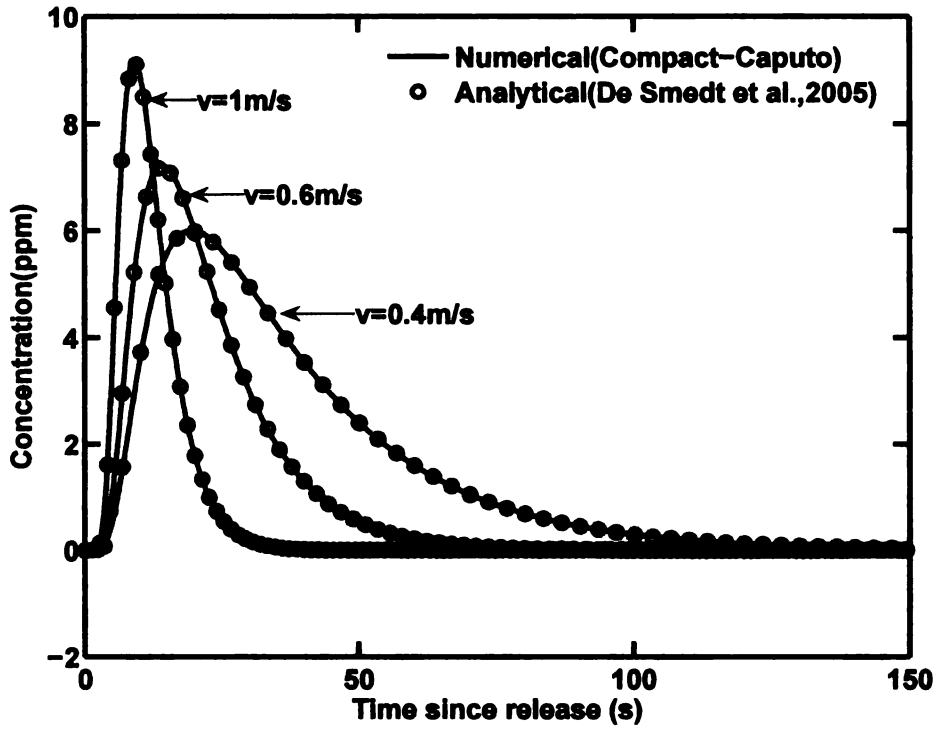


**Figure 5.6.** Comparison of compact-Caputo based fADE with the analytical solution given by De Smedt et al. [2005] for $A = 40$ m$^2$, $A_s = 4$ m$^2$, $D = 1$ m$^\alpha$s$^{-1}$, $\epsilon = 0.0001$ ms$^{-1}$, $M = 100$ g, $\alpha = 2.0$, $\Delta x = 0.33$ m and $x = 10$ m

the total number of parameters were equal to 16 (5 for each reach and a constant $D$). All the parameters in the FSTS model were estimated using global optimization procedure based on genetic and pattern search algorithms as implemented in MATLAB [Goldberg, 1989]. Parameter estimation was done by minimizing the root-mean-square error (RMSE) between the observed data and the simulated values.

We found that the FSTS model (see Figure 5.9) was able to describe the observed tracer concentrations satisfactorily for all the three reaches. A constant $D = 4.14$ was used to describe all the three reaches A, B and C. The $\alpha$ values decreased with downstream distance from 1.98 to 1.75. This was because of the increase in the magnitude of deviation from the Fickian diffusion as the plume travels a larger downstream distance. The higher values of the $(A_s/A)$ with downstream distance are attributed to the alluvium storage and the sediment characteristics (gravel and coarse sand) in reach C. Table 5.1 gives the estimated values for all the three reaches with the normalized RMSE error between observed and simulated values.

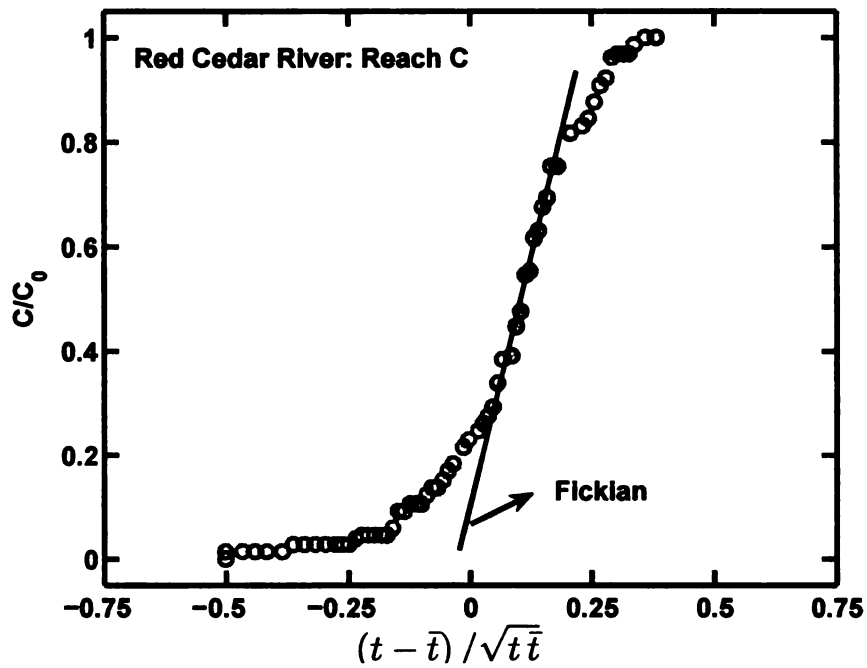


**Figure 5.7.** Probability plot showing the normalized concentration (or probability) as a function of the Z-scores of travel time for the Reach C of the Red Cedar River. Deviation from the straight line indicates a deviation from Fickian diffusion

### 5.3.2 The Grand River, Michigan

We also tested the FSTS model on the Grand River in order to see whether it was able to simulate the scale-dependent dispersion process on a significantly larger reach of 42 km compared to the 5 km reach for the Red Cedar River. This study reach extended from the city of Grand Rapids to the town of Coopersville. The data and analysis based on the TS model (i.e., with a second-order dispersion term) are described in Shen et al. [2007]. The surficial geology of the Grand River Basin is dominated by rivers crisscrossing the moraines and outwash plains formed by extensive glaciation during the Pleistocene. Sampling was carried out at four downstream sites / bridges from the point of injection at Ann Street Bridge near downtown Grand Rapids (see Figure ??). The downstream sampling locations were Wealthy Street (Site 1), $28^{th}$ Street( Site 2), Lake Michigan Drive (Site 3) and 68th Street (Site 4). The study reach was sufficiently long to make watershed influences important Shen et al. [2007], hence we accounted for the lateral inflow in the FSTS model. The average discharge for the river during the tracer study measured by

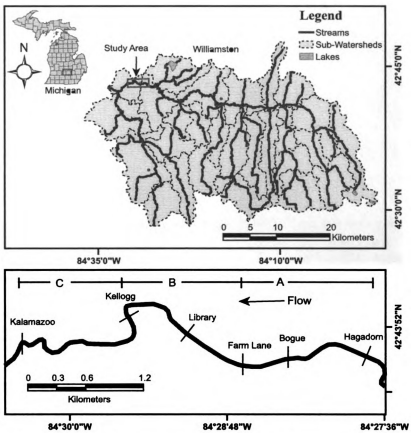


**Figure 5.8.** Red Cedar River Watershed showing the Red Cedar River and the sampling locations (adapted from Phanikumar et al. [2007])

the USGS streamflow gaging station was 91.43 cubic meter per second. Further details can be found in Shen et al. [2007].

In order to correctly estimate the mass of the tracer injected in the main stream channel, we iterated the BTC for reach A and used it for estimating FSTS model parameters for the reaches B,C, and D. The parameters for this site were estimated similar to the Red Cedar river. The RMSE error and the estimated parameters for the reaches is shown in Table 5.2. A constant $D = 3.32$ was used to describe all the three reaches A, B and C. The $\alpha$ values decreased with the downstream distance from 1.99 to 1.62 similar to the Red Cedar river indicating an increase in the magnitude of deviation from the Fickian diffusion with downstream distance.

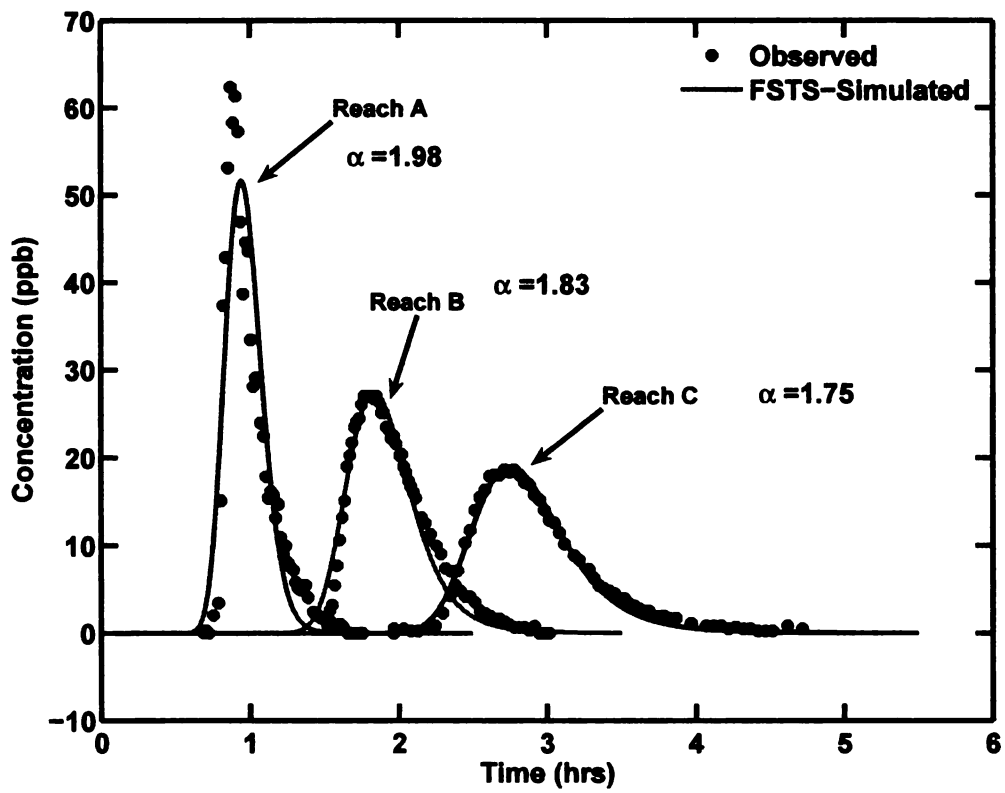


**Figure 5.9.** Fluorescein breakthrough curves for the three reaches A, B and C for the Red Cedar River with a constant dispersion coefficient $D = 4.14$ using the FSTS model

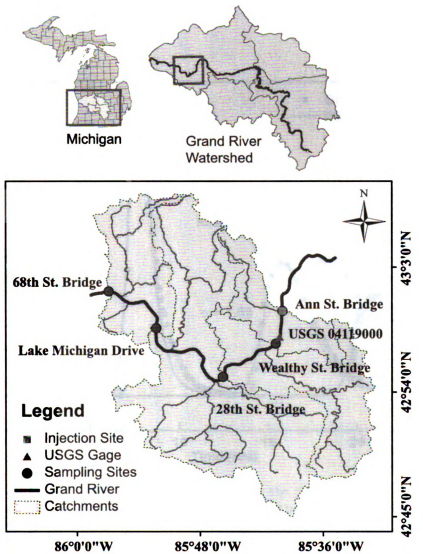


**Figure 5.10.** Grand River Watershed and study region showing the sampling sites (adapted from Shen et al. [2007])

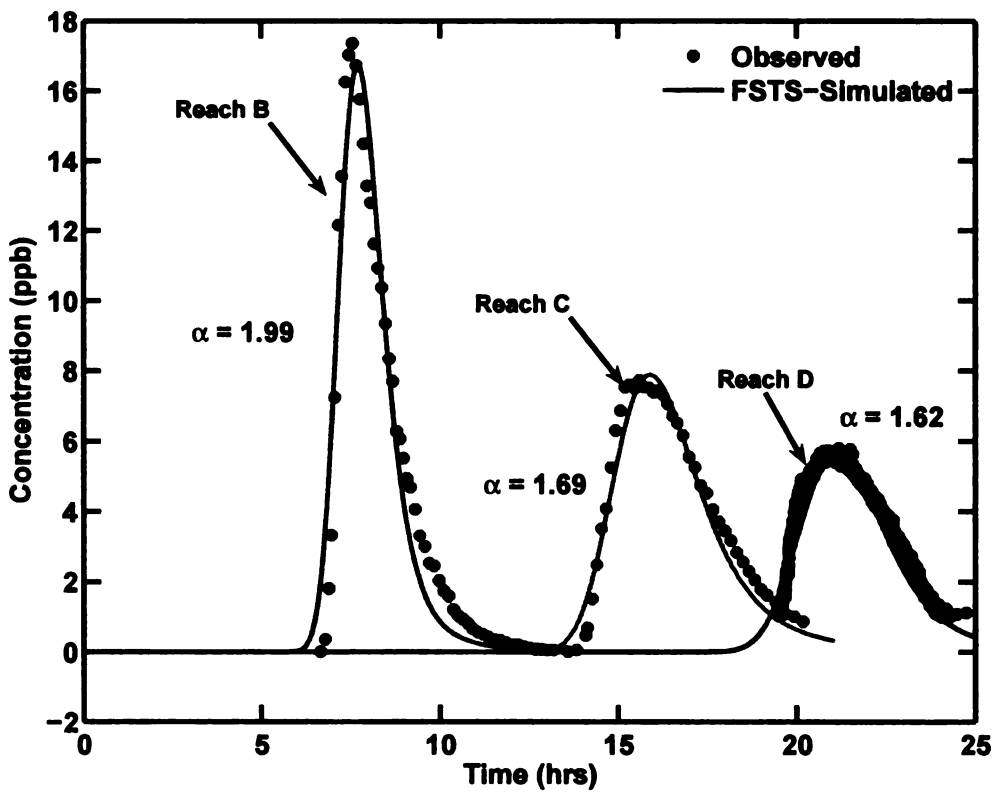


**Figure 5.11.** Rhodamine WT breakthrough curves for the three reaches B, C and D of the Grand River with a constant dispersion coefficient $D = 3.32$ using the FSTS model (data taken from Shen et al. [2007, in review])

**Table 5.1.** Storage zone parameters for the Red Cedar River using FSTS model

| Reach | $A$ | $As$ | $D$ | $\alpha$ | $q_L$ | $\varepsilon \times 10^{-5}$ | $As/A$ | $t_s$ | NRMSE |
|---|---|---|---|---|---|---|---|---|---|
| | ($m^2$) | ($m^2$) | ($m^\alpha/s$) | | ($m^3/s/km$) | ($s^{-1}$) | | (hours) | |
| A | 46.44 | 6.62 | 4.14 | 1.98 | 0.0 | 66.5 | 0.14 | 0.06 | 0.104 |
| B | 41.86 | 7.72 | 4.14 | 1.83 | 0.0 | 61.8 | 0.18 | 0.08 | 0.067 |
| C | 38.81 | 11.16 | 4.14 | 1.75 | 0.0 | 53.2 | 0.29 | 0.15 | 0.037 |

**Table 5.2.** Storage Zone Parameters for the Grand River for the three reaches with a constant $D$ using the FSTS model

| Reach | $A$ | $As$ | $D$ | $\alpha$ | $q_L$ | $\varepsilon \times 10^{-5}$ | $As/A$ | $t_s$ | NRMSE |
|---|---|---|---|---|---|---|---|---|---|
| | ($m^2$) | ($m^2$) | ($m^\alpha/s$) | | ($m^3/s/km$) | ($s^{-1}$) | | (hours) | |
| B | 192.72 | 3.0 | 3.32 | 1.99 | 0.006 | 0.6 | 0.02 | 0.72 | 0.074 |
| C | 193.66 | 3.0 | 3.32 | 1.69 | 0.006 | 0.1 | 0.02 | 4.30 | 0.069 |
| D | 190.97 | 5.18 | 3.32 | 1.62 | 0.001 | 0.4 | 0.03 | 1.88 | 0.090 |

# CHAPTER 6

# Conclusions

The major conclusions of this work are summarized below.

1. The fractional derivative based on the Caputo definition was found to provide a superior description of the fractional-in-space dispersion for the case of instantaneous slug release in a stream. In the past, space-fractional Caputo derivatives were shown to provide a better description (compared to the Grünwald-Letnikov definition) for continuous slug release in a stream; however, this issue was not examined in detail for the case of instantaneous release. The superior performance of the Caputo derivative is likely due to the distribution of the weights as shown in chapter 3.

2. Of the two advection schemes examined in this work, the fourth order accurate compact scheme was found to provide better solutions. The WENO scheme was found to introduce phase and amplitude errors for large wave numbers. Although these schemes have a Courant number restriction, it was not too stringent for the applications considered in this work since constant reach-averaged velocities are used in the models. For the more general case in which the velocities are spatially non-uniform, schemes that do not have a Courant number restriction may be more attractive (e.g., Lagrangian or semi-Lagrangian schemes).

3. We have successfully implemented an operator splitting approach for solving the governing equations. The approach was based on the Strang OS method and the advection and dispersion equations were solved using separate numerical methods.

Comparisons shown in chapter 4 indicate that the OS scheme produced excellent results.

4. One of the objectives of this work was to test whether improved dispersion modeling will enable us to better constrain the TS model parameters such as the storage zone exchange rate. The motivation was provided by the fact that in some stream reaches dispersion was not needed to describe the observed breakthrough data while in other reaches the classical ADE was found adequate. Examination of tracer breakthrough in the Red Cedar River showed that in one of the reaches (Reach C), the early breakthrough was clearly non-Fickian which indicated that a fractional order derivative was needed to describe the transport. Application of our fractional transient storage (FSTS) model showed that one dispersion coefficient but different $\alpha$ values described the observed data well without resulting in any false convergence problems noted earlier for this reach using a standard TS model.

5. Higher order approximations of the fractional derivative are attractive for several reasons (e.g., more accurate solutions on a relatively crude grid means less computational effort while estimating parameters). In this work we described one framework that can be used to obtain higher order accurate solutions based on the Caputo definition of the fractional derivative by evaluating the integer order derivatives to higher order accuracy using a compact scheme.

# APPENDIX A

# Caputo Derivative Operator

The one-dimensional fADE equation to simulate the solute movement in surface and sub-surface system without the source term is given by:

$$\frac{\partial C}{\partial t} + u\frac{\partial C}{\partial x} = D\left(\beta\frac{\partial^{\alpha} C}{\partial x^{\alpha}} + (1-\beta)\frac{\partial^{\alpha} C}{\partial(-x)^{\alpha}}\right) \tag{A.1}$$

The finite difference method described below is based on the method proposed by Zhang et al. [2006] and modified for an infinite domain $[-L, L]$. The finite difference form of equation A.1 can be written as

$$\begin{aligned} &\frac{C_i^{t+\Delta t} - C_i^t}{\Delta t} + \\ &u\frac{C_i^{t+\Delta t} - C_{i-1}^{t+\Delta t}}{\Delta x} = Q_{i-1/2}^{t+\Delta t/2} - Q_{i+1/2}^{t+\Delta t/2} \end{aligned} \tag{A.2}$$

where the fractional dispersive flux can be approximated using the Caputo derivative given by:

$$Q_{i-1/2} = \frac{-D}{\Gamma(2-\alpha)}\left(\int_0^{x_{i-1/2}} \frac{1}{(x_{i-1/2}-y)^{\alpha-1}}\frac{\partial C}{\partial y}dy\right) \tag{A.3}$$

$$Q_{i+1/2} = \frac{-D}{\Gamma(2-\alpha)}\left(\int_0^{x_{i+1/2}} \frac{1}{(x_{i+1/2}-y)^{\alpha-1}}\frac{\partial C}{\partial y}dy\right) \tag{A.4}$$

Assuming that C in $[x - x_{i+1/2}, x - x_{i-1/2}]$ is linearly distributed, the concentration gradient $\partial C/\partial x$ can be approximated by $\left[C(x - x_{i+1/2}) - C(x - x_{i-1/2})\right]/\Delta x$. Sub-

stituting it in equation A.3 to get $Q_{i-1/2}$ as

$$Q_{i-1/2} = \frac{-D}{\Gamma(2-\alpha)} \left( \begin{array}{l} \int_{-L}^{x_{i-1/2}} \frac{\beta C'(x_{i-1/2}-y)}{y^{\alpha-1}} dy \\ + \int_{-L}^{L-x_{i-1/2}} \frac{(1-\beta)C'(x_{i-1/2}+y)}{y^{\alpha-1}} dy \end{array} \right) \tag{A.5}$$

$$\approx \frac{-D}{\Gamma(2-\alpha)} \left[ \begin{array}{l} \sum_{j=0}^{i-1} (C_{i-j} - C_{i-j-1}) \int_{x_{j-1/2}}^{x_{j+1/2}} \frac{\beta}{y^{\alpha-1}} dy \\ + \sum_{j=0}^{N-i} (C_{i+j} - C_{i+j-1}) \int_{x_{j-1/2}}^{x_{j+1/2}} \frac{(1-\beta)}{y^{\alpha-1}} dy \end{array} \right] \tag{A.6}$$

which is equal to

$$Q_{i-1/2} = -\frac{D}{\Gamma(2-\alpha)\Delta x^{\alpha}} \left[ \begin{array}{l} \sum_{j=0}^{i-1} \beta w_j (C_{i-j} - C_{i-j-1}) \\ + \sum_{j=0}^{N-i} (1-\beta) w_j (C_{i+j} - C_{i+j-1}) \end{array} \right] \tag{A.7}$$

where

$$w_j = (j+1)^{2-\alpha} - (j)^{2-\alpha} \tag{A.8}$$

Similarly the flux $Q_{i+1/2}$ can be approximated as

$$Q_{i+1/2} = -\frac{D}{\Gamma(2-\alpha)\Delta x^{\alpha}} \left[ \begin{array}{l} \sum_{j=0}^{i} \beta w_j (C_{i+1-j} - C_{i-j}) \\ + \sum_{j=0}^{N-i-1} (1-\beta) w_j (C_{i+j+1} - C_{i+j}) \end{array} \right] \tag{A.9}$$

In equation A.1 the advection term can be approximated using central differencing given by [Zhang et al., 2006]

$$\frac{\partial C}{\partial x} = \frac{C_{i+1} - C_{i-1}}{2\Delta x} \tag{A.10}$$

Substituting equation A.10 in equation A.1 the finite-difference form of fADE is given by:

$$\frac{C_i^{t+\Delta t}-C_i^t}{\Delta t}+u\frac{C_{i+1}^{t+\Delta t}-C_{i-1}^{t+\Delta t}}{2\Delta x}$$

$$= \frac{D}{\Gamma(2-\alpha)\Delta x^\alpha}\left\{\begin{array}{l} \left(C_{i-1}^{t+\Delta t}-2C_i^{t+\Delta t}+C_{i+1}^{t+\Delta t}\right) \\ +\sum_{j=1}^{i}\beta w_j(C_{i+1-j}^t-C_{i-j}^t) \\ -\sum_{j=1}^{i-1}\beta w_j(C_{i-j}^t-C_{i-j-1}^t) \\ \\ +\sum_{j=1}^{N-i-1}(1-\beta)w_j(C_{i+j+1}^t-C_{i+j}^t) \\ -\sum_{j=1}^{N-i}(1-\beta)w_j(C_{i+j}^t-C_{i+j-1}^t) \end{array}\right\} \tag{A.11}$$

The above equation is a semi-implicit form, since the Gaussian dispersion terms (RHS -first three terms) and the advection terms are solved implicitly while the non-Gaussian terms (remaining RHS terms) are solved explicitly. One can also approximate the advection term to a higher order accuracy using either a WENO or compact scheme discussed in Chapter 2. A prescribed concentration boundary or a prescribed-flux boundary with inlet boundary at $x=-L$ and outlet boundary at $x=L$ can be used to solve the above equation. The prescribed-flux boundary commonly encountered in hydrology can be modeled as a prescribed flux at $x=-L$ and a free drainage at the outlet $x=L$. The boundaries can be modeled as

$$\begin{aligned} uC-D\left(\beta\frac{\partial^{\alpha-1}C}{\partial x^{\alpha-1}}+(1-\beta)\frac{\partial^{\alpha-1}C}{\partial(-x)^{\alpha-1}}\right)_{x=-L} &= uC_{-L} \\ -D\left(\beta\frac{\partial^{\alpha-1}C}{\partial x^{\alpha-1}}+(1-\beta)\frac{\partial^{\alpha-1}C}{\partial(-x)^{\alpha-1}}\right)_{x=L} &= 0 \end{aligned} \tag{A.12}$$

$C_{-L}$ represents the concentration at the inlet boundary. This approach uses an integer-order flux boundary instead of fractional-dispersive boundary given by [Zhang et al., 2006]

$$\begin{aligned} Q_{-N+1/2} &= -\frac{D}{\Gamma(2-\alpha)\Delta x^\alpha}\left[\begin{array}{l}\beta w_0(C_{-N+1}-C_{-N}) \\ +\sum_{j=0}^{N-1}(1-\beta)(C_{-N+1+j}-C_{-N})\end{array}\right] \\ Q_{N-1/2} &= -\frac{D}{\Gamma(2-\alpha)\Delta x^\alpha}\left[\begin{array}{l}\sum_{j=0}^{N-1}\beta w_j(C_{N-j}-C_{N-j-1}) \\ +(1-\beta)(C_{N-1}-C_N)\end{array}\right] \end{aligned} \tag{A.13}$$

# APPENDIX B

# Grünwald-Letnikov Derivative Operator

The value of a fractional derivative operator (based on Grünwald) acting on the function $C(x,t)$ is an infinite series given by [Oldham and Spanier, 1974]

$$\frac{\partial^\alpha C}{\partial x^\alpha} = \lim_{N\to\infty} \frac{1}{\Delta x^\alpha \Gamma(-\alpha)} \sum_{j=0}^{N-1} \frac{\Gamma(j-\alpha)}{\Gamma(j+1)} C(x-jh,t) \tag{B.1}$$

where $\Gamma()$=gamma function, $\Delta x = x/N$; $N$ = positive integer. Oldham and Spanier [1974] presented another definition to the above definition which has a better convergence property and is given by:

$$\frac{\partial^\alpha C}{\partial x^\alpha} = \lim_{N\to\infty} \frac{1}{\Delta x^\alpha \Gamma(-\alpha)} \sum_{j=0}^{N-1} \frac{\Gamma(j-\alpha)}{\Gamma(j+1)} C\left(x+\Delta x-j\Delta x,t\right) \tag{B.2}$$

In analogy, the backward-finite difference form of the above equation is given by Grüwald-Letnikov by induction

$$\frac{\partial^\alpha C}{\partial x^\alpha} = \lim_{N\to\infty} \frac{1}{\Delta x^\alpha \Gamma(-\alpha)} \sum_{j=0}^{N-1} \binom{\alpha}{j} C\left(x-j\Delta x,t\right) \tag{B.3}$$

where the coefficients $\alpha$ over $j$ = weighting factors, reflect the length of the memory of the fractional derivative and is given by [Podlubny, 1999]:

$$w_j^\alpha = \frac{j-1-\alpha}{j} w_{j-1}^\alpha \quad , \quad w_0^\alpha = 1, \quad j = 1,2,3... \tag{B.4}$$

The coefficients of the equation B.1, B.2, and B.3 are equivalent, and can be expressed as

$$\frac{\partial^\alpha C}{\partial x^\alpha} \approx \frac{1}{\Delta x^\alpha} \sum_{j=0}^{N} w_j^\alpha C_{N-j}^t \tag{B.5}$$

which is the Grüwald-Letnikov definition while

$$\frac{\partial^{\alpha} C}{\partial x^{\alpha}} \approx \frac{1}{\Delta x^{\alpha}} \sum_{j=0}^{N+1} w_j^{\alpha} C_{N+1-j}^{t} \tag{B.6}$$

is the Deng-Singh-Bengtsson definition [Deng et al., 2004].

# APPENDIX C

# Grünwald-Letnikov and Caputo Weights

We estimate the normalized weights of the GL and Caputo derivative operators to compare the relative influence of the functional values at various spatial locations for the derivative operators. While the GL derivative is approximated using the shifted GL derivative operator, the Caputo weights are approximated using a finite volume approach. The shifted GL derivative is given by:

$$\frac{\partial^\alpha C}{\partial x^\alpha} \approx \frac{1}{\Delta x^\alpha} \sum_{j=0}^{N+1} w_j^\alpha C_{N+1-j}^t \tag{C.1}$$

where

$$w_j = \left(1 - \frac{\alpha - 1}{i}\right) w_{j-1}, \quad \mathrm{w}_0 = 1, \quad j = 1, 2, 3... \tag{C.2}$$

In case of the GL, since a finite-difference approach is used to approximate the derivative, the coefficients of the series given by equation C.1 is equal to the weight itself and is given by equation C.2. In case of Caputo fractional derivative, the derivative is defined using a finite volume approach given by:

$$\overset{C}{_0}D_x^\alpha C = Q_{i-1/2} - Q_{i+1/2} \tag{C.3}$$

where the flux $Q_{i-1/2}$ is given by:

$$Q_{i-1/2} = -\frac{D}{\Gamma(2-\alpha)\Delta x^\alpha} \sum_{j=0}^{i-1} w_j^c (C_{i-j} - C_{i-j-1}) \tag{C.4}$$

and the flux $Q_{i+1/2}$ is given by:

$$Q_{i+1/2} = -\frac{D}{\Gamma(2-\alpha)\Delta x^\alpha} \sum_{j=0}^{i} w_j^c (C_{i+1-j} - C_{i-j}) \tag{C.5}$$

The weights $w_j^c$ are given by:

$$w_j^c = (j+1)^{2-\alpha} - (j)^{2-\alpha} \tag{C.6}$$

for $1 \leq \alpha < 2$. Substituting the flux values in equation C.3, we get

$$\frac{D}{\Gamma(2-\alpha)\Delta x^\alpha}\left[\sum_{j=0}^{i} w_j^c(C_{i+1-j} - C_{i-j}) - \sum_{j=0}^{i-1} w_j^c(C_{i-j} - C_{i-j-1})\right] \tag{C.7}$$

The above equation can be rewritten and simplified as

$$\begin{aligned} {}_0^C D_x^\alpha C &= \frac{D}{\Gamma(2-\alpha)\Delta x^\alpha}\left[\begin{array}{l} C_{i+1} - 2C_i + C_{i-1} + \sum_{j=1}^{i} w_j^c(C_{i+1-j} - C_{i-j}) \\ -\sum_{j=1}^{i-1} w_j^c(C_{i-j} - C_{i-j-1}) \end{array}\right] \\ &= \frac{D}{\Gamma(2-\alpha)\Delta x^\alpha}\left[\begin{array}{l} C_{i+1} - 2C_i + C_{i-1} + \sum_{j=1}^{i-1} w_j^c(C_{i+1-j} - 2C_{i-j} + C_{i-j-1}) \\ +w_i^c(C_1 - C_0) \end{array}\right] \end{aligned} \tag{C.8}$$

Collecting the common terms from the above equation and rearranging it, we get

$${}_0^C D_x^\alpha C = \frac{D}{\Gamma(2-\alpha)\Delta x^\alpha}\left\{\begin{array}{l} w_0^c C_{i+1} + (-2w_0^c + w_1^c)C_i + (w_0^c - 2w_1^c + w_2^c)C_{i-1} + \\ (w_1^c - 2w_2^c + w_3^c)C_{i-2} + (w_2^c - 2w_3^c + w_4^c)C_{i-3} + \\ \quad \cdots (w_{j-1}^c - 2w_j^c + w_{j+1}^c)C_{i-j} + \cdots \\ \quad +(w_{i-2}^c - 2w_{i-1}^c + w_i^c)C_1 + (w_{i-1}^c - w_i^c)C_0 \end{array}\right. \tag{C.9}$$

We replaced constant 1 by $w_0^c$ in order to have a consistent subscript notation.

# BIBLIOGRAPHY


S. Abarbanel and A. Kumar. Compact high-order schemes for the euler equations. *Journal of Scientific Computing*, 3(3):275–288, 1988.

J. David Allan. *Stream ecology : structure and function of running waters.* Chapman & Hall, London ; New York, 1st edition, 1995. J. David Allan.ill. ; 26 cm.Includes bibliographical references (p. 343-377) and indexes.

M. W. Becker and A. M. Shapiro. Tracer transport in fractured crystalline rock: Evidence of nondiffusive breakthrough tailing. *Water Resources Research*, 36(7):1677–1686, 2000.

K. E. Bencala and R. A. Walters. Simulation of solute transport in a mountain pool-and-riffle stream: A transient storage model. 19(3), 1983.

D. A. Benson. *The fractional advection-dispersion equation: Development and application.* Dissertation of doctorial degree, University of Nevada Reno, 1998.

D. A. Benson, S. W. Wheatcraft, and M. M. Meerschaert. Application of a fractional advection-dispersion equation. *Water Resources Research*, 36(6):1403–1412, 2000.

D. A. Benson, C. Tadjeran, M. M. Meerschaert, I. Farnham, and G. Pohll. Radial fractional-order dispersion through fractured rock. *Water Resources Research*, 40(12): –, 2004.

B. Berkowitz and H. Scher. On characterization of anomalous-dispersion in porous and fractured media. *Water Resources Research*, 31(6):1461–1466, 1995.

D. B. Booth. Challenges and prospects for restoring urban streams: a perspective from the pacific northwest of north america. *Journal of the North American Benthological Society*, 24(3):724–737, 2005.

A. Burgel, T. Grahs, and T. Sonar. From continuous recovery to discrete filtering in numerical approximations of conservation laws. *Applied Numerical Mathematics*, 42 (1-3):47–60, 2002.

A. Cadiou and C. Tenaud. Implicit weno shock capturing scheme for unsteady flows. application to one-dimensional euler equations. *International Journal for Numerical Methods in Fluids*, 45(2):197–229, 2004.

M. Caputo and F. Mainardi. New dissipation model based on memory mechanism. *Pure and Applied Geophysics*, 91(8):134, 1971.

Ryuichi Chiba, Sergei Fomin, Vladimir Chugunov, Toru Takahashi, Yuichi Niibori, Toshiyuki Hashida, Kazuyuki Tohji, Noriyoshi Tsuchiya, and Balachandran Jeyadevan. Numerical simulation for non-fickian diffusion into fractured porous rock, 2006.

J. E. Cohen. Human population: The next half century. *Science*, 302(5648):1172–1175, 2003.

J. Constantz. Interaction between stream temperature, streamflow, and groundwater exchanges in alpine streams. *Water Resources Research*, 34(7):1609–1615, 1998.

B. Costa and W. S. Don. High order hybrid central - weno finite difference scheme for conservation laws. *Journal of Computational and Applied Mathematics*, 204(2):209–218, 2007.

D. J. Dangelo, J. R. Webster, S. V. Gregory, and J. L. Meyer. Transient storage in appalachian and cascade mountain streams as related to hydraulic characteristics. *Journal of the North American Benthological Society*, 12(3):223–235, 1993.

P. M. Davis, T. C. Atkinson, and T. M. L. Wigley. Longitudinal dispersion in natural channels: 2. the roles of shear flow dispersion and dead zones in the river severn, uk. 4 (3):355–371, 2000.

F. De Smedt, W. Brevis, and P. Debels. Analytical solution for solute transport resulting from instantaneous injection in streams with transient storage. *Journal of Hydrology*, 315:25–39, 2005.

A. O. Demuren, R. V. Wilson, and M. Carpenter. Higher-order compact schemes for numerical simulation of incompressible flows, part i: Theoretical development. *Numerical Heat Transfer Part B-Fundamentals*, 39(3):207–230, 2001.

Z. Q. Deng, V. P. Singh, and L. Bengtsson. Numerical solution of fractional advection-dispersion equation. *Journal of Hydraulic Engineering-Asce*, 130(5):422–431, 2004.

Z. Q. Deng, L. Bengtsson, and V. P. Singh. Parameter estimation for fractional dispersion model for rivers. *Environmental Fluid Mechanics*, 6(5):451–475, 2006.

A. Dolezal and S. S. M. Wong. Relativistic hydrodynamics and essentially nonoscillatory shock capturing schemes. *Journal of Computational Physics*, 120(2):266–277, 1995.

J. H. Duff and F. J. Triska. Denitrification in sediments from the hyporheic zone adjacent to a small forested stream. *Canadian Journal of Fisheries and Aquatic Sciences*, 47(6): 1140–1147, 1990.

J. H. Duff, F. Murphy, C. C. Fuller, F. J. Triska, J. W. Harvey, and A. P. Jackman. A mini drivepoint sampler for measuring pore water solute concentrations in the hyporheic zone of sand-bottom streams. *Limnology and Oceanography*, 43(6):1378–1383, 1998.

R. P. Fedkiw, G. Sapiro, and C. W. Shu. Shock capturing, level sets, and pde based methods in computer vision and image processing: a review of osher's contributions. *Journal of Computational Physics*, 185(2):309–341, 2003.

A. G. Fernald, P. J. Wigington, and D. H. Landers. Transient storage and hyporheic flow along the willamette river, oregon: Field measurements and model estimates. *Water Resources Research*, 37(6):1681–1694, 2001.

Hugo B. Fischer. *Mixing in inland and coastal waters.* Academic Press, New York, 1979.

C. Gallo and G. Manzini. A mixed finite element finite volume approach for solving biodegradation transport in groundwater. *International Journal for Numerical Methods in Fluids*, 26(5):533–556, 1998.

David E. Goldberg. *Genetic algorithms in search, optimization, and machine learning.* Addison-Wesley Pub. Co., Reading, Mass., 1989.

R. Gorenflo, F. Mainardi, D. Moretti, and P. Paradisi. Time fractional diffusion: A discrete random walk approach. *Nonlinear Dynamics*, 29(1-4):129–143, 2002.

D. Gottlieb and C. W. Shu. On the gibbs phenomenon and its resolution. *Siam Review*, 39(4):644–668, 1997.

S. Gottlieb, D. Gottlieb, and C. W. Shu. Recovering high-order accuracy in weno computations of steady-state hyperbolic systems. *Journal of Scientific Computing*, 28(2-3): 307–318, 2006.

R. Haggerty, S. A. McKenna, and L. C. Meigs. On the late-time behavior of tracer test breakthrough curves. *Water Resources Research*, 36(12):3467–3479, 2000.

E. L. Harbott, M. R. Grace, J. A. Webb, and B. T. Hart. Small-scale temporal variation and the effect of urbanisation on extracellular enzyme activity in streams. *Journal of Environmental Monitoring*, 7(9):861–868, 2005.

A. Harten, B. Engquist, S. Osher, and S. R. Chakravarthy. Uniformly high-order accurate essentially nonoscillatory schemes .3. *Journal of Computational Physics*, 71(2):231–303, 1987.

C. Harvey and S. M. Gorelick. Rate-limited mass transfer or macrodispersion: Which dominates plume evolution at the macrodispersion experiment(made) site? 36(3):637–650, 2000.

M. Yousuff Hussaini, B. Van Leer, and J. Van Rosendale. *Upwind and High-Resolution Schemes.* Springer-Verlag Telos, 1997.

G. S. Jiang and C. W. Shu. Efficient implementation of weighted eno schemes. *Journal of Computational Physics*, 126(1):202–228, 1996.

H. E. Jobson. Predicting river travel time from hydraulic characteristics. *Journal of Hydraulic Engineering-Asce*, 127(11):911–918, 2001.

J. B. Jones and R. M. Holmes. Surface-subsurface interactions in stream ecosystems. *Trends in Ecology & Evolution*, 11(6):239–242, 1996.

K. Jonsson, H. Johansson, and A. Worman. Hyporheic exchange of reactive and conservative solutes in streams - tracer methodology and model interpretation. *Journal of Hydrology*, 278(1-4):153–171, 2003.

L. A. Khan and P. L. F. Liu. An operator splitting algorithm for the three-dimensional advection-diffusion equation. *International Journal for Numerical Methods in Fluids*, 28(3):461–476, 1998.

L. A. Khan and P. L. F. Liu. An operator splitting algorithm for coupled one-dimensional advection-diffusion-reaction equations. *Computer Methods in Applied Mechanics and Engineering*, 127(1-4):181–201, 1995.

P. Kumar and O. P. Agrawal. An approximate method for numerical solution of fractional differential equations. *Signal Processing*, 86(10):2602–2610, 2006.

J. M. Lees, L. A. Camacho, and S. Chapra. On the relationship of transient-storage and aggregated dead zone models to solute transport in streams. 36(1):213, 1999.

S. K. Lele. Compact finite-difference schemes with spectral-like resolution. *Journal of Computational Physics*, 103(1):16–42, 1992.

Ming Li. *Numerical solutions for the incompressible Navier-Stokes equations*. PhD thesis.

F. Liu, V. Anh, and I. Turner. Numerical solution of the space fractional fokker-planck equation. *Journal of Computational and Applied Mathematics*, 166(1):209–219, 2004.

X. D. Liu, S. Osher, and T. Chan. Weighted essentially nonoscillatory schemes. *Journal of Computational Physics*, 115(1):200–212, 1994.

S. L. Lowery and W. C. Reynolds. Numerical simulation of a spatially-developing mixing layer. Technical Report Rep. TF-26, 1986.

C. Lubich. Discretized fractional calculus. *Siam Journal on Mathematical Analysis*, 17 (3):704–719, 1986.

V. E. Lynch, B. A. Carreras, D. Del-Castillo-Negrete, K. M. Ferreira-Mejias, and H. R. Hicks. Numerical methods for the solution of partial differential equations of fractional order. *Journal of Computational Physics*, 192(2):406–421, 2003. 747ZX Times Cited:21 Cited References Count:18.

G. I. Marchuk and N. N. Yanenko. Solution of multidimensional kinetic equation by splitting method. *Doklady Akademii Nauk Sssr*, 157(6):1291–1310, 1964.

A. Marion and M. Zaramella. Diffusive behavior of bedform-induced hyporheic-exchange in rivers. *Journal of Environmental Engineering-Asce*, 131(9):1260–1266, 2005.

A. Marion, M. Zaramella, and A. I. Packman. Parameter estimation of the transient storage model for stream-subsurface exchange. *Journal of Environmental Engineering-Asce*, 129(5):456–463, 2003.

M. M. Meerschaert and C. Tadjeran. Finite difference approximations for fractional advection-dispersion flow equations. *Journal of Computational and Applied Mathematics*, 172(1):65–77, 2004.

J. L. Meyer, M. J. Paul, and W. K. Taulbee. Stream ecosystem function in urbanizing landscapes. *Journal of the North American Benthological Society*, 24(3):602–612, 2005.

Kenneth S. Miller and Bertram Ross. *An introduction to the fractional calculus and fractional differential equations.* Wiley, New York, 1993.

E. W. Montroll and G. H. Weiss. Random walks on lattices .2. *Journal of Mathematical Physics*, 6(2):167–175, 1965.

P. J. Mulholland. Dissolved organic matter concentration and flux in streams. *Journal of the North American Benthological Society*, 16(1):131–141, 1997.

S. P. Neuman. Adaptive eulerian-lagrangian finite element method for advection-dispersion. 20:321–37, 1984.

K. Nishimoto. *An Essence of Nishimoto's Fractional Calculus (calculus in the 21st Century): Integrations and Differentiations of Arbitrary Order.* Descartes Press Co., 1991.

J. A. Ochoa-Tapia, F. J. Valdes-Parada, and J. Alvarez-Ramirez. A fractional-order darcy's law. *Physica a-Statistical Mechanics and Its Applications*, 374(1):1–14, 2007.

Z. Odibat. Approximations of fractional integrals and caputo fractional derivatives. *Applied Mathematics and Computation*, 178(2):527–533, 2006.

A Ogata and R. B. Banks. A solution of the differential equation of longitudinaldispersion in porous media. *Geological Survey Professional Paper,Movement in EarthMaterials.*, 1961.

Keith B. Oldham and Jerome Spanier. *The fractional calculus; theory and applications of differentiation and integration to arbitrary order.* Mathematics in science and engineering ; v. 111. Academic Press, New York,, 1974.

M. S. Phanikumar. Thermosolutal convection in a rectangular enclosure with strong side-walls and bottom heating. *International Journal of Heat and Fluid Flow*, 15(4): 325–336, 1994.

M. S. Phanikumar and D. W. Hyndman. Interactions between sorption and biodegradation: Exploring bioavailability and pulsed nutrient injection efficiency. *Water Resources Research*, 39(5):–, 2003.

M. S. Phanikumar, I. Aslam, C. P. Shen, D. T. Long, and T. C. Voice. Separating surface storage from hyporheic retention in natural streams using wavelet decomposition of acoustic doppler current profiles. *Water Resources Research*, 43(5), 2007.

S. Pirozzoli. Conservative hybrid compact-weno schemes for shock-turbulence interaction. *Journal of Computational Physics*, 178(1):81–117, 2002.

Igor Podlubny. *Fractional differential equations : an introduction to fractional derivatives, fractional differential equations, to methods of their solution and some of their applications.* Mathematics in science and engineering ; v. 198. Academic Press, San Diego, 1999.

William H. Press. *Numerical recipes in C++ : the art of scientific computing.* Cambridge University Press, Cambridge ; New York, 2nd edition, 2002.

Patrick J. Roache. *Fundamentals of computational fluid dynamics.* Hermosa Publishers, Albuquerque, N.M., 1998.

A. H. Roy, M. C. Freeman, B. J. Freeman, S. J. Wenger, W. E. Ensign, and J. L. Meyer. Investigating hydrologic alteration as a mechanism of fish assemblage shifts in urbanizing streams. *Journal of the North American Benthological Society*, 24(3):656–678, 2005.

R. L. Runkel. *One-dimensional Transport with Inflow and Storage (OTIS): A Solute Transport Model for Streams and Rivers.* US Dept. of the Interior, US Geological Survey; Information Services distributor, 1998.

R. L. Runkel and R. E. Broshears. One-dimensional transport with inflow and storage (otis)a solute transport model for small streams: Boulder, colo., university of colorado, 1991.

Muhammad Sahimi. Fractal and superdiffusive transport and hydrodynamic dispersion in heterogeneous porous media. *Transport in Porous Media*, 13(1):3–40, 1993. 10.1007/BF00613269.

S. G. Samko, A. A. Kilbas, and O. I. Marichev. *Fractional integrals and derivatives : theory and applications.* Gordon and Breach Science Publishers, Switzerland ; Philadelphia, Pa., USA, 1993.

B. H. Schmid. Simplification in longitudinal transport modeling: case of instantaneous slug releases. *Journal of Hydrologic Engineering*, 9(4):319–324, 2004.

R. Schumer, D. A. Benson, M. M. Meerschaert, and S. W. Wheatcraft. Eulerian derivation of the fractional advection-dispersion equation. *Journal of Contaminant Hydrology*, 48 (1-2):69–88, 2001.

R. Schumer, D. A. Benson, M. M. Meerschaert, and B. Baeumer. Multiscaling fractional advection-dispersion equations and their solutions. *Water Resources Research*, 39(1):–, 2003.

K. Sebastian and C. W. Shu. Multidomain weno finite difference method with interpolation at subdomain interfaces. *Journal of Scientific Computing*, 19(1-3):405–438, 2003.

S. Serna and A. Marquina. Power eno methods: a fifth-order accurate weighted power eno method. *Journal of Computational Physics*, 194(2):632–658, 2004.

C. Shen, M. S. Phanikumar, T.T. Fong, I. Aslam, S.L. Molloy, and J.B. Rose. The transport of bacteriophage p22 relative to rhodamine wt in suraface waters: The grand river, michigan. *Environmental Science & Technology*, 2007.

C. W. Shu. *Essentially Non-oscillatory and Weighted Essentially Non-oscillatory Schemes for Hyperbolic Conservation Laws.* Institute for Computer Applications in Science and Engineering, NASA Langley Research Center; National Technical Information Service, distributor, 1997.

G. Sposito and W. Jury. Fundamental problems in the stochastic convection-dispersion model of solute transport in aquifers and field soils. (1):77–88, 1986.

Y. C. Tai, S. Noelle, J. M. N. T. Gray, and K. Hutter. Shock-capturing and front-tracking methods for granular avalanches. *Journal of Computational Physics*, 175(1):269–301, 2002.

G. Taylor. Conditions under which dispersion of a solute in a stream of solvent can be used to measure molecular diffusion. *Proceedings of the Royal Society of London Series a-Mathematical and Physical Sciences*, 225(1163):473–477, 1954.

C. W. Tsai, K. Z. Kuai, M. Bursik, and D. Hess. Nonlinear modeling of dam-break flood wave induced sediment transport and morphological evolution in rivers. *AGU Fall Meeting Abstracts*, 54:02–02, 2004.

H. M. Valett, J. A. Morrice, C. N. Dahm, and M. E. Campana. Parent lithology, surface-groundwater exchange, and nitrate retention in headwater streams. *Limnology and Oceanography*, 41(2):333–345, 1996.

P. J. van der Houwen and B. P. Sommeijer. Splitting methods for three-dimensional transport models with interaction terms. *Journal of Scientific Computing*, 12(3):215–231, 1997. 10.1023/A:1025645326705.

S. Wallis. The numerical solution of the advection-dispersion equation: A review of some basic principles. *Acta Geophysica*, 55(1):85–94, 2007.

C. Wei and G. Morrison. Bacterial enzyme-activity and metal speciation in urban river sediments. *Hydrobiologia*, 235:597–603, 1992. Jm308 Times Cited:10 Cited References Count:15.

M. Weilbeer. *Efficient Numerical Methods for Fractional Differential Equations and their Analytical Background.* PhD thesis, Institut computational mathematics, 2006.

S. W. Wheatcraft and S. W. Tyler. An explanation of scale-dependent dispersivity in heterogeneous aquifers using concepts of fractal geometry. *Water Resources Research*, 24(4):566–578, 1988.

S. M. Wondzell and F. J. Swanson. Seasonal and storm dynamics of the hyporheic zone of a 4th-order mountain stream .2. nitrogen cycling. *Journal of the North American Benthological Society*, 15(1):20–34, 1996.

A. Worman. Analytical solution and timescale for transport of reacting solutes in rivers and streams. *Water Resources Research*, 34(10):2703–2716, 1998.

A. Worman. Effect of flow-induced exchange in hyporheic zones on longitudinal transport of solutes in streams and rivers (vol 38, pg 1001, 2002). *Water Resources Research*, 38 (6):–, 2002.

Z. Yong, D. A. Benson, M. M. Meerschaert, and H. P. Scheffler. On using random walks to solve the space-fractional advection-dispersion equations. *Journal of Statistical Physics*, 123(1):89–110, 2006.

Y. Zhang, D. A. Benson, M. M. Meerschaert, E. M. LaBolle, and H. P. Scheffler. Random walk approximation of fractional-order multiscaling anomalous diffusion. *Physical Review E*, 74(2), 2006.

Y. Zhang, D. A. Benson, M. M. Meerschaert, and E. M. LaBolle. Space-fractional advection-dispersion equations with variable parameters: Diverse formulas, numerical solutions, and application to the macrodispersion experiment site data. *Water Resources Research*, 43(5):–, 2007.